# SUBMERGED BREAKWATERS AS A MEASURE TO REDUCE WAVE OVERTOPPING AT VERTICAL SEAWALLS

**A Thesis Submitted to**
**the Graduate School of**
**İzmir Institute of Technology**
**in Partial Fulfillment of the Requirements for Degree of**

**MASTER OF SCIENCE**

**in Civil Engineering**

**by**

**Rabia KARAGÖZ**

**December 2024**
**İZMİR**

We approve the thesis of **Rabia KARAGÖZ**

**Examining Committee Members:**

**Asst. Prof. Dr. Doğan KISACIK**
Department of Civil Engineering, İzmir Institute of Technology

**Assoc. Prof. Dr. Bergüzar ÖZBAHÇECİ**
Department of Civil Engineering, İzmir Institute of Technology

**Asst. Prof. Dr. Gülizar ÖZYURT TARAKCIOĞLU**
Department of Civil Engineering, Middle East Technical University

**11 December 2024**

**Asst. Prof. Dr. Doğan KISACIK**
Supervisor
Department of Civil Engineering
İzmir Institute of Technology

**Prof. Dr. Nurhan ECEMİŞ**
Head of the Department of Civil Engineering

**Prof. Dr. Mehtap EANES**
Dean of the Graduate School

# ACKNOWLEDGEMENTS

First of all, I would like to express my deepest gratitude to my advisor, Asst. Prof. Dr. Doğan Kısacık, for his invaluable guidance and support throughout this journey. His expertise in laboratory studies and coastal engineering has greatly shaped this research and enriched my understanding of the field. I am sincerely thankful for his feedback, patience, and mentorship, which have been a constant source of motivation.

I sincerely thank Assoc. Prof. Dr. Bergüzar Özbahçeci for her inspiring lectures during my undergraduate studies, which sparked my interest in coastal engineering. I am also grateful for her valuable suggestions and constructive feedback as a thesis jury member, which greatly enhanced this work.

I sincerely thank Asst. Prof. Dr. Gülizar Özyurt Tarakcıoğlu, a member of my thesis jury, for her valuable contributions during the defense. Her insightful remarks and constructive feedback greatly helped to improve this study.

This study was funded by the Scientific and Technological Research Council of Turkey, TUBITAK under 122M553.

I sincerely thank Nisa Bahadıroğlu for her unwavering support and kindness throughout this thesis journey. Her tireless efforts and dedication in laboratory studies, along with her exceptional assistance, have been invaluable. Beyond her expertise, her encouragement during challenging times and her valuable friendship has been a source of strength, for which I am deeply grateful.

I would like to thank Kadir Aktaş for his invaluable assistance and expertise during the laboratory studies. His patience in answering my questions and his support throughout this process have been greatly appreciated.

I would also like to thank my dear friend Onur Deniz Türkseven for his endless support, encouragement, and help with laboratory studies throughout this research journey.

I am grateful to my dear friend Semih Can for his sincere support, friendship, and help with the laboratory studies.

I sincerely thank Serkan Koç, Binhan Arık, İlay Develi, Baran Mungan, Yağız Erbay, and Beyzanur Sönmez for their friendship and support in laboratory studies.

I deeply appreciate my lovely friends Bahadır Öztürk, Hilal Çelik Karaca, Yaren Türkseven, and Ekin Gültepe for their friendship and understanding.

I would like to extend my heartfelt gratitude to my dear friends Hande Aydemir, Seçil Melis Altıparmak, Hayriye Dönmez, Busenur Yeter, and Can Açıkgöz for their unwavering support and encouragement. Their presence has been a source of comfort and strength during challenging times, and their kindness and understanding have been truly uplifting.

Finally, I would like to express my deepest gratitude to my beloved mother Havva Karagöz, my precious father Bahadır Karagöz, and my lovely brother Hüseyin Karagöz. Their presence has always made me feel supported and never alone. Without them, this achievement would not have been possible. During the most challenging times of my life, they provided unwavering and unconditional support without hesitation or complaint, for which I am profoundly thankful.

*To my lovely parents,*

# ABSTRACT


## SUBMERGED BREAKWATERS AS A MEASURE TO REDUCE WAVE OVERTOPPING AT VERTICAL SEAWALLS

Rapid urbanization and population growth in coastal cities are increasing pressure on urban areas. This pressure is fed by climate change caused by global warming. Sea level rise, one of the most significant impacts of climate change, increases flood risk of urban areas by reducing the effectiveness of coastal protection structures, especially during storms. Therefore, submerged breakwater can be used as a solution to reduce wave-overtopping. This study is 2D, small-scale experimental research carried out in IZTECH Hydraulics Laboratory within the scope of TUBITAK project 122M553 and investigates the performance of submerged breakwaters in reducing wave overtopping on vertical seawalls. It is shown that submerged breakwaters can be used as an effective coastal defense system by reducing the overtopping discharge by up to 90%. The effectiveness of the submerged breakwater is expressed through a reduction factor ($\gamma_{sub}$), which quantifies its impact on wave overtopping. Reduction factor is influenced by geometric parameters of the submerged breakwater, such as breakwater height and crest width, as well as hydrodynamic conditions including wave height, wavelength, and water depth. Based on 128 different experimental tests, relationship between these parameters and wave overtopping reduction is quantified, and the reduction factor is formulated as a function of submerged breakwater's design parameters. Reduction factor is then integrated into widely accepted EurOtop (2018) wave overtopping prediction formula to provide an estimate of wave overtopping discharge in the presence of a submerged breakwater. Furthermore, the effectiveness of wave-transmission formulas proposed in literature is evaluated by comparing them with the data set generated in this study.

# ÖZET

## DİKEY DENİZ DUVARLARINDA DALGA AŞMASINI AZALTMAK İÇİN ÖNLEM OLARAK BATIK DALGAKIRANLAR

Kıyı kentlerindeki hızlı kentleşme ve artan nüfus, kentsel alanlar üzerindeki baskıyı artırmakta. Bu durum küresel ısınmanın tetiklediği iklim değişikliğiyle daha da şiddetlenmektedir. İklim değişikliğinin en belirgin etkilerinden biri olan deniz seviyesinin yükselmesi, özellikle fırtına koşullarıyla birleştiğinde kıyı koruma yapılarının etkinliğini azaltarak kentsel bölgelerin taşkın riskini artırmaktadır. Bu bağlamda, dalga aşmasını azaltmak için batık bir dalgakıran çözüm olarak kullanılabilir. Bu çalışma, İYTE Hidrolik Laboratuvarında, 122M553 kodlu TÜBİTAK projesi kapsamında gerçekleştirilen 2 boyutlu, küçük ölçekli deneysel bir araştırma olup, dikey deniz duvarlarında dalga aşmasını azaltmada batık dalgakıranların etkinliğini incelemektedir. Batık dalgakıranların, dalga aşma debisini %90'a kadar azaltarak etkin bir tamamlayıcı kıyı savunma sistemi olarak kullanılabileceği gösterilmiştir. Batık dalgakıranın etkinliği, dalgaların aşması üzerindeki etkisini ölçen bir indirgeme katsayısı ($\gamma_{sub}$) ile ifade edilir. Bu indirgeme katsayısı, dalgakıran yüksekliği ve kret genişliği gibi batık dalgakıranın geometrik parametreleri ile dalga yüksekliği, dalga boyu ve su derinliği gibi hidrodinamik koşullardan da etkilenir. Bu parametrelerin etkisi dalga aşmasındaki azalmanın belirlenmesinde önemli bir rol oynar. 128 farklı deney testi kullanılarak, dalga aşmasındaki azalma niceliksel olarak belirlenmiştir. Daha sonra batık dalgakıranın tasarım parametrelerinin bir fonksiyonu olarak ifade edilmiş azaltma faktörü tanımlanmıştır. Bu indirgeme katsayısı, yaygın olarak kabul gören EurOtop (2018) dalga aşması tahmin formülüne entegre edilerek, batık dalgakıranın dikey deniz duvarı önüne yerleştirilmesi durumunda, dalga aşma deşarjının tahmin edilmesini sağlar. Ayrıca bu deneysel çalışmada, literatürde önerilen dalga iletim formüllerinin etkinliği, bu çalışmada üretilen veri seti ile karşılaştırılarak değerlendirilmiştir.

# TABLE OF CONTENTS

# LIST OF FIGURES

**Figure** **Page**

**Figure** **Page**

**Figure** **Page**

**Figure** **Page**

**Figure** **Page**

# LIST OF TABLES

# CHAPTER 1

# INTRODUCTION

The large and rapidly increasing human population, settlements and economic activities in coastal areas increase the vulnerability of these areas to natural disasters. As noted by Small et al. (2003), these densely populated areas host a variety of natural processes that are often modified by human activities and create vulnerability to natural disasters. The establishment of special economic zones has encouraged more intensive development by increasing the geographical advantages of coastal areas (McGranahan et al., 2007). This further increases the risk of vulnerability to natural disasters.

The combination of human settlement, economic activities and infrastructure development efforts collectively increases the risk profile of coastal areas. These factors make coastal areas vulnerable to natural risks such as storms, floods and sea level rise. Sea level rise is one of the severe results of the climate change caused by global warming. When sea level rise is considered together with the storm conditions, the resilience of the coastal protection structures is quite inadequate to protect the city from coastal flooding. Therefore, some measures must be taken for adaptation of the coastal structures to sea level rise.

İzmir, one of the important coastal cities in Türkiye, is also at risk of coastal flooding at times when storms are intense, especially in the winter season, negatively affecting life in this region. Figure 1.1 illustrates the coastal flooding caused by overtopping in the Kordon Region of Izmir. Also, according to Intergovernmental Panel on Climate Change (IPCC) report, climate change due to global warming will cause rise in sea levels and wave heights soon. As a result of rising sea levels and increasing wave heights, coastal areas may experience flooding and low-lying areas may be inundated.

Kisacik et al. (2019), states that crest of seawall is not high enough to reduce wave overtopping, the simplest course of action would be to increase the crest heights of these structures, as the local administrations and the people are opposed to any obstruction to the scenery. Kisacik et al. (2022) noted that it is preferable to limit the crest heights of such structures, as many coastal areas serve recreational purposes where accessibility to the sea and the preservation of scenic views are important.

If it is not possible to increase the crest level, submerged breakwater may be an alternative solution to protect the coastal areas from the flooding (van Gent et al., 2022). The crest of the submerged breakwater is positioned below the still water level (SWL) to break the incident waves by creating a shallow region. Therefore, the transmitted waves approaching the structure will have relatively lower energy. Consequently, the overtopping discharge will decrease due to the submerged breakwater.

Submerged breakwaters are economically more advantageous than conventional rubble mound breakwaters (Ahrens, 1987). The most important reason for this is that the crest elevation in submerged breakwaters is low. Another advantage of the submerged breakwater is that submerged breakwaters are more aesthetically pleasing than conventional breakwaters for coastal areas.

In Izmir Bay both coastal protection structures, vertical seawalls and rubble mounds are inadequate to protect the coastline against flooding. Since vertical seawalls are the most critical case, this study focuses on reducing the overtopping discharge on vertical seawalls.

This study aims to evaluate the effectiveness of submerged breakwaters in mitigating wave overtopping at vertical seawalls through physical model tests. To achieve this, experimental investigations were conducted in the Hydraulic Laboratory at Izmir Institute of Technology (IZTECH), where the impact of submerged breakwaters was quantified using a gamma reduction factor, representing their influence on overtopping discharge.

A submerged breakwater solution was proposed to mitigate the risk of flooding while preserving the visual aesthetics of both the seaside and the landward areas. This approach provides the advantage of reducing wave overtopping without obstructing views or altering the natural coastal environment. By dissipating wave energy before it reaches the shoreline, submerged breakwaters are designed to maintain a balance between functionality and aesthetics, enhancing coastal protection systems.

In addition to quantifying wave overtopping reduction, the study also examined wave transmission phenomena associated with submerged breakwaters. Understanding wave transmission is crucial for assessing how much energy passes through or over the breakwater, affecting the wave climate on the protected side. The results of this study are expected to contribute valuable insights into the performance of submerged breakwaters as a supplementary coastal defense strategy and provide a basis for comparison with existing findings in the literature.

Figure 1.1. Flooding photos of Kordon region, İzmir during storm conditions.
(Source: İzmir Sponge City Report, 2022)

## 1.1. The Structure of Thesis

This thesis consists of 4 main chapters apart from the current introduction section.

Chapter 2 provides an overview of the relevant academic literature about wave transmission and wave overtopping on vertical seawall.

In chapter 3, the detailed experimental set-up and test program are presented. Also, in chapter 3 hydrodynamic conditions the hydrodynamic conditions under which the experiments were conducted are presented in detail. This chapter provides a comprehensive overview of the experimental setup, including dimensional analysis and reflection analysis, to guarantee accurate representation of the wave and structural interactions. Through these analyses, the chapter lays a foundational understanding of the parameters impacting wave transmission and wave overtopping discharge, serving as a basis for the study's quantitative assessments.

Chapter 4 presents the experimental results, detailed analyses of wave transmission and the findings related to gamma reduction. The data obtained from these experiments provide useful insights into the performance of submerged breakwaters in wave energy dissipation and overtopping reduction.

Chapter 5 concludes the study by summarizing the key findings and discussing their implications for coastal protection. Additionally, this chapter proposes directions for future research, offering recommendations that could expand on the current findings and explore new approaches to enhance the effectiveness of submerged breakwaters in various hydrodynamic conditions.

# CHAPTER 2

# LITERATURE REVIEW

## 2.1. Wave Transmission

The amount of wave passing to the back of the structure after being partially absorbed by an artificial or natural obstacle is called wave transmission. The transmission coefficient, $K_t$, is defined as the ratio of the transmitted wave height ($H_{m0,\,t}$) to the incident wave height ($H_{m0,\,i}$) or the square root of the ratio of the transmitted wave energy to the incident wave energy, as shown in Eq. 2. 1.

$$K_t = \frac{H_{m0_t}}{H_{m0_i}} = \left(\frac{E_t}{E_i}\right)^{0.5} \tag{2. 1}$$

Here,

$H_{m0t}$: Spectral wave height transmitted through the structure.

$H_{m0i}$: Spectral wave height of approaching the structure.

$E_t$: The energy of the wave transmitted through the structure.

$E_i$: The energy of the wave approaching the structure.

Transmitted wave energy dependent on characteristic features of incident waves in other words wave height, wave period and wave steepness, the geometry of the structure, crest width, height and slope of the structure, and permeability of the structure.

Many studies on wave transmission have been conducted in literature, and Van der Meer (1990a) was the first to formulate it as stated in Eq. 2. 2, with the limitation that the wave transmission coefficient between 0.1 and 0.8. In this formula, the wave transmission coefficient, $K_t$, decreases linearly according to the relative crest of the freeboard ( $\frac{F}{Hm0_i}$). Besides F is negative for submerged structures.

$$K_t = 0.80\ for - 2.0 < \frac{F}{Hm0_i} < -1.13$$

$$K_t = 0.46 - 0.3\frac{F}{Hm0_i} \; for \; -1.13 < \frac{F}{Hm0_i} < 1.2 \tag{2. 2}$$

$$K_t = 0.1 \; for \; 1.2 < \frac{F}{Hm0_i} < 2$$

here;

F: Crest freeboard. $F = h_t - h'$
where, $h_t$ is water depth in front of the structure and $h'$ is structure's height.
$H_{m0i}$: Spectral wave height approaching the structure.
However, this formula does not consider the crest width effects.

Meer et al. (1994) proposed the following formula, considering both the crest width effect and the nominal rock diameter effect on wave transmission on both emergent and submerged structures.

$$K_t = a\frac{F}{Dn_{50}} + b \tag{2. 3}$$

Where $D_{n50}$ is the nominal rock diameter of breakwater, and a and b coefficients are defined as,

$$a = 0.031\frac{Hm0_i}{Dn_{50}} - 0.24 \tag{2. 4}$$

for emergent breakwaters,

$$b = -5.42S_{0p} + 0.0323\frac{Hm0_i}{Dn_{50}} - 0.0017\left(\frac{B}{Dn_{50}}\right)^{1.84} + 0.51 \tag{2. 5}$$

for submerged breakwaters

$$b = -2.6S_{0p} + 0.05\frac{Hm0_i}{Dn_{50}} + 0.85 \tag{2. 6}$$

Here $S_{0p}$ is the wave steepness based on peak wave period, $\frac{2\pi H_{m0i}}{gT_p^2}$ .

For conventional emergent breakwaters $K_t$ is limited between 0.075 and 0.75 and for submerged type breakwaters Kt is minimum 0.15, maximum 0.60 for $\frac{F}{Dn_{50}} < -2$. The general wave transmission formula is valid with the range of $1 < \frac{Hm0_i}{Dn_{50}} < 6$ and $0.01 < S_{0p} < 0.05$. According to Meer et al. (1994), $\frac{Hm0_i}{Dn_{50}} > 6$ causes instability in the structure and $S_{0p} > 0.05$ can cause the breaking of waves.

d'Angremond et al. (1996) performed advanced analyses and formulated wave transmission on permeable and impermeable structures, demonstrating the effect of both the structure's crest width and height, as well as wave steepness.

For permeable breakwaters,

$$K_t = -0.4\frac{F}{Hm0_i} + \left(\frac{B}{Hm0_i}\right)^{-0.31} \times \left(1 - e^{-0.5\xi}\right) \times 0.64 \qquad (2.7)$$

For impermeable breakwaters,

$$K_t = -0.4\frac{F}{Hm0_i} + \left(\frac{B}{Hm0_i}\right)^{-0.31} \times \left(1 - e^{-0.5\xi}\right) \times 0.80 \qquad (2.8)$$

Where,

$$\xi = \frac{tan\alpha}{\sqrt{\frac{Hm0}{L}}} \qquad (2.9)$$

The limitation value of the $K_t$ is in these formulas, $0.075 < K_t < 0.80$

here;

B: Crest width

F: Crest freeboard.

$H_{m0i}$: Wave height approaching the structure.

$\xi$: Surf similarity parameter (Iribarren number)

$tan\alpha$: front slope of the breakwater face

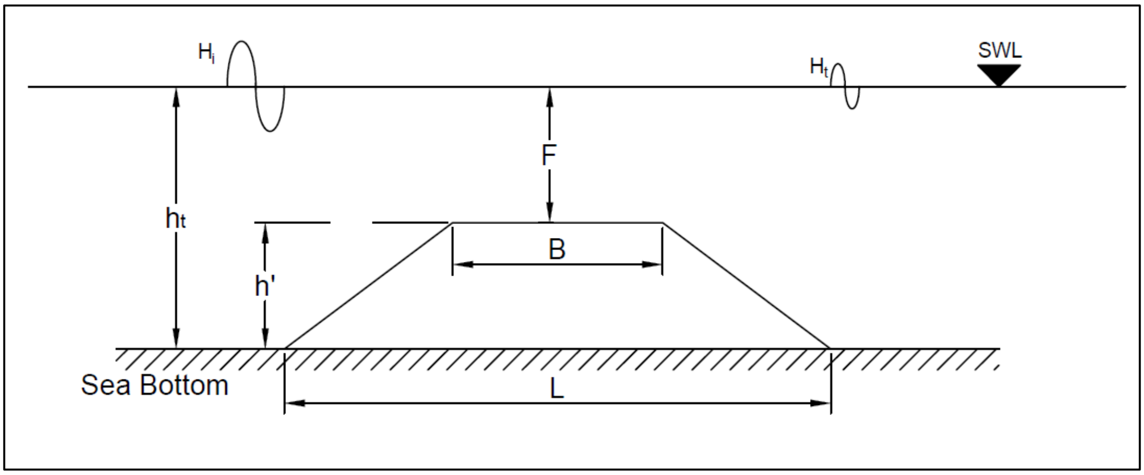


Figure 2.1.Submerged Breakwater Parameters Representation

Seabrook et al. (2000) suggested the following formula as a result of physical model analysis which shown in Figure 2.2.

$$K_t = 1 - \left( e^{0.65\frac{F}{Hm0_i} - 1.09\frac{H_{m0i}}{B}} - 0.047\left(\frac{B * F}{L * D_{n50}}\right) + 0.067\left(\frac{F * H_{m0i}}{B * D_{n50}}\right)\right) \tag{2.10}$$

The formula shows that relative submergence, crest width, incident wave height parameters are the most important parameters for wave transmission. Also, it is recommended that the formula be examined under these boundary condition ranges,

$$-7.08 \leq \left(\frac{B * F}{L * D_{n50}}\right) \leq 0$$

$$-2.14 \leq \left(\frac{F * H_{m0i}}{B * D_{n50}}\right) \leq 0 \tag{2.11}$$

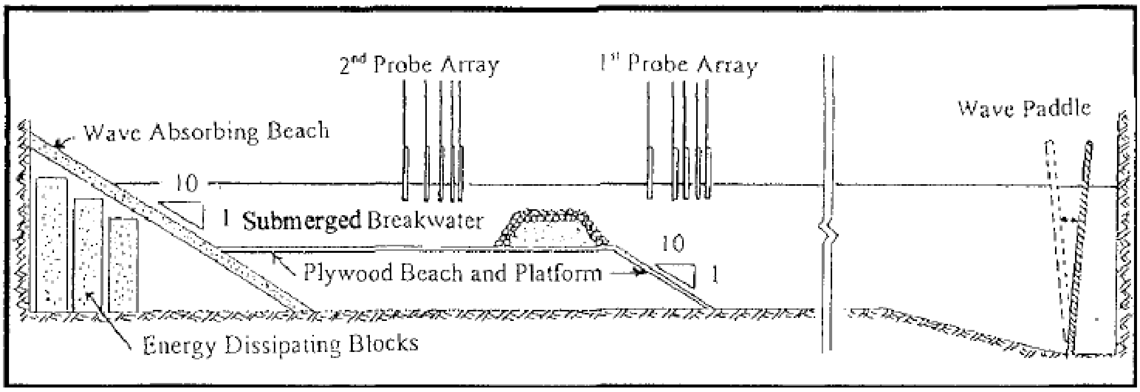


Figure 2.2. 2-D Experimental Setup
(Source: Seabrook et al., 2000)

Calabrese et al. (2003) proposed the following formula for wave transmission in low crested and submerged breakwaters in large-scale experiments, replacing $D_{n50}$ with B in the formula used by Meer et al. (1994):

$$K_t = a\frac{F}{B} + b \tag{2.12}$$

Where a and b coefficients are defined as,

$$a = (0.6957\frac{Hm0_i}{ht} - 0.7021)e^{0.2568\frac{B}{H_{m0i}}} \tag{2.13}$$

$$b = (1 - 0.562e^{-0.0507\xi})e^{-0.0507\frac{B}{H_{moi}}} \quad (2.14)$$

With the ranges between,

$$-0.4 \leq \frac{F}{B} \leq 0.3$$

$$1.06 \leq \frac{B}{Hm0_i} \leq 8.13 \quad (2.15)$$

$$0.31 \leq \frac{Hm0_i}{ht} \leq 0.61$$

$$3 \leq \xi \leq 5.20$$

Briganti et al. (2003) obtained consistent results showing that the formula proposed by d'Angremond et al. (1996) is valid for $\frac{B}{Hm0_i}$<10 and extended the formula to be used for wider-crested submerged breakwaters with $\frac{B}{Hm0_i}$>10. The following formula is,

$$K_t = -0.35\frac{F}{Hm0_i} + 0.51(\frac{B}{Hm0_i})^{-0.65} \times (1 - e^{-0.41\xi}) \quad (2.16)$$

Meer et al. (2005) extended that formula for $\frac{B}{Hm0_i} > 12$ ,

$$K_t = -0.3\frac{F}{Hm0_i} + 0.75\left(1 - e^{-0.5\xi 0p}\right) \quad for\ \xi_{0p} < 3 \quad (2.17)$$

Here Kt is between -0.075 and 0.8.

Charles Friebel et al. (2003), proposed the formula below for $K_t$ for submerged breakwaters wave transmission.

$$K_t = -0.4969exp(\frac{F}{Hm0_i}) - 0.0292(\frac{B}{h_t}) - 0.4257(\frac{h'}{h_t}) - 0.0696log(\frac{B}{L}) + 0.1359(\frac{F}{B}) + 1.0905 \quad (2.18)$$

The formula is valid for,

$$-8.639 \leq (\frac{F}{Hm0_i}) \leq 0.000$$

$$0.286 \leq (\frac{B}{h_t}) \leq 8.750$$

$$0.440 \le (\frac{h'}{h_t}) \le 1.000 \tag{2.19}$$

$$0.024 \le (\frac{B}{L}) \le 1.890$$

$$-1.050 \le (\frac{F}{B}) \le 0.000$$

where,

B: Crest width

h': height of the submerged breakwater

$h_t$ : water depth at the toe of the submerged breakwater

F: Crest freeboard.

$H_{m0i}$: Wave height approaching the structure.

L: wavelength at local depth.

Kurdistani et al. (2022) proposed the formula below for wave transmission at submerged porous breakwaters from a numerical simulation modelling with Flow-3D.

$$K_t = 0.576 \ln\left(0.428(1 + cot\alpha)^{0.042} (1 - \frac{F}{Hm0_i})^{0.75} (\frac{B_{eff}}{D_{n50}})^{0.125} (\frac{L_p}{B_{eff}})^{0.39} \omega^{0.413} \Psi^{-0.18}\right) + 0.923 \tag{2.20}$$

Here $B_{eff}$ is $\frac{4B+bottom\ width}{5}$ for submerged breakwaters. ω is non dimensional wave parameter defined as $(\frac{1}{2\pi})\tanh(\frac{2\pi h_t}{L})$ and ψ is non dimensional wave damping parameter defined as $\frac{n^{0.5}hx}{BH_{m0}}$,

where *n* = porosity, and *x* = horizontal coordinate inside the breakwater core.

Recently, Van Gent et al. (2023) conducted physical model tests at DELTARES and proposed a new wave transmission formulation at submerged structures and compared the new expression with Daemen (1991) and Calabrese et al. (2003).

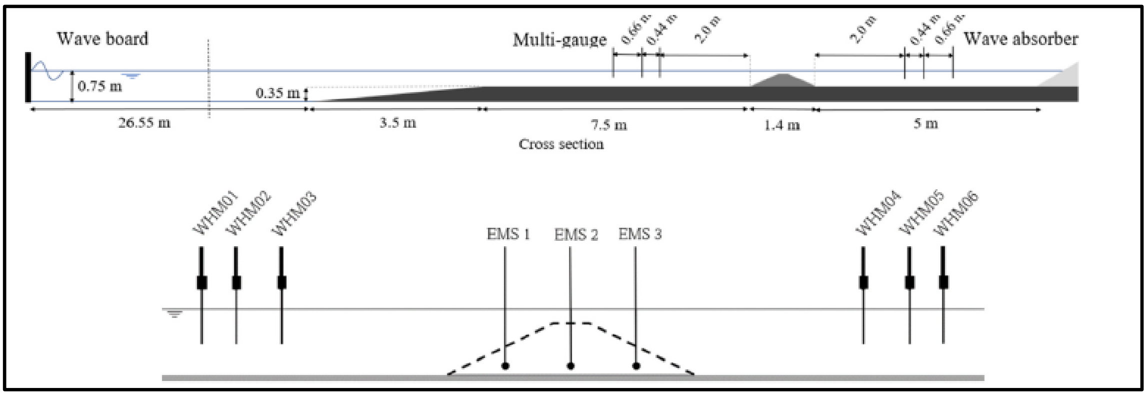


Figure 2.3. Cross-section of the foreshore in the flume
(Source: van Gent et al., 2023)

The new formulation is,

$$K_t = c_1 \tanh\left((-(\frac{F}{Hm0_i} + c_2(\frac{B}{L_{m-1,0}})^{c_3} + c_4\,)\right) + c_5 \tag{2.21}$$

Where,

Table 2.1. Coefficients for Eq. 2.21
(Source: van Gent et al., 2023)

| Structure Type | $c_1$ | $c_2$ | $c_3$ | $c_4$ | $c_5$ |
|---|---|---|---|---|---|
| Impermeable structure | 0.47 | 3.1 | 0.75 | 0 | 0.5 |
| Permeable structure (rubble mound structure) | 0.43 | 3.1 | 0.75 | -0.25 | 0.5 |
| Perforated structure | 0.13 | 3.1 | 0.75 | -0.15 | 0.82 |
| Perforated structure with screen | 0.4 | 3.1 | 0.75 | -0.15 | 0.5 |
| Perforated structure with perforated screen | 0.17 | 3.1 | 0.75 | -0.15 | 0.75 |

## 2.2. Wave Overtopping on Vertical Sea Walls

In the literature, TAW (2002), EurOtop (2007), EurOtop (2016) and EurOtop (2018) manuals provide technical information for the calculation and estimation of wave overtopping amount. One of the widely used manuals today is EurOtop (2018) manual. In EurOtop (2018); wave overtopping behavior of different structural designs under various wave conditions is analyzed with laboratory experiments conducted on coastal structures with different structural features such as slope, surface roughness, width, height and using these collected data sets, the relationships between the parameters affecting the wave overtopping amount and wave overtopping are analyzed and empirical formulas are developed.

Owen (1980) conducted some of the earliest studies on wave overtopping discharge and proposed the following Eq. 2.22, demonstrating that as the crest freeboard $R_c$ increases, wave overtopping discharge q decreases exponentially. Figure 2.4 shows the description of vertical seawall wave overtopping and parameters related to that term.

$$\frac{q}{\sqrt{gH_{m0}{}^{3}}} = aexp\left(-b\frac{R_c}{H_{m0}}\right) \tag{2.22}$$

where a and b are fitting coefficients.

Franco et al. (1994) suggested coefficients, $a = 0.2 \; and \; b = -4.3$ for formula x and with the boundary conditions $0.03 < \frac{R_c}{H_{m0}} < 3.2$ and for deep water conditions. On the other hand, for intermediate and shallower water Allsop et al. (1995) suggested coefficients, $a = 0.05$ and $b = -2.78$. The suggestion is valid for $0.03 < \frac{R_c}{H_{m0}} < 3.2$.

Allsop et al. (1995) stated that wave overtopping calculations on vertical seawalls can always be expressed not by an exponential equation but also by the power equation, and for this purpose they determined the h* parameter using data obtained from model studies where wave breaking occurred. Meer et al. (2014) stated that the h* parameter is used as a measure of impulsiveness, with a transition from non-impulsive to impulsive overtopping conditions at the wall taking place over the range $0.2 \le h* \le 0.3$.

$$h^{*} = 1.3\frac{h}{H_{m0}}\frac{2\pi h}{gT_{m-1,0}^{2}} \tag{2.23}$$

Based on the findings outlined, EurOtop (2007) stated that for non-impulsive conditions (h*>0.3)

$$\frac{q}{\sqrt{gH_{m0}{}^{3}}} = 0.04exp\left(-2.6\frac{R_c}{H_{m0}}\right) \; valid \; for \; 0.1 < \frac{R_c}{H_{m0}} < 3.5 \tag{2.24}$$

For impulsive condition (h* < 0.2)

$$\frac{q}{{h_*}^2\sqrt{gh^3}} = 1.5\times10^{-4} exp\left(h_*\frac{R_c}{H_{m0}}\right)^{-3.1}$$
$$valid\ for \quad 0.03 < h_*\frac{R_c}{H_{m0}} < 1 \tag{2.25}$$

More comprehensive research on vertical seawall wave overtopping was conducted considering CLASH data and experimental set-ups were studied. As a result, the equations on vertical seawall wave overtopping in EurOtop (2016) and EurOtop (2018) were reworked and updated. For example, Goda (2000) stated that foreshore local water depth is important.

The current formulas mentioned in EurOtop (2018) are as follows.

For no influence of foreshore,

$$\frac{q}{\sqrt{g{H_{m0}}^3}} = 0.047\times\exp\left(-(2.35\frac{R_c}{H_{m0}})^{1.3}\right) \tag{2.26}$$

EurOtop (2018), recommends for a design approach, increase the average discharge by about one standard deviation, so the new recommended formula is below,

$$\frac{q}{\sqrt{g{H_{m0}}^3}} = 0.054\times\exp\left(-(2.35\frac{R_c}{H_{m0}})^{1.3}\right) \tag{2.27}$$

If there is influence of foreshore impulsive or non-impulsive conditions are checked. Meer et al. (2014) stated that $\frac{h^2}{H_{m0}L_{m-1,0}} = 0.23$ was used to determine impulsive or non-impulsive conditions. This is roughly equal to h*=0.3, because of the different wave period measure used. Where $L_{m-1,0}$ is deep water wavelength based on $T_{m-1,0}$. ($L_{m-1,0} = gT^2_{m-1,0}/2\pi$)

$$\frac{h^2}{H_{m0}L_{m-1,0}} > 0.23\ (treat\ as\ non-impulsive\ conditions)$$

$$\frac{h^2}{H_{m0}L_{m-1,0}} \le 0.23\ (treat\ as\ impulsive\ conditions)$$

For non-impulsive condition,

$$\frac{q}{\sqrt{gH_{m0}{}^{3}}} = 0.05exp\left(-2.78\frac{R_c}{H_{m0}}\right) \tag{2.28}$$

One standard deviation (σ) increased,

$$\frac{q}{\sqrt{gH_{m0}{}^{3}}} = 0.062exp\left(-2.78\frac{R_c}{H_{m0}}\right) \tag{2.29}$$

For impulsive condition,

$$\frac{q}{\sqrt{g*H_{m0}{}^{3}}} = 0.011*\left(\frac{H_{m0}}{h*s_{m-1,0}}\right)^{0.5} exp\left(-2.2\frac{R_c}{H_{m0}}\right)$$

$$\left(valid\ for\ 0 < \frac{R_c}{H_{m0}} < 1.35\right) \tag{2.30}$$

$$\frac{q}{\sqrt{g*H_{m0}{}^{3}}} = 0.0014*\left(\frac{H_{m0}}{h*s_{m-1,0}}\right)^{0.5} \left(\frac{R_c}{H_{m0}}\right)^{-3}$$

$$\left(valid\ for\ \frac{R_c}{H_{m0}} > 1.35\right) \tag{2.31}$$

One standard deviation (σ) increased,

$$\frac{q}{\sqrt{g*H_{m0}{}^{3}}} = 0.0155*\left(\frac{H_{m0}}{h*s_{m-1,0}}\right)^{0.5} exp\left(-2.2\frac{R_c}{H_{m0}}\right)$$

$$\left(valid\ for\ 0 < \frac{R_c}{H_{m0}} < 1.35\right) \tag{2.32}$$

$$\frac{q}{\sqrt{g*H_{m0}{}^{3}}} = 0.0020*\left(\frac{H_{m0}}{h*s_{m-1,0}}\right)^{0.5} \left(\frac{R_c}{H_{m0}}\right)^{-3}$$

$$\left(valid\ for\ \frac{R_c}{H_{m0}} > 1.35\right) \tag{2.33}$$

where $S_{m-1,0}\ is\ the\ wave\ steepness,\ \ 2\pi H_{m0}/gT_{m-1,0}^{2}$

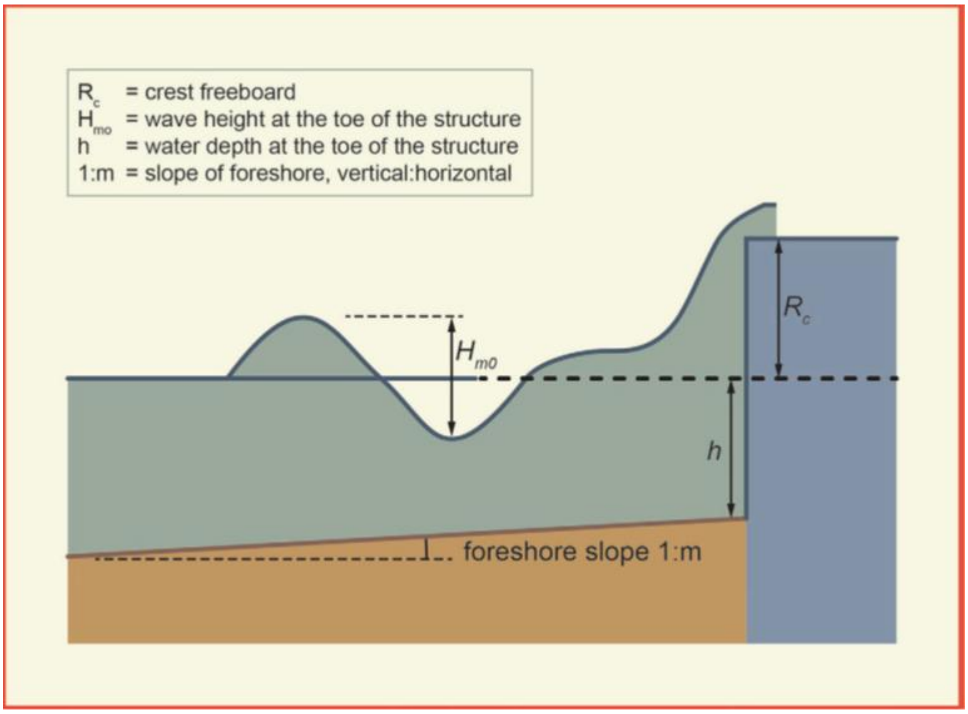


Figure 2.4. Overtopping at vertical seawall
(Source: EurOtop, 2018)

The literature on wave transmission and wave overtopping discharge on vertical sea walls individually, currently contains a large number of research. However, in most of these studies, there is no coastal structure behind the low-crested structure or submerged structure.

Van Gent, (2024) investigates the impact of submerged and emerged coastal structures on the structure-induced wave setup, particularly focusing on the magnitude of mean water level setup between these structures. Also, how factors such as structural permeability and the distance between the submerged low-crested structures (LCS) and the coastal structure influence the mean water level setup.

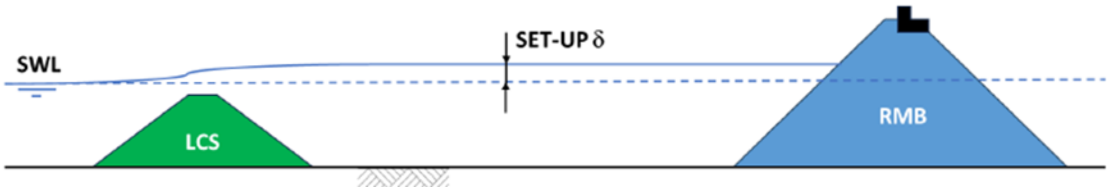


Figure 2.5. Experimental set-up of rubble mound breakwater behind the submerged breakwater (Source: Van Gent, 2024)

Another research by Rambabu and Srineash (2024) conducted a numerical study primarily focused on evaluating surface elevation near the seawall, examining wave reflection characteristics, and analyzing hydrodynamic pressures exerted on the seawall when it is protected by a submerged breakwater. Although the two studies mentioned above were conducted with a coastal structure behind a low-crested structure, the wave overtopping reduction on vertical seawall by a submerged or low-crested structure is a subject that has not yet been studied in literature. Therefore, this subject was studied with the experimental setup prepared in this study and the gaps in the literature were tried to be eliminated.

# CHAPTER 3

# METHODOLOGY

## 3.1. The Experimental Setup

Small-scale 2D laboratory experiments were conducted to investigate and quantify the effectiveness of submerged breakwaters in reducing wave overtopping at vertical seawalls under impulsive wave conditions. A total of 128 experiments were carried out in the wave flume, with systematic variations in wave and structural parameters to ensure comprehensive data collection across different hydrodynamic conditions.

All physical model tests are conducted in the wave flume at the Hydraulics Laboratory of the İzmir Institute of Technology (IZTECH, Turkey) (Figure 3.1). The wave flume is made of steel and glass with dimensions of 40 m in length, (8-meter section of the 40 m long wave channel was made of thick glass to facilitate observation during the experiments), 1.4 m in height, and 1 m in width.

A piston type wavemaker in flume has the capacity to produce regular and irregular waves with a power of 5kW (Aktaş, 2020). At the end of the flume, a 1/5 sloped passive absorption system made up of rocks was constructed to minimize the reflections occurring in the wave flume (Figure 3.2). The HR Wallingford Wave Measurement System™, consisting of 60 cm twin-wire analog wave probes and a wave gauge monitoring device with a built-in 16-bit A/D converter, is used to convert voltage differences into water surface profiles (Aktaş, 2020). The calibration of these wave gauge systems was performed daily before the experiments started.

Figure 3.1. Wave Flume at IZTECH Hydraulics Laboratory

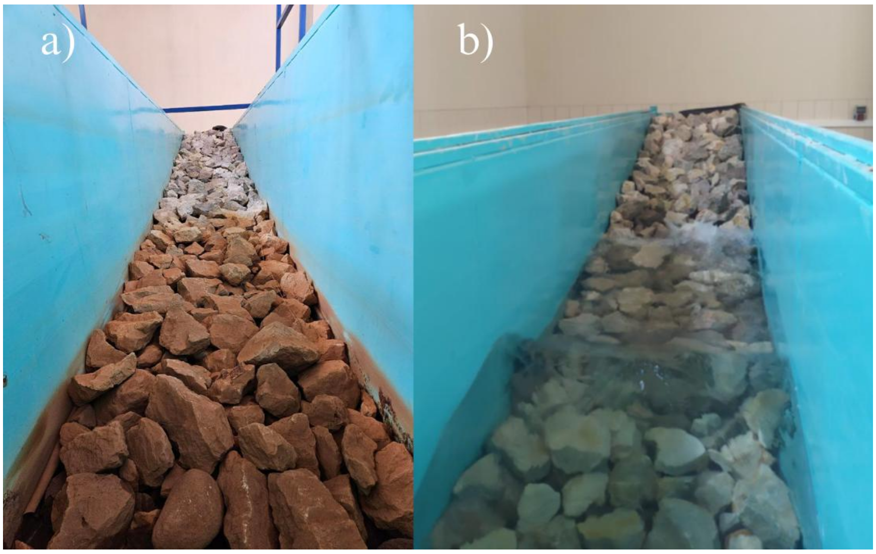


Figure 3.2. a) Passive absorption system without water in flume b) Passive absorption system with water in flume

In the experiments conducted by Romano et al. (2015), it was suggested to work with minimum of 500 waves in the experiments for wave overtopping calculation. On the other hand, the convergence tests conducted on the confidence intervals in their experiments show that the difference in the confidence interval between a 500-wave time series and a 1000-wave time series is less than 20%. Also, EurOtop (2018) stated that physical model tests suggest that between 500 and 1000 random waves are required to avoid significant variations in extreme statistics. Considering all this information and studies, 1000 irregular waves with JONSWAP spectrum was selected as a statistical representation of a real sea state that guarantees consistent results.

To achieve accurate reproduction of all hydrodynamic conditions, the largest Froude model scale was set to 1:16 after considering the flume's water depth and wavemaker capacity. The experimental model is located on a horizontal platform approximately 20.9 m away from the wave generator, 0.18 m above the bottom of the wave flume. The horizontal platform starts with a 1/30 transition slope approximately 10.5 m in front of the wave generator, and 1.5 m is left between the submerged breakwater and the vertical sea wall. (Figure 3.3). According to the Dokuz Eylül University scientific research project (BAP) numbered BAP-2016.KB.FEN.014 by Kisacik et al. (2017), and the İzmir Sponge City Report (2022) the critical $R_c$ value for vertical walls is determined as 1.2 m under the still water level condition. Also, still water level is determined as 2.8 m in the prototype conditions by Kisacik et al. (2017), and the İzmir Sponge City Report (2022). Accordingly, the scaled model height of the vertical wall was determined as 0.25 m. In the following chapters, the models in the experimental setup will be explained in more detail.

Behind the vertical seawall model there is an overtopping tank to measure the amount of overtopping discharge in each experiment. A 0.1-meter-wide chute integrated into the vertical seawall model directs the overtopped water into this tank. At the end of each test, the accumulated water in the tank was measured, and this is used to calculate the mean wave overtopping discharge $q$ (expressed in $m^3/s$ per meter of vertical seawall crest width). Figure 3.3 shows the characteristics of the model and its placement within the wave flume. Additionally, the figure illustrates the dimensions of the setup, with the top part representing the side view of the wave flume and the bottom part representing the top view of the wave flume.

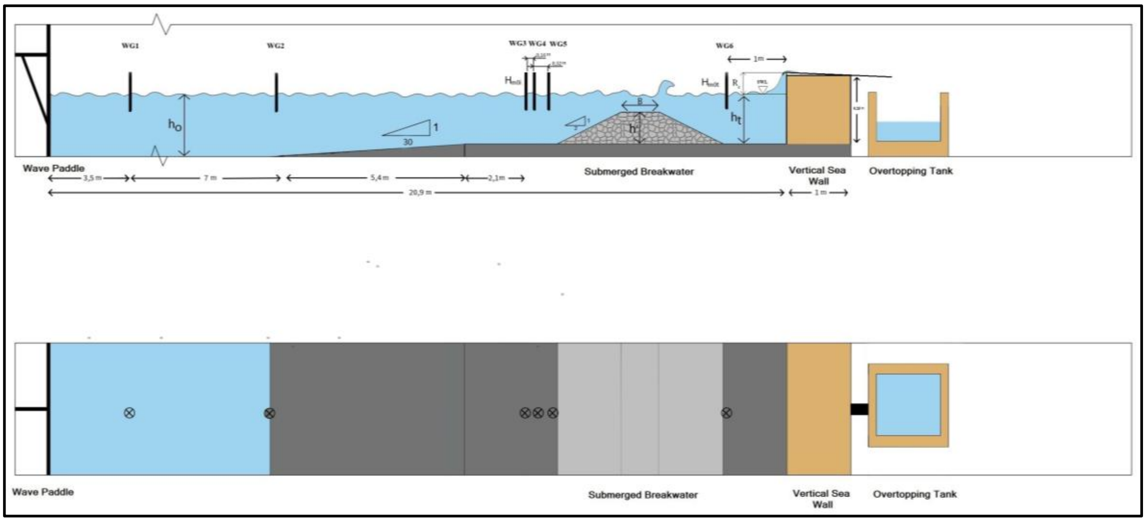


Figure 3.3. Experimental Set-up (upper panel side view; lower panel top view)

The model was instrumented with 6 wave gauges to measure incident, transmitted and reflected waves. Gauge 1 is in front of the wave paddle, gauge 2 is located at the toe of foreshore slope and used to take measurements before the wave transformation along the foreshore slope. Gauge 3,4,5 are positioned in front of the submerged breakwater to measure incident and reflected spectral wave heights ($H_{m0,i}$, $H_{m0,r}$), and wave periods ($T_{m-1,0}$) by using (Mansard et al., 1980) 3-gauge-procedure reflection analysis method. The 6$^{th}$ wave gauge is behind the submerged breakwater, i.e. in front of the vertical sea wall to measure the transmitted spectral wave heights ($H_{m0, t}$). The positions of all wave gauges within the wave flume are also represented in Figure 3.3 .

The experimental set-up consists of,

- The case with no structure to measure undisturbed wave conditions.
- Only submerged breakwater case to measure transmitted wave height (Model X),
- Submerged breakwater with vertical seawall case to measure overtopping discharge (Model Y),
- The simple vertical wall case to measure reference overtopping discharges. (Reference Case)

### 3.1.1. No Structure Condition

The Figure 3.4 below shows the experimental setup used in the wave flume, where no structure is present, to determine the incident wave height ($H_{m0,\ i}$) and wave period ($T_{m-1,0}$) for calculating wave overtopping under conditions with minimal reflection. In the no-structure case, although there is no physical structure in the flume, a passive absorption system is present (see Figure 3.2), introducing some level of wave reflection. To address this the reflected waves were separated using the 3-gauge procedure method, which was developed by (Mansard et al., 1980). The values of $H_{m0}$ and $T_{m-1,0}$, used in the overtopping calculations, were measured at the 3$^{rd}$, 4$^{th}$, and 5$^{th}$ wave gauges and processed with the 3-gauge procedure method. This method is effectively isolating the incident wave height from the reflections caused by the passive absorption system.

Later sections will provide a more detailed examination of reflection analysis, which will elucidate the significance of minimizing wave reflection and its impact on experimental accuracy. (See Chapter 3.4.2)

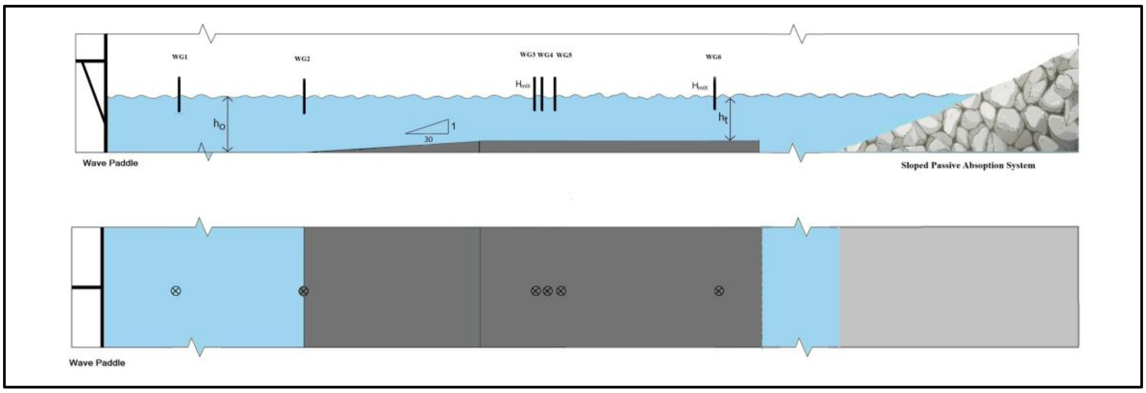


Figure 3.4. No structure condition experimental setup (upper panel side view; lower panel top view)

### 3.1.2. Submerged Breakwater (Model X)

Figure 3.5 and Figure 3.6 show the details of the Model X which includes submerged breakwater, B is the breakwater's crest width and h' is the breakwaters height. The submerged breakwater is built from stones with a nominal diameter between $0.027\ m \leq Dn_{50} \leq 0.035\ m$, with the weight of the stones calculated using zero damage condition as stated by the Hudson formula below Eq. 3. 1.

$$W = \frac{\gamma_s \times H_{m0,i}^3}{K_D \times cot\theta \times (\frac{\gamma_s}{\gamma_w} - 1)^3} \quad (3.1)$$

where $\gamma_s$ and $\gamma_w$ are the specific weight of stone and water, respectively, $H_{m0}$ is the design wave height, $K_D$ is the stability coefficient, and $\theta$ is the angle of the sloping face of the breakwater.

In order to ensure zero damage, each breakwater geometry was fixed to the shape of the breakwater using metal wire mesh. It was particularly preferred that the openings of the metal wire mesh were wider than the gaps between the breakwater stones. This choice was made in order not to affect the permeability of the breakwater and to preserve the natural flow characteristics between the stones. In this way, the experimental conditions were arranged to reflect the realistic behavior of the breakwater structure.

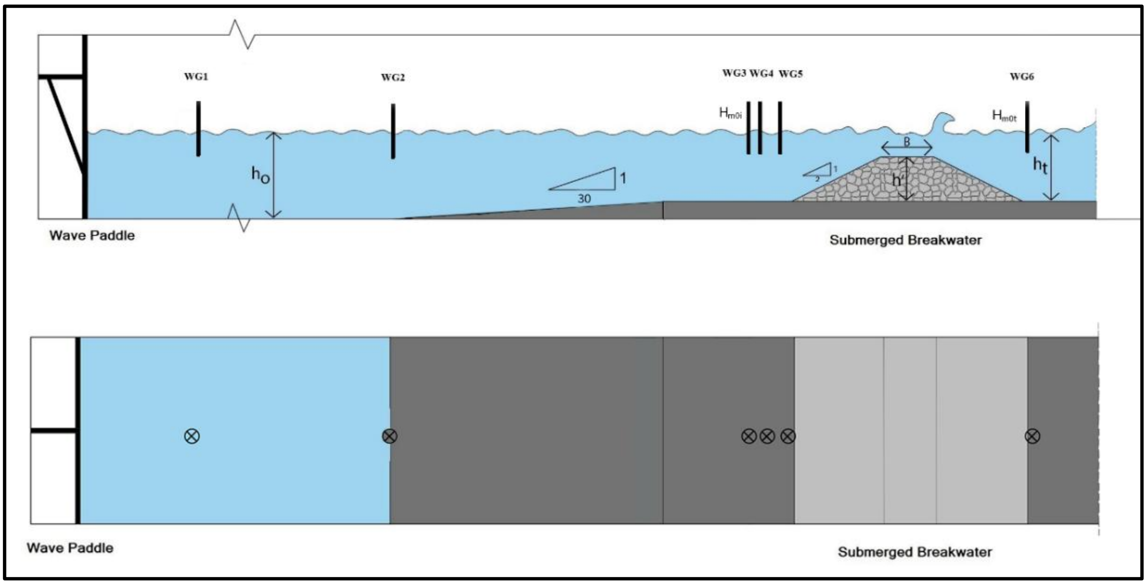


Figure 3.5. Model X experimental setup (upper panel side view; lower panel top view)

The height of the submerged breakwater (h') is between 0.09 m and 0.21 m with a slope of 1:2. The crest width (B) is determined between $3D_{n50} \leq B \leq 8D_{n50}$, considering the suggestion of Rock Manual (2007) $3D_{n50}$ for the minimum crest width. The values of submerged breakwater heights and crest widths are summarized in Table 3.1.

Table 3.1. Submerged breakwater parameters

| Height (h') (m) | | Crest Width (B) (m) | | |
|---|---|---|---|---|
| $h'_1$ | = 0.09 | $B_1$ | = $3D_{n50}$ | = 0.09 |
| $h'_2$ | = 0.12 | $B_2$ | = $4D_{n50}$ | = 0.12 |
| $h'_3$ | = 0.15 | $B_3$ | = $6D_{n50}$ | = 0.18 |
| $h'_4$ | = 0.18 | $B_4$ | = $8D_{n50}$ | = 0.24 |
| $h'_5$ | = 0.21 | | | |

In the experimental process, five different submerged breakwater heights (h') and four different submerged breakwater crest widths (B) were tested. However, a total of 15 distinct geometric configurations were employed (see Table 3.2). Experimental designs were carefully designed to replicate feasible and possible breakwater configurations. On purpose, combinations that were inconsistent with the functional requirements of breakwaters, such as an excessively wide crest width and a very small breakwater height, were excluded. Thus, a balanced range of configurations was chosen to guarantee that the results of the investigation could be used to inform engineering applications that are both realistic and effective. This approach aimed to generate experimental results that are in close alignment with practical design constraints, thereby increasing the feasibility in the development of submerged breakwater solutions. The studied geometric configurations are shown in the Table 3.2 below.

Table 3.2. Submerged breakwater geometric configurations

| | | | |
|---|---|---|---|
| $h'_1$<br>$h'_2$ | B1 | B2 | B3 |
| $h'_3$<br>$h'_4$<br>$h'_5$ | B2 | B3 | B4 |

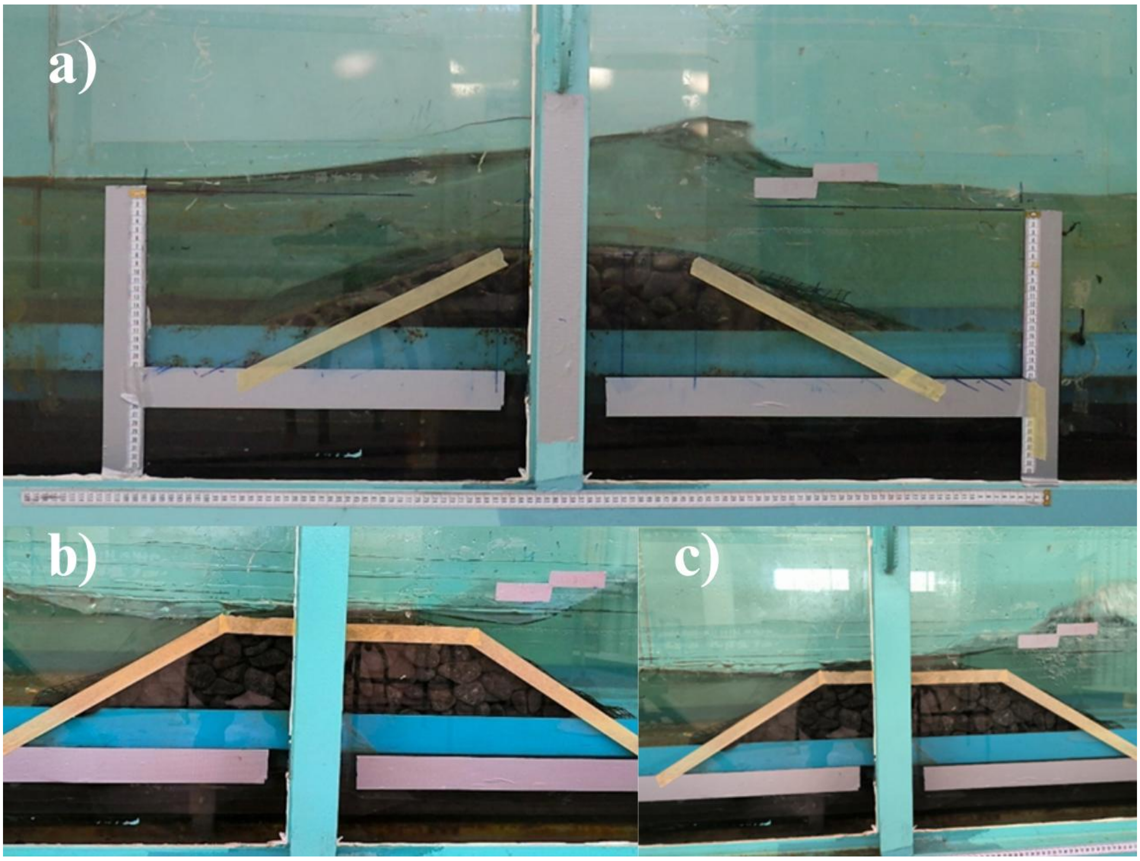


Figure 3.6. a) Visualization of wave breaking in Model X. b&c) Visualization of Model X under wave conditions.

### 3.1.3. Submerged Breakwater with Vertical Seawall (Model Y)

Model Y includes both submerged breakwater and vertical seawall. $h_t$ is water depth at the toe of the submerged breakwater and vertical seawall, $R_c$ is the total crest freeboard. This part aims to evaluate the reduction effect of submerged breakwater on overtopping discharge. In this part of the experiments the submerged breakwater, the vertical seawall and an overtopping tank are located in the wave flume to simulate real-world conditions more effectively (Figure 3.7, Figure 3.8 and Figure 3.10). The geometric parameters of the submerged breakwater from Model X were systematically applied in Model Y, and the effect of the geometric parameters of the submerged breakwater on the wave overtopping amount is examined by measuring the wave overtopping in each test.

The vertical seawall model is made of wooden material. Its heigh is 0.25 m and the width and the length of the vertical seawall model is about 1 m. The overtopping tank is also made of wooden material. The inner length and width of the overtopping tank is 0.77m x 0.77m and the height of nearly 0.46m. However, to position the 0.1 m wide chute see Figure 3.10, that directs overtopped water into the tank, the surface behind the vertical seawall model was cut to allow the chute to fit properly. This setup also enabled a very mild slope to be provided, facilitating the smooth transfer of overtopped water from the vertical seawall model to the tank.

The distance between the submerged breakwater and the vertical seawall was determined based on the midpoint of the crest width of each submerged breakwater model. For this study, this distance was kept fixed at 1.8 m.

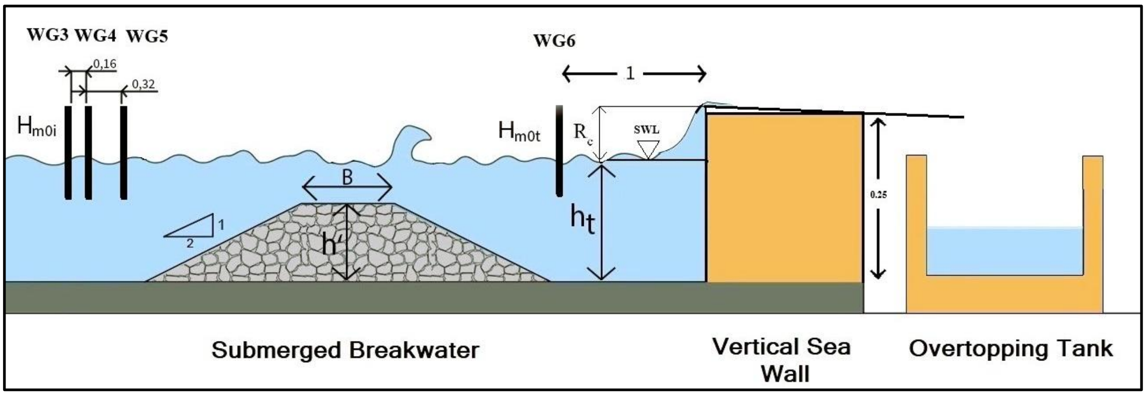


Figure 3.7. Submerged breakwater with vertical seawall (Model Y)

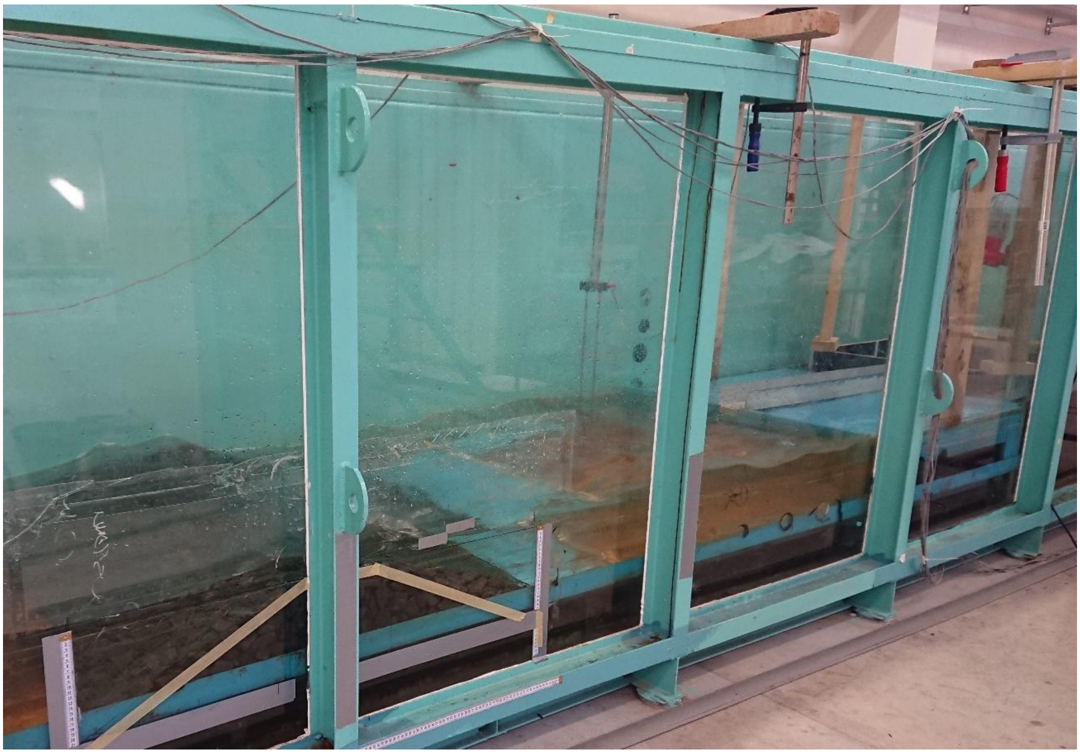

Figure 3.8. Visualization of submerged breakwater and vertical seawall

### 3.1.4. The Simple Vertical Seawall (Reference Case)

These experiments are conducted to measure the reference overtopping discharge for each hydrodynamic condition. In this case, only the vertical seawall model and overtopping tank are included. Reference overtopping discharges were measured without the submerged breakwater under the specified hydrodynamic conditions to provide reference values for Model Y. This allows the effect of the submerged breakwater on wave overtopping to be defined as a reduction factor ($\gamma_{sub}$) based on the wave overtopping discharges measured in this set-up. Figure 3.9 illustrates the model characteristics.

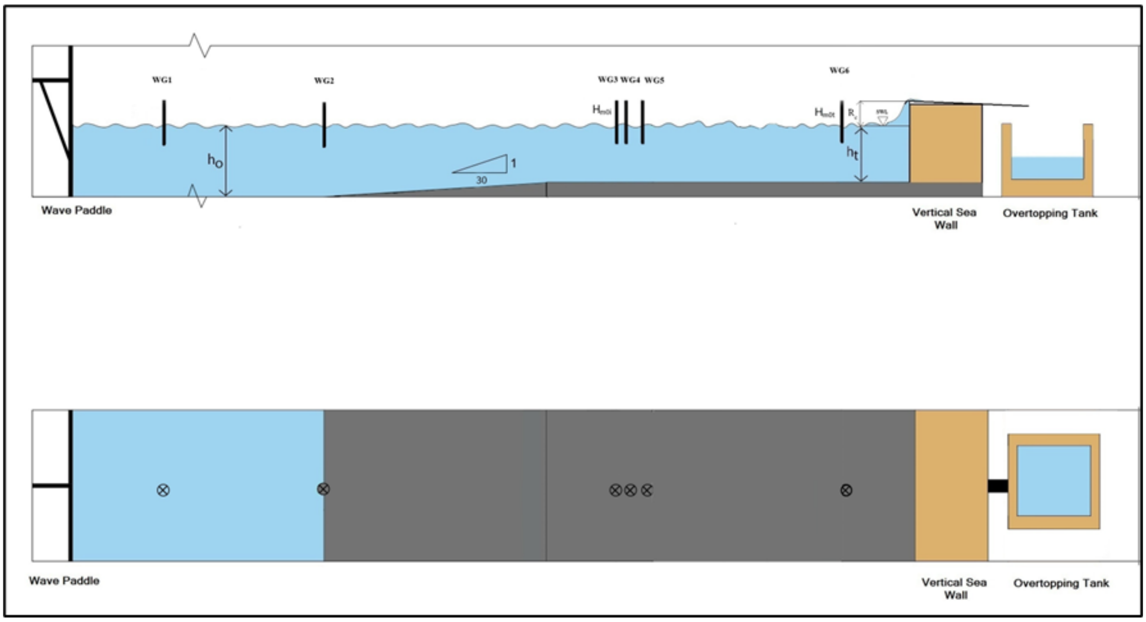


Figure 3.9. The reference case model (upper panel side view; lower panel top view)

The reference discharge values obtained in this setup serve as a critical baseline for evaluating comparisons and analyses of the submerged breakwater's effectiveness across varying experimental scenarios. These values not only help in quantifying the reduction in wave overtopping but also provide a foundation for comparing the experimental results, with datasets used in the EurOtop guidelines, allowing the consistency and reliability of the measured data to be quantified against values derived from the formula in EurOtop (2018).

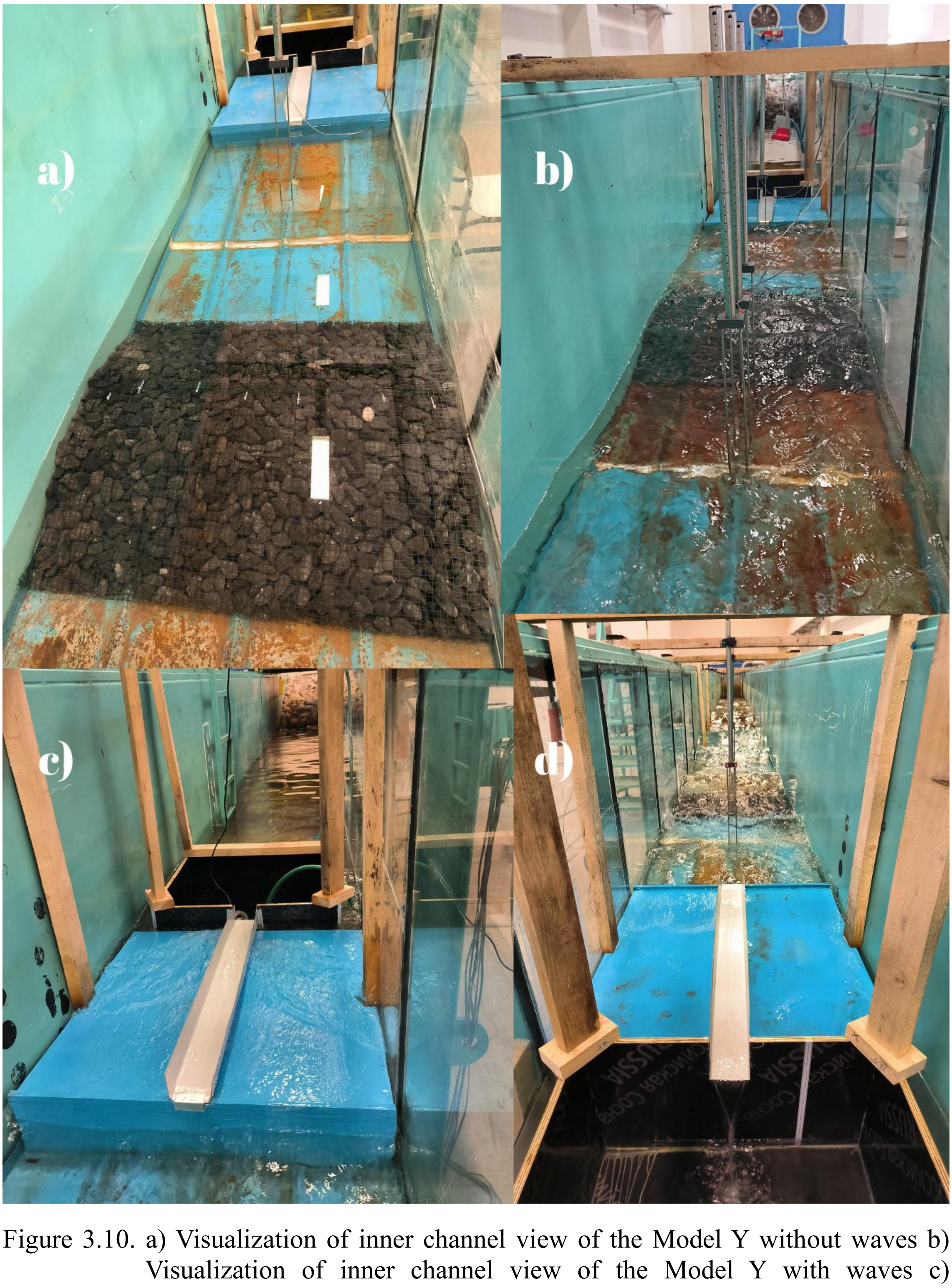


Figure 3.10. a) Visualization of inner channel view of the Model Y without waves b) Visualization of inner channel view of the Model Y with waves c) Visualization of inner channel view vertical seawall model and overtopping tank. d) Visualization of wave overtopping collection with 0.1m wide chute.

## 3.2. Hydrodynamic Conditions

The studied range of hydrodynamic conditions were determined by Kisacik et al. (2017) for BAP project with consideration of the Izmir Bay prototype conditions with 1:16 Froude scale. Two different water depths were used in front of the structure and two different wave heights and periods were tested for each water depth. Additionally, in experiments, the steepness of 0.04 is considered to reflect Mediterranean conditions. (See Table 3.3)

Table 3.3. Target hydrodynamic conditions

| | $h_0$ (m) | $h_t$ (m) | $H_{m0}$ (m) | $T_{m-1,0}$ (s) | $L_0$(m) | $S_0$ |
|---|---|---|---|---|---|---|
| H1 | 0.4 | 0.22 | 0.075 | 1.15 | 2.065 | 0.036 |
| H2 | 0.4 | 0.22 | 0.091 | 1.26 | 2.479 | 0.037 |
| H3 | 0.4175 | 0.2375 | 0.075 | 1.15 | 2.065 | 0.036 |
| H4 | 0.4175 | 0.2375 | 0.091 | 1.26 | 2.479 | 0.037 |

where;

$$s_0 = wave\ steepness$$

$$s_0 = \frac{H_{m0}}{L_0} \tag{3. 2}$$

$$L_0 = Deep\ water\ wave\ length\ = \frac{g.{T_{m-1,0}}^2}{2\pi}$$

When determining the hydrodynamic conditions, water level is determined first. As a result of the field measurements made by Kisacik et al. (2017) within the scope of the BAP Project for the Gulf of Izmir, the still water level (+0.00) (SWL) was determined as 2.8m. However, climate change, global warming, storm conditions and water level increases due to these should also be considered. Kisacik et al. (2017), stated in their study that the extreme water level change for Izmir Bay could be 1 m. As a result, the high-water level (+1.00) (HWL) for Izmir Bay was determined as 3.8 m.

The wave model of İzmir Bay was simulated using the third-generation nearshore wave model SWAN (Simulating Waves Nearshore) studies conducted within the scope of

BAP project studied by Kisacik et al. (2017), Ak (2021) and Sponge City Report (2022). SWAN was developed at Delft University of Technology, that computes random, short-crested wind-generated waves in coastal regions and inland waters. (SWAN Manual, 2017). The waves simulated in this study are compelled by the most recent reanalysis of offshore wind data from the European Centre for Medium-Range Weather Forecasts (ECMWF), ERA5 (Sponge City Report, 2022). According to model results, the wave climate in some important regions of Izmir Bay is shown in Table 3.4.

Table 3.4. Wave climate of İzmir Bay

| Locations | $H_{m0}$ (m) | $T_p$ (s) |
|---|---|---|
| Bostanlı | 1.13 | 3.87 |
| Poligon | 1.46 | 4.16 |
| Karşıyaka | 1.17 | 4.62 |
| Mavişehir | 0.74 | 3.74 |
| Konak | 1.43 | 4.85 |
| Bayraklı | 1.20 | 4.77 |

As seen in Table 3.4, the highest significant wave height was determined as 1.46 m, and the average of all wave heights was determined as 1.2 m by eliminating the lowest wave heights.

## 3.3. Test Program

The performance of submerged breakwater on both dissipating the energy of incident waves and reducing the overtopping discharge should be analyzed separately. Therefore, Model X and Model Y experiments were carried out under the same hydrodynamic conditions and geometric design conditions. The first part (Model-X) is related to the effect of submerged breakwater geometry on the transmitted wave condition, so it includes only submerged breakwater without the vertical seawall behind it. The wave conditions measured behind the submerged breakwater are compared with those obtained from tests conducted at the exact location but without a submerged breakwater. This procedure is repeated for fifteen different geometric configurations of submerged breakwater performed under four different hydrodynamic conditions (see Table 3.3).

The second part (Model-Y) is to evaluate the reduction effect of submerged breakwater on overtopping discharge. In this concept, the submerged breakwater, the vertical seawall, and an overtopping tank are located in the wave flume. The fifteen different geometric configurations of submerged breakwater are tested under four different hydrodynamic conditions. After each test, the amount of water overtopping from the crest of the vertical wall is measured and recorded as mean overtopping discharge (referred to as q). For more accurate quantification of the reduction in overtopping discharge, reference tests are performed including only the vertical seawall without the submerged breakwater in front of it. Both Model-Y and reference tests are performed with the same relative freeboard ($R_c/H_{m0}$) under the same hydrodynamic conditions.

Based on this information, four experiments are required for the case with no structure to test four different hydrodynamic conditions. Additionally, four experiments will be conducted in the scenario with only the vertical seawall model, serving as a reference for wave overtopping. Each model (Model X and Model Y) will be tested with 15 different geometric configurations under the four hydrodynamic conditions, resulting in a total of 60 experiments. In total, the experimental program consists of 128 separate experiments. Also, several experiments with the same target spectrum were conducted to ensure the repeatability of both wave properties and overtopping discharges.

Table 3.5. Test matrix for empty and reference case.

| | **Test Number** | **Wall Existence** | **h'** | **B** | **Hydrodynamic Condition** |
|---|---|---|---|---|---|
| **Empty Case** | T000_1 | - | - | - | H1 |
| | T000_2 | - | - | - | H2 |
| | T000_3 | - | - | - | H3 |
| | T000_4 | - | - | - | H4 |
| **Reference Case** | T000_5 | W | - | - | H1 |
| | T000_6 | W | - | - | H2 |
| | T000_7 | W | - | - | H3 |
| | T000_8 | W | - | - | H4 |

Table 3.6. The test parameter matrix for Model X

| Model X | | | | |
|---|---|---|---|---|
| **Geometric Configuration** | **Wall Existence** | **h'** | **B** | **Hydrodynamic Condition** |
| G01 | - | h1' | B1 | H1&H2&H3&H4 |
| G02 | - | h1' | B2 | H1&H2&H3&H4 |
| G03 | - | h1' | B3 | H1&H2&H3&H4 |
| G04 | - | h2' | B1 | H1&H2&H3&H4 |
| G05 | - | h2' | B2 | H1&H2&H3&H4 |
| G06 | - | h2' | B3 | H1&H2&H3&H4 |
| G07 | - | h3' | B2 | H1&H2&H3&H4 |
| G08 | - | h3' | B3 | H1&H2&H3&H4 |
| G09 | - | h3' | B4 | H1&H2&H3&H4 |
| G10 | - | h4' | B2 | H1&H2&H3&H4 |
| G11 | - | h4' | B3 | H1&H2&H3&H4 |
| G12 | - | h4' | B4 | H1&H2&H3&H4 |
| G13 | - | h5' | B2 | H1&H2&H3&H4 |
| G14 | - | h5' | B3 | H1&H2&H3&H4 |
| G15 | - | h5' | B4 | H1&H2&H3&H4 |

Table 3.7. The test parameter matrix for Model Y

| Model Y | | | | |
|---|---|---|---|---|
| **Geometric Configuration** | **Wall Existence** | **h'** | **B** | **Hydrodynamic Condition** |
| G01 | W | h1' | B1 | H1&H2&H3&H4 |
| G02 | W | h1' | B2 | H1&H2&H3&H4 |
| G03 | W | h1' | B3 | H1&H2&H3&H4 |
| G04 | W | h2' | B1 | H1&H2&H3&H4 |
| G05 | W | h2' | B2 | H1&H2&H3&H4 |
| G06 | W | h2' | B3 | H1&H2&H3&H4 |
| G07 | W | h3' | B2 | H1&H2&H3&H4 |
| G08 | W | h3' | B3 | H1&H2&H3&H4 |
| G09 | W | h3' | B4 | H1&H2&H3&H4 |
| G10 | W | h4' | B2 | H1&H2&H3&H4 |
| G11 | W | h4' | B3 | H1&H2&H3&H4 |
| G12 | W | h4' | B4 | H1&H2&H3&H4 |
| G13 | W | h5' | B2 | H1&H2&H3&H4 |
| G14 | W | h5' | B3 | H1&H2&H3&H4 |
| G15 | W | h5' | B4 | H1&H2&H3&H4 |

## 3.4. Data Analysis

All wave measurements were analyzed using the "WaveLab" software developed by Aalborg University. (See Figure 3.11)

Each test and its repeat trials were conducted over a duration of 1220 seconds. To avoid the initiation phase at the beginning of each test and the damping phase at the end, a specific time window was selected for analysis. For all tests, this time window begins at t = 50 s and ends at t = tend - 50 s. The first 50 seconds were excluded to eliminate the effects of the zero-wave duration and the initiation phase, during which wave generation had just started, and synchronization across wave probes was still stabilizing. Similarly, the final 50 seconds were excluded to avoid the damping effects caused by the paddle stopping, which could artificially reduce wave heights. This approach ensured that the analyses were based on stable and reliable data, eliminating transient effects during both the initiation and damping phases.

Both time domain and frequency domain analyses were conducted separately for each wave gauge, and the results ($H_{m0}$, $T_{m-1,0}$, $T_p$, $H_s$) were recorded.

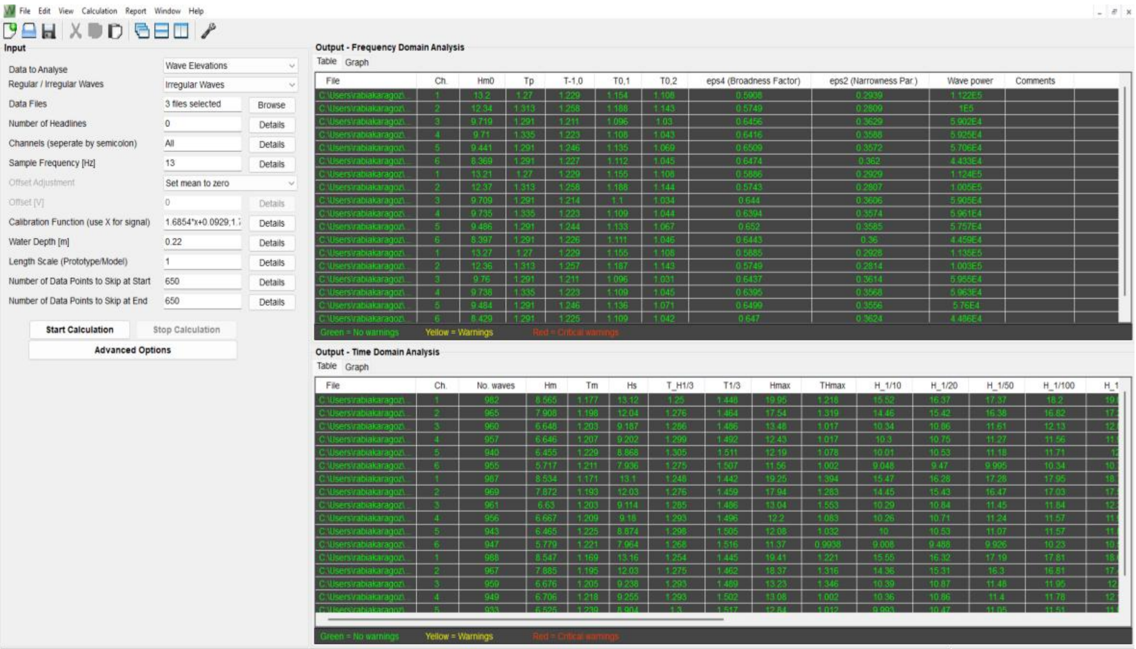


Figure 3.11. "WaveLab" Software data analysis

### 3.4.1. Dimensional Analysis

The aim of the dimensional analysis study is to produce dimensionless parameters and examine the physical meanings of these parameters while examining the effect of the submerged breakwater on the wave overtopping process.

Parameters which affect the wave transmission on submerged breakwater are related to the geometry of submerged breakwater, fluid and flow parameters.

Table 3.8. Wave Transmission Parameters for Submerged Breakwaters

| | Parameters | Definitions | Units | Dimensions |
|---|---|---|---|---|
| Geometric | B | crest width of breakwater | m | $L^1M^0T^0$ |
| | $F(h_t\text{-}h')$ | freeboard | m | $L^1M^0T^0$ |
| | h' | height of structure (at its axis) | m | $L^1M^0T^0$ |
| | $D_{n50}$ | nominal rock diameter of armour layer ($=(M_{n50}/\rho\alpha)^{1/3}$) | m | $L^1M^0T^0$ |
| | m | front slope of the breakwater face (=tanθ) | - | - |
| | $h_t$ | water depth | m | $L^1M^0T^0$ |
| Flow | g | Gravitational acceleration | $m/s^2$ | $L^1M^0T^{-2}$ |
| | $H_i$ | incident wave height ($H_{moi}$) at the toe of the structure | m | $L^1M^0T^0$ |
| | $H_t$ | transmitted wave height | m | $L^1M^0T^0$ |
| | L | wavelength at spectral peak | m | $L^1M^0T^0$ |
| | T | period at spectral peak | s | $L^0M^0T^1$ |
| Fluid | ρ | Water density | $kg/m^3$ | $L^{-3}M^1T^0$ |
| | μ | Water dynamic viscosity | kg/m*s | $L^{-1}M^1T^{-1}$ |

The parameters for dimensional analysis:

$F (A_1, A_2, A_3, A_4, A_5, A_6, A_7, A_8, A_9, A_{10}) = F (B, h_t, h', H_i, H_t, L, g, \rho, \mu, m)$

As shown in the Table 3.9 the parameters classified as geometric, kinematic, dynamic and non-dimensional and according to Buckingham π-theorem there are 12 possible scenarios with 7 non-dimensional parameters. It should be noted that $K_t$ is the ratio of $H_t$ to $H_i$. Therefore, it was not considered as a repeating parameter in the dimensional analysis process.

Table 3.9. Classification of parameters

| Geometric | Kinematic | Dynamic | Non-Dimensional |
|---|---|---|---|
| B | g | ρ | m |
| $h_t$ | | μ | $K_t$ |
| h' | | | |
| $H_i$ | | | |
| $H_t$ | | | |
| L | | | |

Dimensional Analysis Calculation for Scenario 1

$$repeating\ parameters(r) = (\ B, g, \rho)$$

$$\pi_1 = B^a g^b \rho^c h'$$

$$L^0 M^0 T^0 = (L^1 M^0 T^0)^a (L^1 M^0 T^{-2})^b (L^{-3} M^1 T^0)^c (L^1 M^0 T^0)$$

$$a = -1\ ; b = 0\ ; c = 0$$

$$\pi_1 = B^{-1} g^0 \rho^0 h_t$$

$$\pi_1 = \frac{h'}{B}$$

$$\pi_2 = \frac{h_t}{B} \quad ; \quad \pi_3 = \frac{H_t}{B} \quad ; \quad \pi_4 = \frac{H_i}{B} \quad ; \quad \pi_5 = \frac{L}{B}\ ; \ \pi_6 = \frac{\mu}{\rho \times \sqrt{B^3 \times g}} \quad ; \quad \pi_7 = m$$

The repeating parameters for other scenarios are listed in Table 3.10 but their calculations are not detailed.

Table 3.10. Non-dimensional π variables for all scenarios

| | Scenario 1 | Scenario 2 | Scenario 3 | Scenario 4 | Scenario 5 | Scenario 6 | Scenario 7 | Scenario 8 | Scenario 9 | Scenario 10 | Scenario 11 | Scenario 12 |
|---|---|---|---|---|---|---|---|---|---|---|---|---|
| Repeating Parameters | B,g,ρ | ht,g,ρ | h',g,ρ | Ht,g,ρ | Hi,g,ρ | L,g,ρ | B,g,μ | ht,g,μ | h',g,μ | Ht,g,μ | Hi,g,μ | L,g,μ |
| $\pi_1$ | h'/B | B/ht | B/h' | B/Ht | B/Hi | B/L | h'/B | B/ht | B/h' | B/Ht | B/Hi | B/L |
| $\pi_2$ | ht/B | h'/ht | ht/h' | ht/Ht | ht/Hi | ht/L | ht/B | h'/ht | ht/h' | ht/Ht | ht/Hi | ht/L |
| $\pi_3$ | Ht/B | Ht/ht | Ht/h' | h'/Ht | h'/Hi | h'/L | Ht/B | Ht/ht | Ht/h' | h'/Ht | h'/Hi | h'/L |
| $\pi_4$ | Hi/B | Hi/ht | Hi/h' | Hi/Ht | Ht/Hi = Kt | Ht/L | Hi/B | Hi/ht | Hi/h' | Hi/Ht | Ht/Hi = Kt | Ht/L |
| $\pi_5$ | L/B | L/ht | L/h' | L/Ht | L/Hi | Hi/L | L/B | L/ht | L/h' | L/Ht | L/Hi | Hi/L |
| $\pi_6$ | $\frac{\mu}{\rho \times \sqrt{B^3 \times g}}$ | $\frac{\mu}{\rho \times \sqrt{F^3 \times g}}$ | $\frac{\mu}{\rho \times \sqrt{F^3 \times g}}$ | $\frac{\mu}{\rho \times \sqrt{F^3 \times g}}$ | $\frac{\mu}{\rho \times \sqrt{F^3 \times g}}$ | $\frac{\mu}{\rho \times \sqrt{F^3 \times g}}$ | $\frac{\mu}{\rho \times \sqrt{F^3 \times g}}$ | $\frac{\mu}{\rho \times \sqrt{F^3 \times g}}$ | $\frac{\mu}{\rho \times \sqrt{F^3 \times g}}$ | $\frac{\mu}{\rho \times \sqrt{F^3 \times g}}$ | $\frac{\mu}{\rho \times \sqrt{F^3 \times g}}$ | $\frac{\mu}{\rho \times \sqrt{F^3 \times g}}$ |
| $\pi_7$ | m | m | m | m | m | m | m | m | m | m | m | m |

### 3.4.2. Reflection Analysis

In experimental processes, wave reflection generally occurs from any obstacle. Reflections are particularly significant levels when a vertical structure is present making it impossible to directly measure the incident wave height $H_{moi}$ in such a system. If the reflected waves are not separated from the incident waves, the superposition of incident and reflected wave measurements may lead to unrealistic results. Therefore, minimizing wave reflections in the wave flume is crucial for obtaining more realistic results. Different methods have been proposed to separate the reflected and incident waves.

The initial technique was suggested by Goda et al. (1976). In this approach, wave data was simultaneously collected from two adjacent locations by two wave gauges. Utilizing Fourier components, wave height of the reflected and incident waves characteristics are determined.

In this study, the 3-gauge wave reflection analysis method developed by Mansard et al. (1980) was used to separate the incident waves from the reflected waves and the method needs three wave gauges positioned at specific intervals from one another, based on the wavelength at the average depth where the gauges are located.

$$x_{3,4} = \frac{L}{10}, \qquad \frac{L}{6} < x_{3,5} < \frac{L}{3}, \qquad x_{3,5} \neq \frac{L}{5} \ and \ x_{3,5} \neq \frac{3L}{10} \tag{3. 3}$$

Table 3.11. Distance between wave gauges according to wavelengths.

| Water Depth $h_t$ (m) | Period T (s) | Wave Gauge Numbers | Wavelength L (m) | Distance between gauge 3-4 (m) | Distance between gauge 3-5 (m) |
|---|---|---|---|---|---|
| 0.22 | 1.15 | 3-4-5 | 1.5002 | 0.16 | 0.48 |
| 0.22 | 1.26 | | 1.6782 | | |
| 0.2375 | 1.15 | | 1.5432 | | |
| 0.2375 | 1.26 | | 1.7295 | | |

This approach is particularly well-suited for the precise separation of incident and reflected waves through the use of multiple wave gauge measurements, thereby delivering a more precise representation of the wave field. (Mansard & Funke, 1980) achieved a wider frequency range with this method and reduced noise compared to the two-gauge method. The goal is to realize a more realistic simulation of sea state conditions through the application of this technique, which will result in more accurate experimental results.

To verify the accuracy of the obtained incident wave height, it was compared with the incident wave height measured under no-structure conditions (see Chapter 3.1.1), where all structures were removed from the wave flume and reference case incident wave height with using the technique of Mansard et al. (1980) (see Figure 3.12). While the values are similar, minor differences exist. The average difference between the incident wave heights calculated in the two models is 2% and maximum difference is 2.9%, meaning that technique works well. These differences are attributed to the uneven surface of the foreshore constructed on the flume bed and the imperfect performance of the passive absorption system.

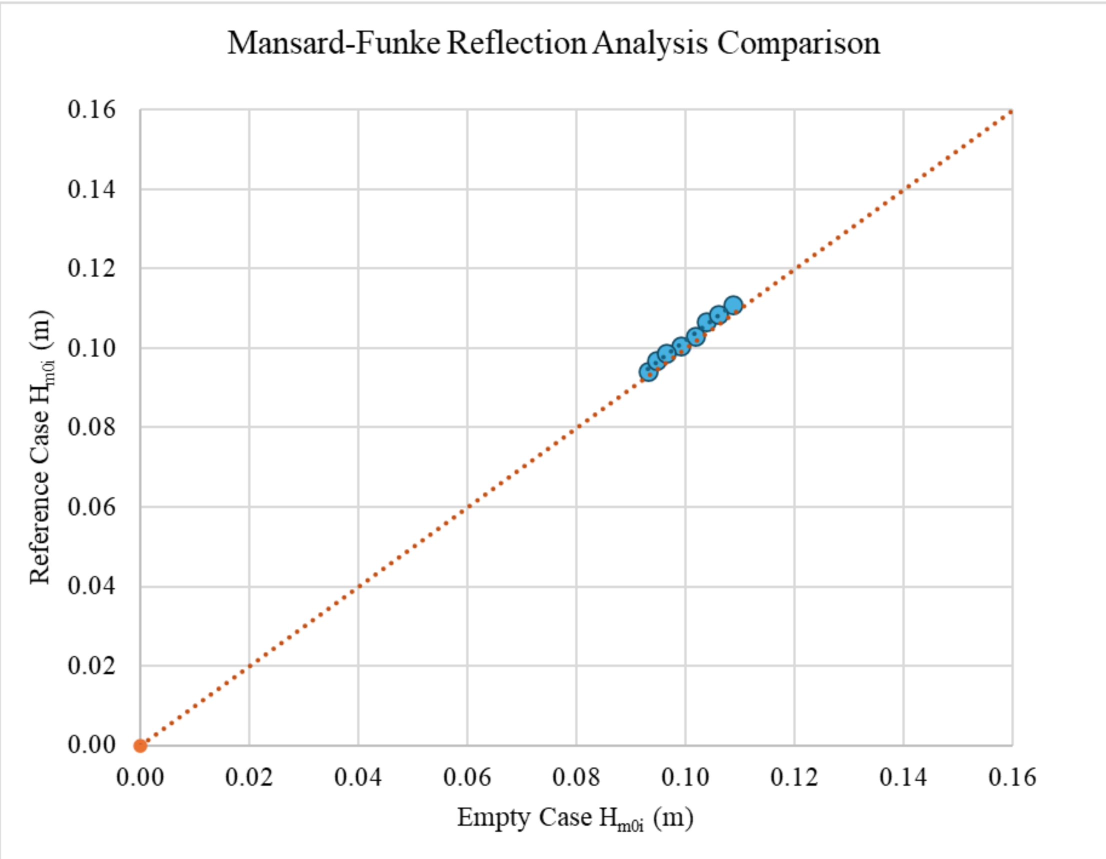


Figure 3.12. No Structure and Reference Case incident waves comparison

The Figure 3.13 below presents the average results of the reflection coefficients conducted for all hydrodynamic cases and all models. These results emphasize the influence of structural factors on wave reflection in experimental setups. As expected, the reflection is highest in the reference case, which involves only a vertical wall. Similarly, in Model Y, the presence of the vertical wall results in a relatively high reflection. Also, the reflection is lowest in the no-structure case; however, the reflection coefficient $C_r$ is approximately 0.2. This is primarily due to irregularities in the flume and the flume bed, as well as the insufficient performance of the passive absorption system at these depths, as previously discussed.

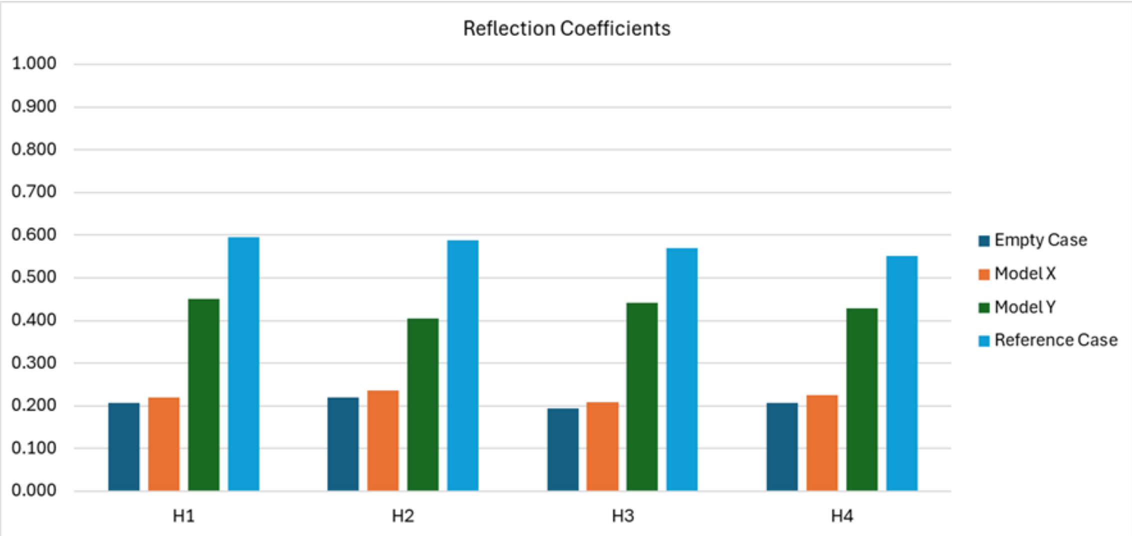


Figure 3.13. Reflection coefficients for all hydrodynamic cases and all models

In addition, the analysis of wave reflection for transmitted wave height was conducted using the Eq. 3. 4 proposed by Goda et al. (1976).

$$H_i = \frac{1}{\sqrt{1 + C_r^2}} H_s$$
$$H_r = \frac{C_r}{\sqrt{1 + C_r^2}} H_s \tag{3. 4}$$

Where, $H_s$ denotes the significant or other representative wave height of composite waves observed by the wave gauge (Goda et al., 1976).

Measurements of the transmitted wave height were obtained from the 6$^{th}$ wave gauge result, which was positioned behind the breakwater. (See Figure 3.3) However, because only a single wave gauge was placed behind the breakwater, it was not possible to conduct a direct reflection analysis in this region by the help of Mansard et al. (1980)'s 3-gauge wave reflection analysis method. Yet, the sixth wave gauge, where transmitted wave height measurements were taken, was still affected by wave reflection within the flume. To address this, the reflection coefficient was determined using empty-case experiments, where no structure was present. (See Chapter 3.1.1) These experiments provided the reflection characteristics of the flume itself, allowing for the accurate calculation of incident wave height in the absence of the structure. The same reflection coefficients obtained from these tests were then applied in the analysis of the transmitted wave height.

# CHAPTER 4

# RESULTS AND DISCUSSIONS

This research primarily aims to evaluate the performance of submerged breakwaters in reducing overtopping discharge when designed in front of vertical sea walls. Another important aspect of this study is to evaluate the effectiveness of submerged breakwaters in relation to wave transmission. The findings obtained from the conducted experiments are discussed under this topic.

Initially, overtopping discharge measurements for the reference case model without a submerged breakwater (simple vertical wall case) were compared with estimates from the EurOtop (2018) database, which is used to predict overtopping discharge for simple vertical walls. Additionally, these measurements were compared with predictions from the EurOtop (2018) formulations and with results from overtopping discharge experiments previously conducted on simple vertical walls in other laboratories. The purpose of this comparison is to assess the accuracy and consistency of the data obtained at IZTECH by benchmarking against EurOtop (2018) database measurements and those from other labs.

Secondly, the reduction effect on overtopping discharge is quantified by examining changes in the hydrodynamic conditions and submerged breakwater parameters when a submerged breakwater (Model Y) is positioned in front of the vertical seawall. In this situation, the reference case and Model Y have the same relative freeboard ($R_c/H_{m0}$), which enables a direct comparison of performance under equivalent conditions.

The primary objective of this study is to develop a reduction factor, denoted as $\gamma_{sub}$, aimed at quantifying the effectiveness of submerged breakwaters in reducing overtopping discharge for vertical seawalls. This factor is derived in reference to the EurOtop (2018) formulation for vertical steep walls (Equation 7.9), facilitating a systematic approach to evaluate the performance impact of submerged breakwaters within established overtopping prediction frameworks.

Another key research focus is the investigation of wave transmission behavior of submerged breakwaters under varying geometric parameters and hydrodynamic conditions. The concept of wave transmission has been extensively studied in literature, with numerous formulations developed. This study aims to compare the data obtained from experiments conducted in the IZTECH laboratory with existing formulations in the literature, providing a basis for evaluating the consistency and applicability of these findings.

## 4.1. Wave Transmission Analysis

As noted in the literature review in Section 2.1 and included in the formulations, the transmitted wave at a submerged breakwater is influenced by key parameters such as $D_{n50}$, the front slope of the breakwater face, and permeability. However, these parameters were held constant in this study, so variations dependent on them could not be observed. The geometric parameters influencing wave transmission over a submerged breakwater and wave overtopping reduction by a submerged breakwater are the breakwater height and crest width. Since the cross-sectional area of the breakwater can be determined using these parameters, the analyses are carried out based on variations in the breakwater's cross-sectional area.

In this experimental study, the efficiency of the wave transmission formulas proposed in the literature, as discussed in Section 2.1, was evaluated by comparison with the dataset produced in this study. In the following sections of this chapter, detailed analyses will be presented, comparing the wave transmission coefficients calculated from the formulas ($Kt$ calculated) with those obtained from the laboratory data ($Kt$ measured).

$H_{m0}$ incident values in the no structure case and the transmitted wave height, measured by the wave gauge behind the submerged breakwater (WG6), are used to calculate transmission coefficients. Also, Model X allows for a detailed assessment of how transmitted wave height is influenced by structural parameters and wave characteristics, providing insights essential for optimizing coastal defenses.

Figure 4.1 shows the measured wave transmission coefficients on vertical axis and the non-dimensional freeboard ($F/H_{m0i}$) on the horizontal axis where F is the difference between the water depth ($h_t$) and the breakwater height (h'). Also, in Figure 4.1, all measured wave transmission coefficients ($K_t$) are above 0.4, and for conditions with the lowest $F/H_{m0i}$, the wave transmission coefficients are observed to approach $Kt = 1$. In cases with a structure of very low elevation or without any structure, the wave transmission coefficient is expected to approach $Kt = 1$. The current test results show a trend that aligns with this expectation.

Similarly, as shown in Figure 4.1 and Figure 4.2 , under the same hydrodynamic conditions and breakwater height, a wider crest clearly results in a lower wave transmission coefficient. This is because a wider crest provides a larger surface area for wave energy dissipation, reducing the amount of energy transmitted past the structure. Experimental results confirm this trend across a range of crest widths, demonstrating that increasing the crest width significantly improves the breakwater's efficiency in reducing wave transmission. These findings highlight the importance of crest width as a design parameter for optimizing the performance of submerged breakwaters.

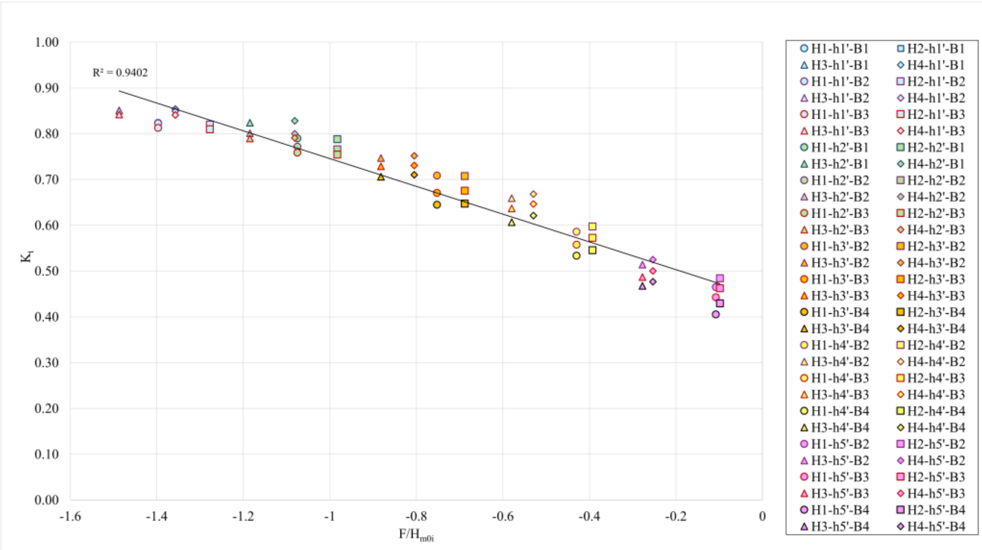


Figure 4.1. Measured wave transmission for all test vs $F/H_{m0i}$

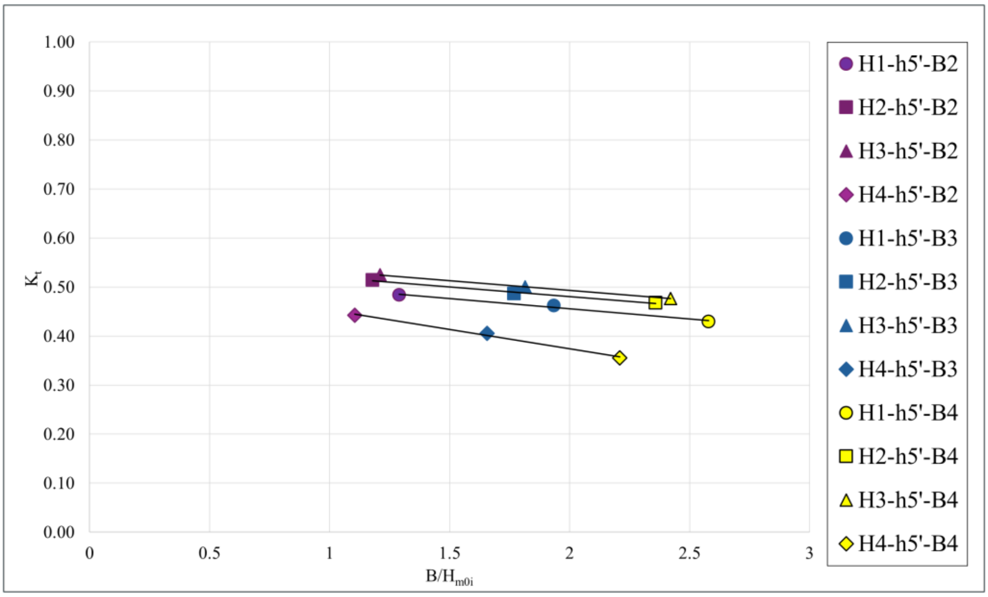


Figure 4.2. Measured wave transmission for h5’ height vs $F/H_{m0i}$

Figure 4.3 to Figure 4.10 show the changes in spectral shape for incident and transmitted waves under all hydrodynamic conditions analyzed in this experimental work. Blue area shows the incident waves, orange area shows the transmitted waves spectral shapes. The horizontal x-axis shows the frequency with unit Hz and the vertical y-axis shows the spectral density with unit ($m^2$.s). The largest breakwater geometry, G15, reduced energy more effectively than the smallest geometry, G01. This indicates that larger breakwater structures are more efficient in attenuating wave energy, resulting in more significant modifications to the spectral shape of the transmitted waves.

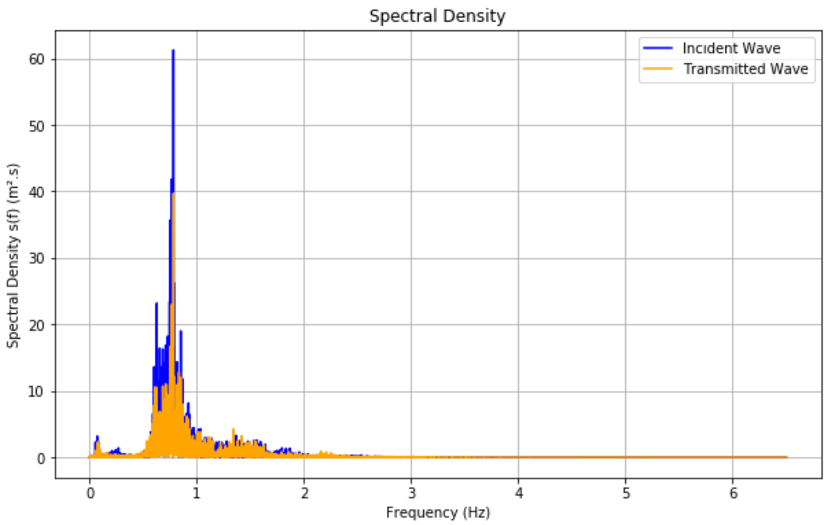


Figure 4.3. H1 Hydrodynamic Condition - G01 submerged breakwater geometric configuration variance spectrum

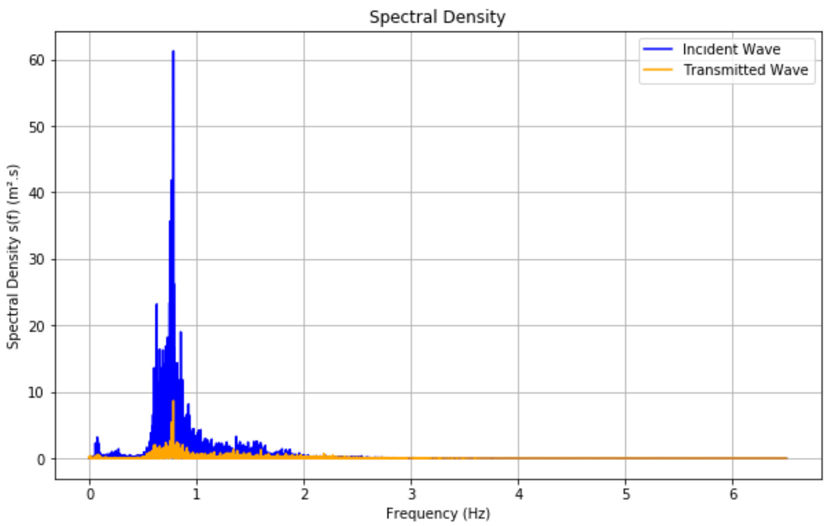


Figure 4.4. H1 Hydrodynamic Condition – G15 submerged breakwater geometric configuration variance spectrum

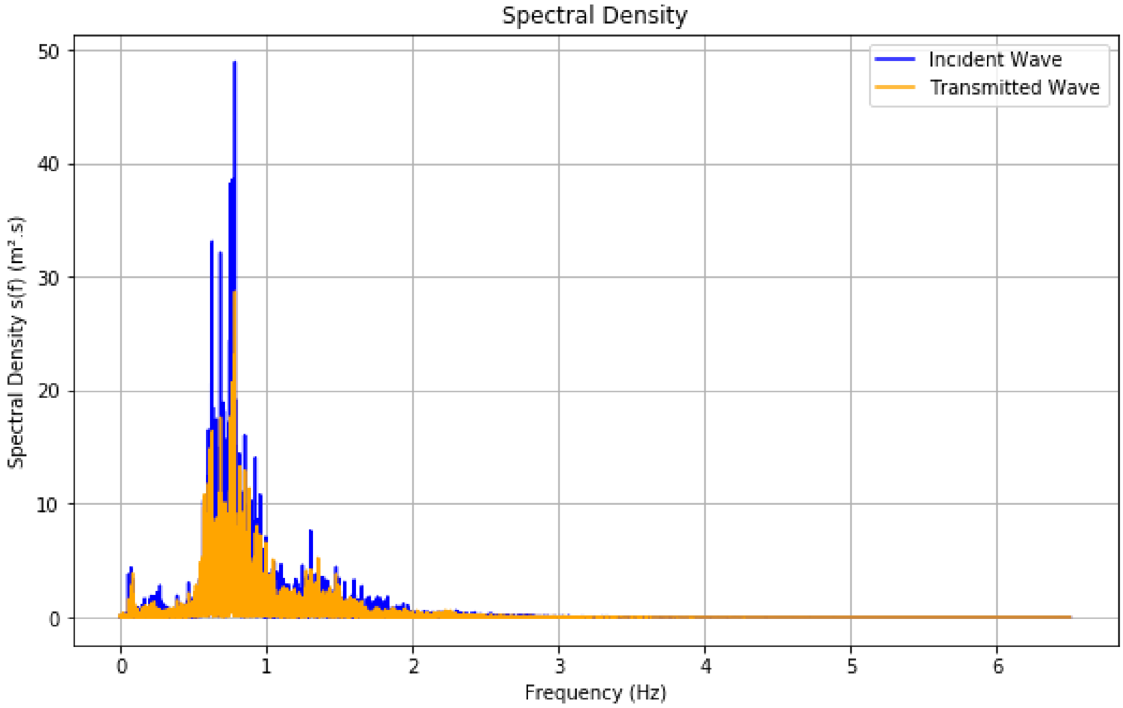


Figure 4.5. H2 Hydrodynamic Condition – G01 submerged breakwater geometric configuration variance spectrum

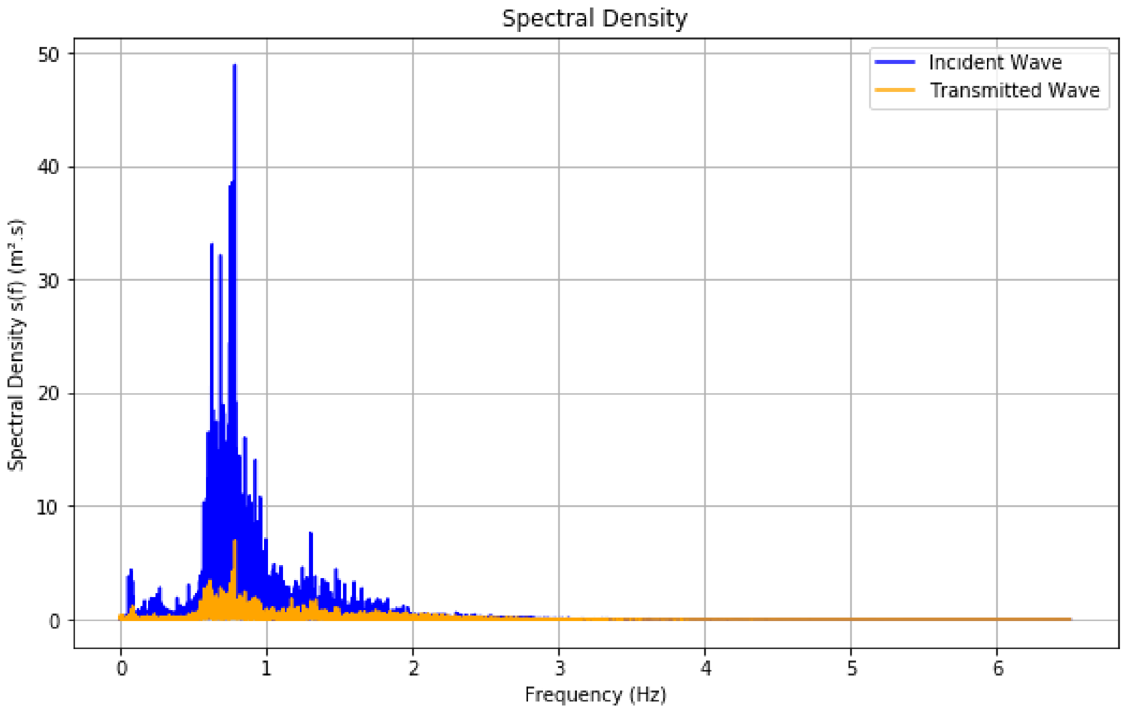


Figure 4.6. H2 Hydrodynamic Condition – G15 submerged breakwater geometric configuration variance spectrum

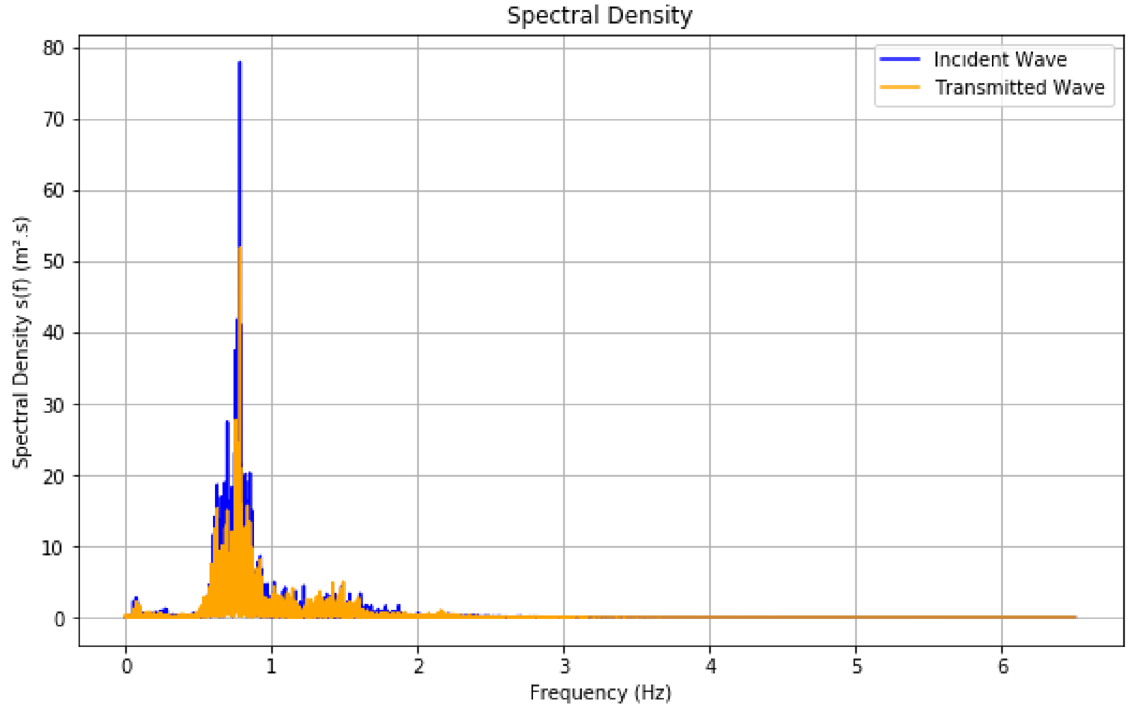


Figure 4.7. H3 Hydrodynamic Condition – G01 submerged breakwater geometric configuration variance spectrum

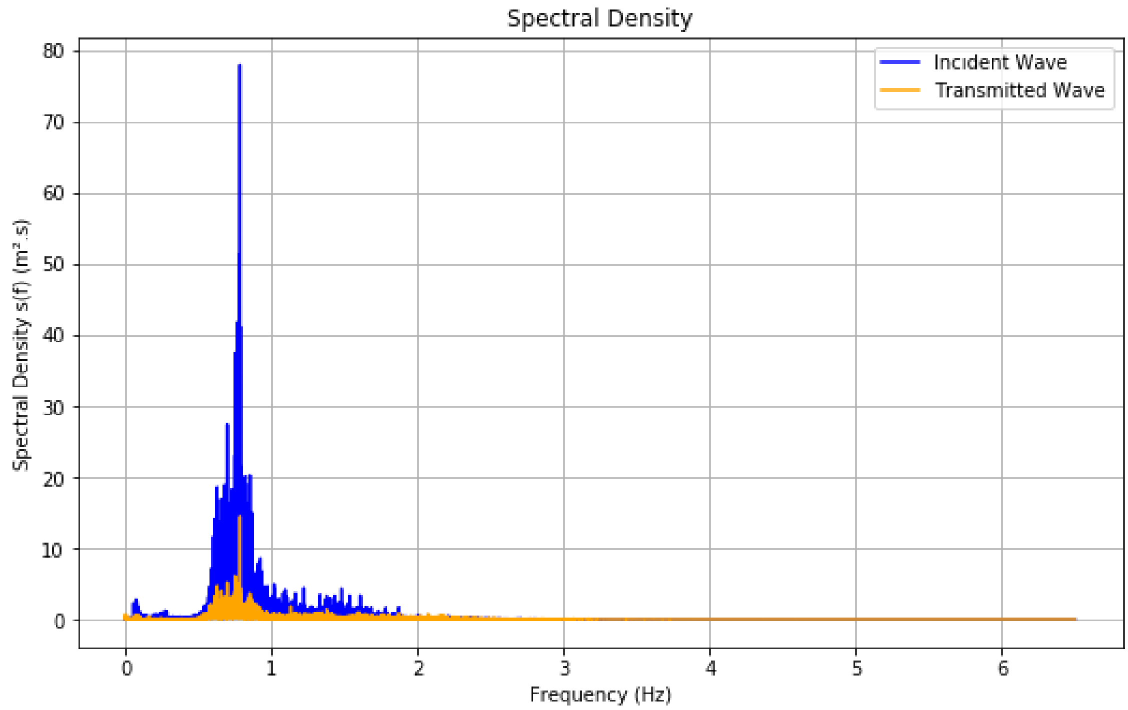


Figure 4.8. H3 Hydrodynamic Condition – G15 submerged breakwater geometric configuration variance spectrum

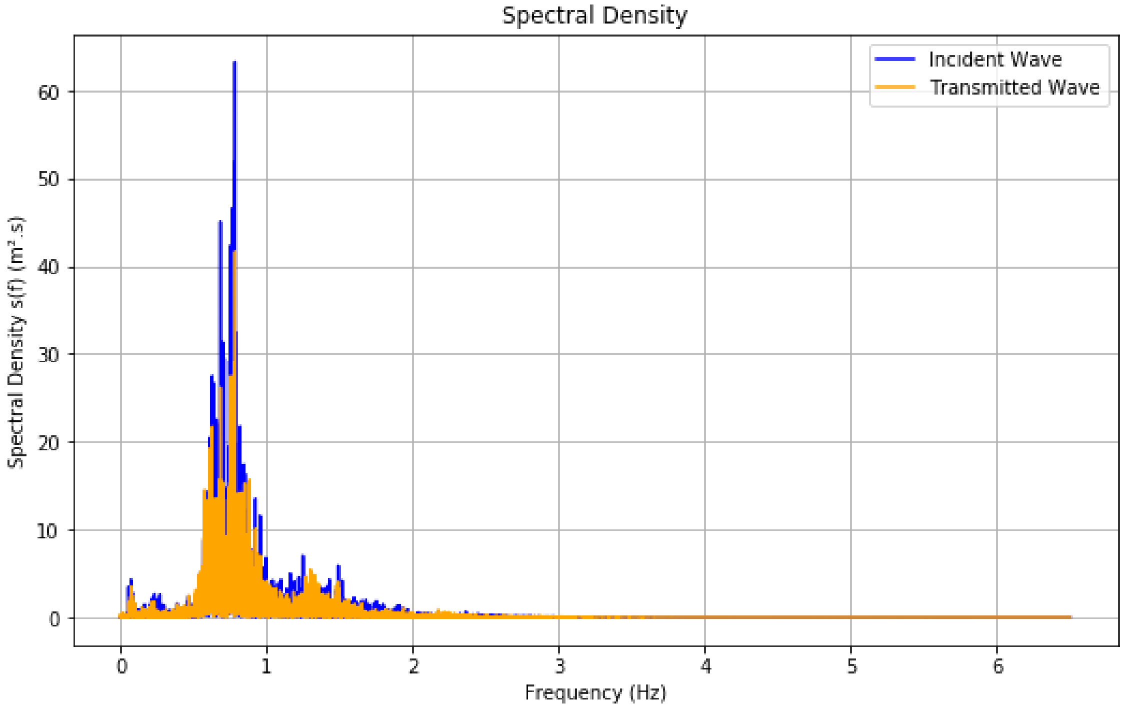


Figure 4.9. H4 Hydrodynamic Condition – G01 submerged breakwater geometric configuration variance spectrum

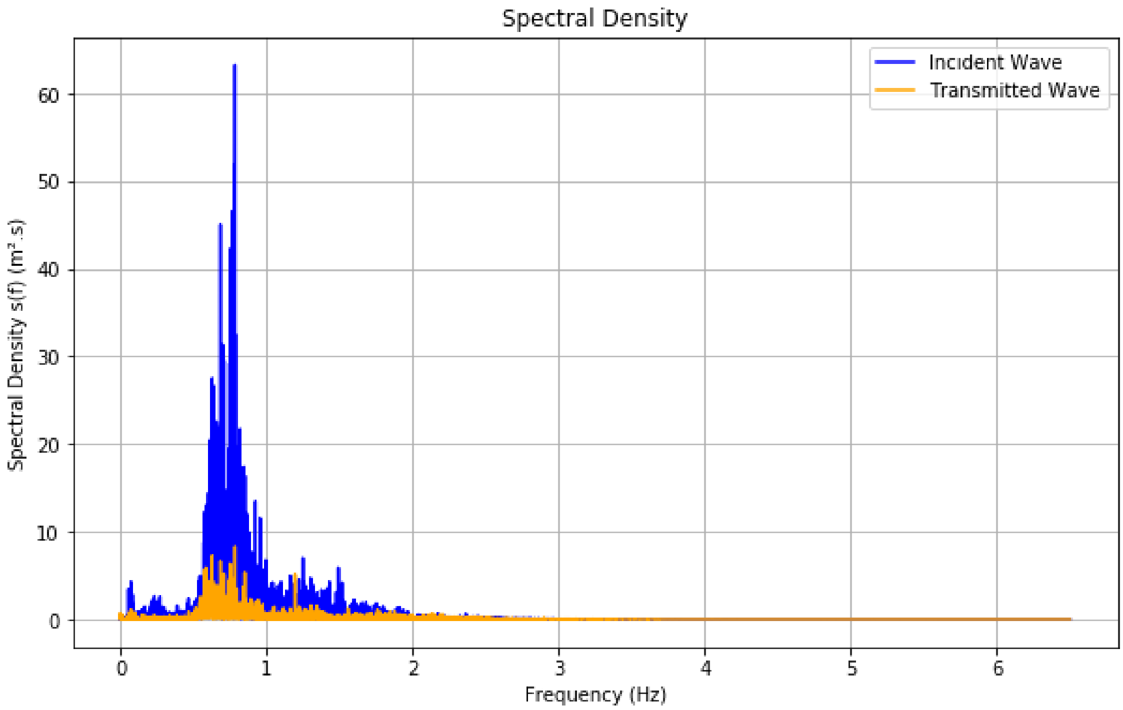


Figure 4.10. H4 Hydrodynamic Condition – G15 submerged breakwater geometric configuration variance spectrum

### 4.1.1. Existing Formula for Wave Transmission and Present Dataset

Figure 4.11 shows the calculated $K_t$ using Meer (1990a) formulation Eq. 2. 2 versus the measured $K_t$. Based on van der Meer's (1990a) approach, the $K_t$ values range from a maximum 0.8 to minimum 0.1. In this study the relative crest freeboard is within the range of $-1.5 < \frac{F}{Hm0_i} < -0.09$. As a result, some data points outside the ranges specified by Meer (1990a) and are highlighted as red dots in the Figure 4.11 and these red dots are not included in $R^2$ calculation.

In comparing the experimentally measured $K_t$ values to those calculated using the referenced formula, a strong correlation $R^2 = 0.9488$ was observed. This high $R^2$ indicates a close alignment between experimental measurements and theoretical predictions. However, the trend line deviates slightly from the $y = x$ line. This divergence suggests that values less than 0.6 the formula overestimates and values greater than 0.6 the formula underestimates, but the formula provides a generally accurate representation of $K_t$ according to $R^2$. The scatter in the graph can be attributed to the fact that the given formulation does not take into account the effect of the crest width.

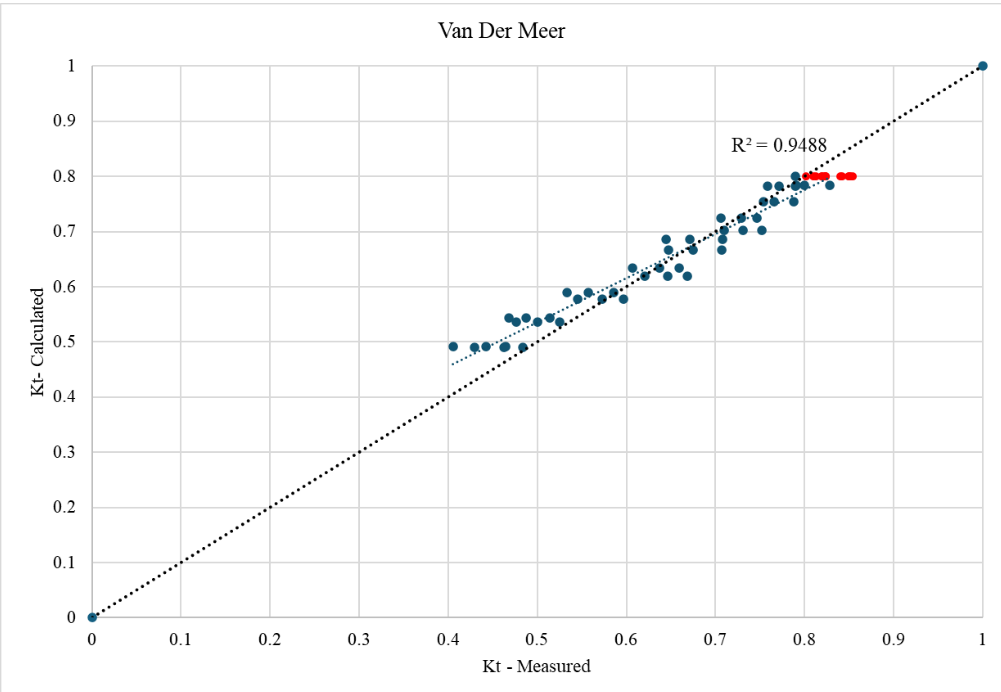


Figure 4.11. Comparison between wave transmission coefficients calculated from the Meer, (1990a) formula and measured from the produced data

Figure 4.12 presents the calculated wave transmission data, using d'Angremond et al. (1996)'s Eq. 2. 7 on the vertical axis and the measured wave transmission coefficients on the horizontal axis. d'Angremond et al. (1996) highlighted the importance of relative crest width and relative crest freeboard in their formula (see Eq. 2. 7). In this study, the range of relative crest width is $0.8 < \frac{B}{Hm0_i} < 2.6$. According to the suggested formula, the maximum $K_t$ value is 0.8 and the minimum $K_t$ value is 0.075. Therefore, these values are indicated as red dots in the figure and not included in $R^2$ calculation. d'Angremond et al. (1996) formula slightly underestimate, and trend is parallel or more or less same slope and measurements within the formula's limitations still show a strong correlation, yielding an $R^2$ value of 0.9612. his high correlation can be attributed to the d'Angremond et al. (1996) formula's consideration of both crest width and freeboard effects simultaneously, providing a more comprehensive analysis of wave transmission.

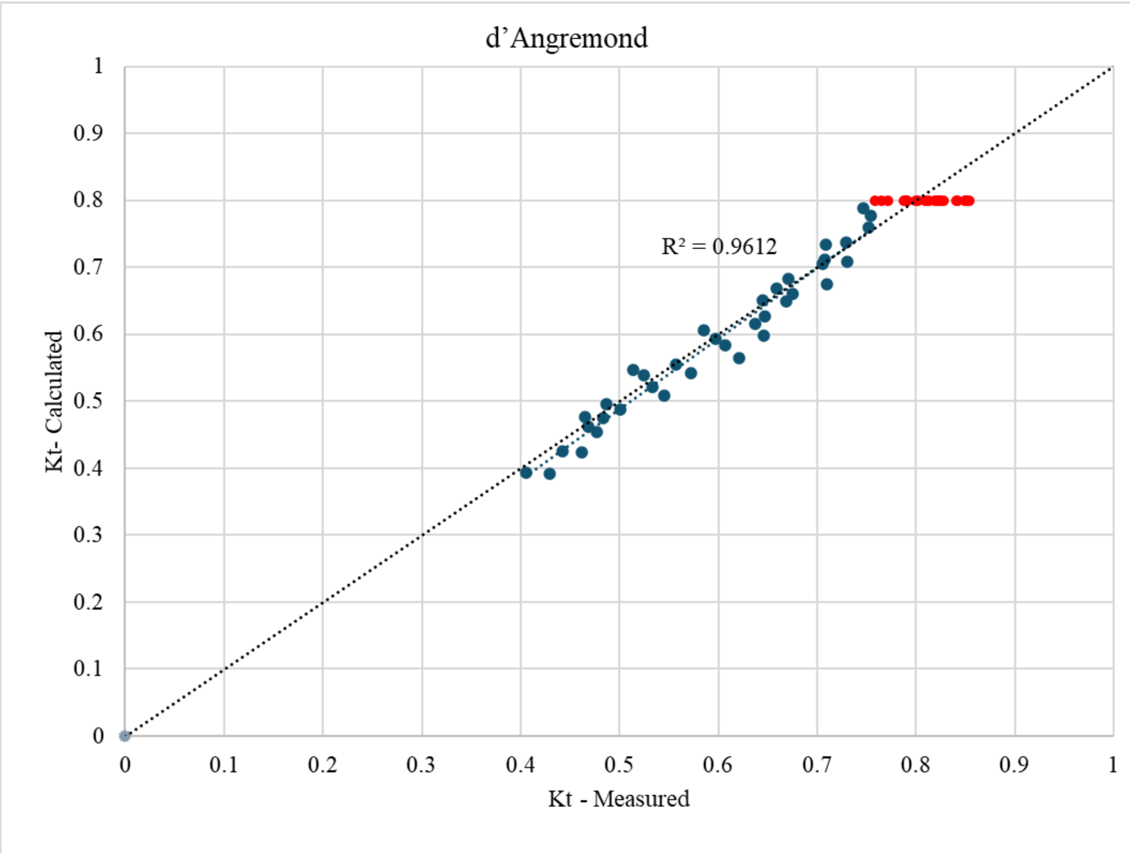


Figure 4.12. Comparison between wave transmission coefficients calculated from the d'Angremond, et al. (1996) formula and measured from the produced data

Figure 4.13 shows the calculated wave transmission data, with Equations 2.10, and 2.11 on the vertical axis and the measured wave transmission coefficients on the horizontal axis. In the formula suggested by Seabrook et al. (2000), a wider range was used for crest width (from 0.3 m to 3.5 m). When Seabrook et al. (2000) compared their data with previously proposed formulas, they found these equations unsuitable for representing breakwaters with wider crests. This observation motivated the development of Eq. 2.10, as explained. The figure below shows a greater degree of scatter, with an $R^2$ value of 0.7152, indicating a relatively low correlation. The values shown in red, fall outside the ranges recommended by Seabrook et al. (2000) in Eq. 2.11. These data points, indicated by red dots which are not included $R^2$ calculation, represent the breakwaters in the dataset with the lowest crest elevations and narrowest crests.

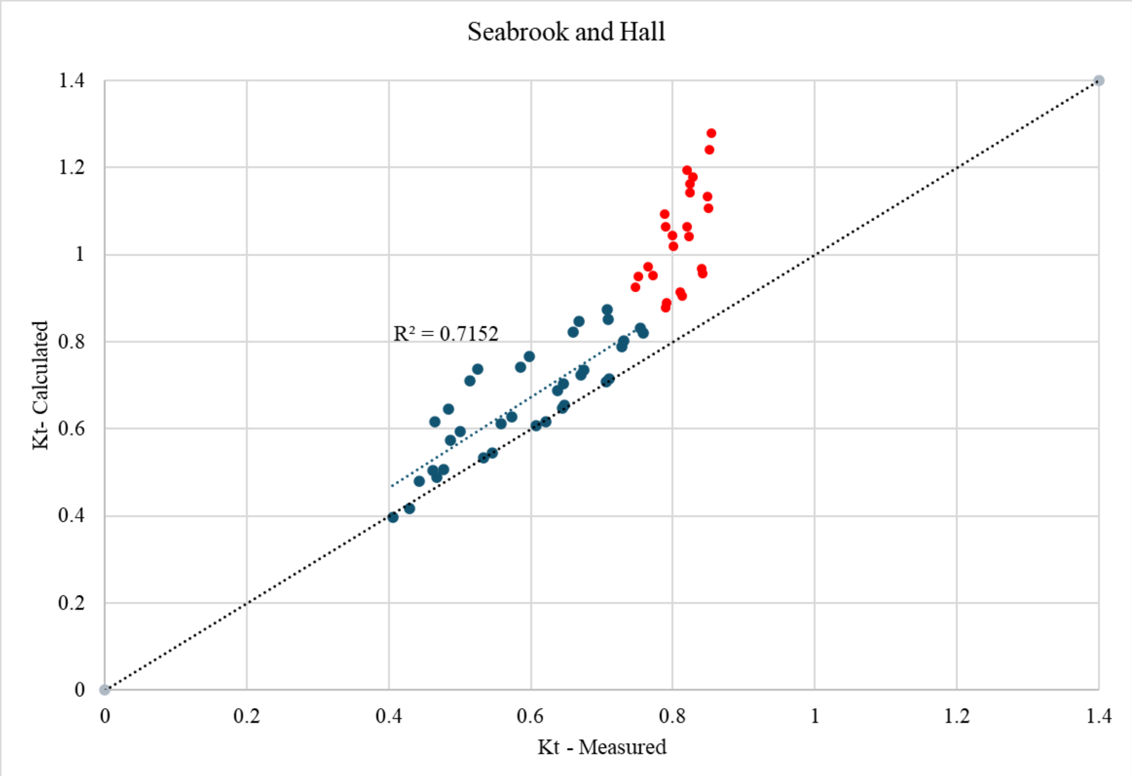


Figure 4.13. Comparison between wave transmission coefficients calculated from the Seabrook et al. (2000) formula and measured from the produced data

Figure 4.14 presents the calculated wave transmission data, using Charles Friebel et al. (2003) equations 2.18 and 2.19 on the vertical axis and the measured wave transmission coefficients on the horizontal axis. Additionally, the data points lie below the $y = x$ line, indicating that the formula underestimates the values for this dataset but still show a strong correlation, with an $R^2$ value of 0.9462. In Eq. 2.19, Charles Friebel et al. (2003) stated the ratio of structure height to water depth is between $0.44 \leq (\frac{h'}{h_t}) \leq 1.0$, however in this study this ratio is in between $0.37 \leq (\frac{h'}{h_t}) \leq 0.95$. The values, which are outside the recommended range according to the formula, are shown with red dots in the graph below and these data points are not included in calculation of $R^2$.

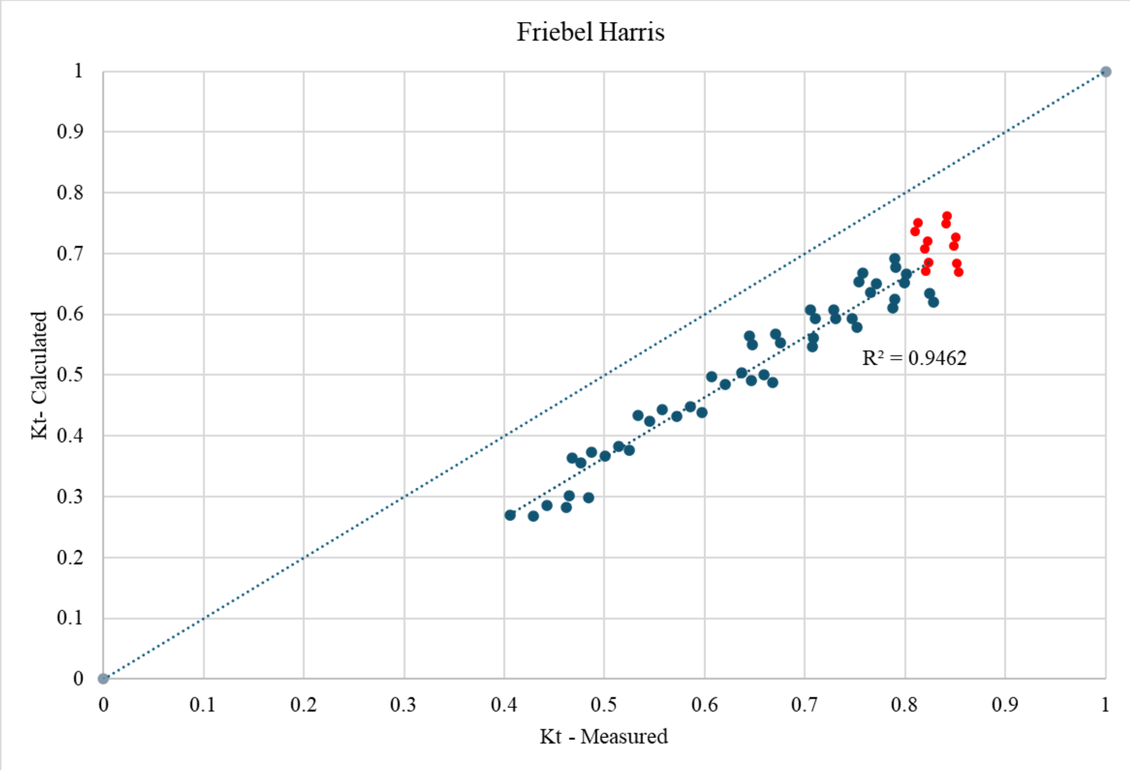


Figure 4.14. Comparison between wave transmission coefficients calculated from the Charles Friebel et al., (2003) formula and measured from the produced data

Figure 4.15 presents the wave transmission data calculated using Van Gent et al. (2023) Eq. 2.21 plotted on the vertical axis, and the measured wave transmission coefficients on the horizontal axis. The resulting $R^2$ value is 0.9854, indicating a high correlation. Compared to other formulas available in the literature, this equation shows the closest alignment with the experimental data. In Eq.2.21, the effects of both submergence depth and crest width are analyzed together with wave height and wavelength. Unlike other empirical formulations in the literature, Eq.2.21 incorporates a hyperbolic tangent function, which distinguishes it from other approaches. Eq.2.21 yielded the highest correlation among the tested equations, suggesting that the tanh function effectively captures the nonlinear relationship between the influencing parameters.

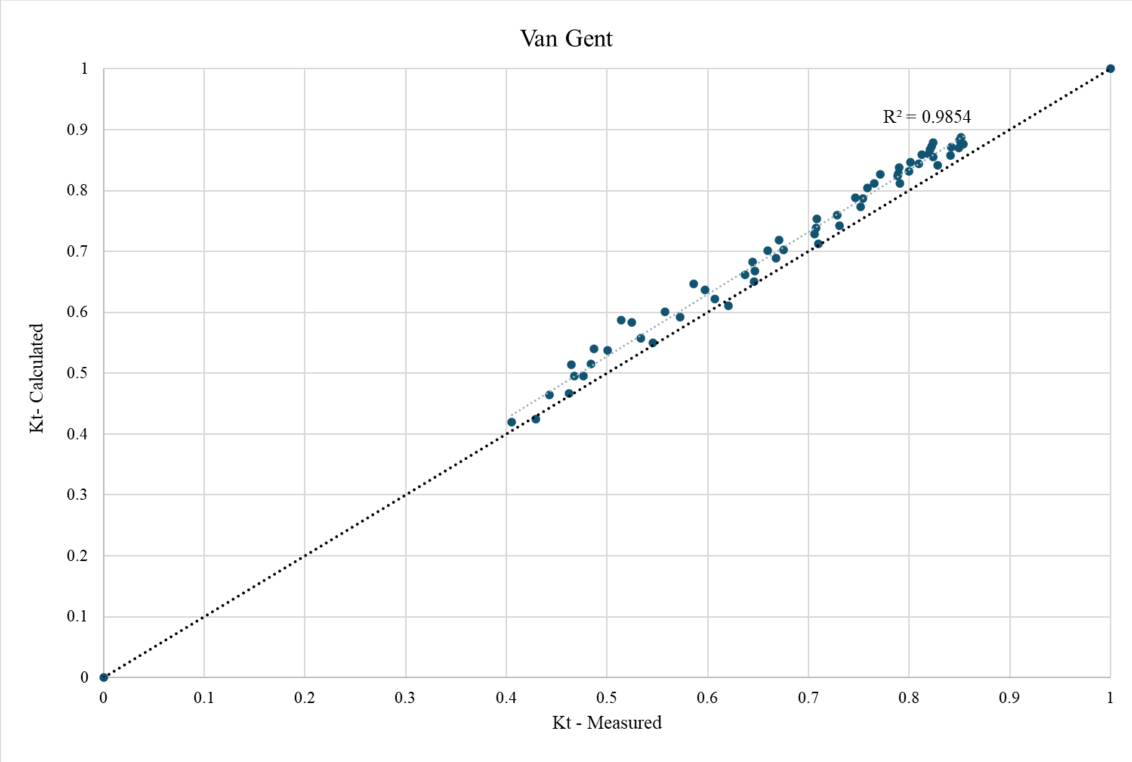


Figure 4.15. Comparison between wave transmission coefficients calculated from the Van Gent et al. (2023) formula and measured from the produced data

## 4.2. Overtopping at Reference Case

This thesis aims to quantify the reduction factor in the wave overtopping formulations due to the submerged breakwaters located in front of vertical seawall. Initially, reference experiments were conducted in a wave flume under the same hydrodynamic conditions, without the presence of the submerged breakwater. The observed data were compared to the simple vertical wall equations presented in EurOtop (2018). To establish a robust correlation with the EurOtop (2018) findings, additional experiments were carried out at two different water depths, distinct from those used in the overtopping tests involving the submerged breakwater. These two water depths were chosen to be between the depths used as a baseline, allowing a clearer trend line to be established. The experimental conditions are thoroughly summarized in the accompanying Table 4.1.

Table 4.1. Reference case parameters and overtopping discharge

| condition | $T_{m-1,0\ (s)}$ | $H_{mo}$(m) | $h_t$(m) | $R_c$(m) | $h/L_0$ | $L_{(m-1,0)\ (m)}$ | $S_{m-1,0}$ |
|---|---|---|---|---|---|---|---|
| H1 | 1.247 | 0.093 | 0.220 | 0.030 | 0.091 | 2.427 | 0.038 |
| H2 | 1.278 | 0.102 | 0.220 | 0.030 | 0.086 | 2.551 | 0.040 |
| H3 | 1.259 | 0.099 | 0.2375 | 0.013 | 0.096 | 2.475 | 0.040 |
| H4 | 1.298 | 0.109 | 0.2375 | 0.013 | 0.090 | 2.628 | 0.041 |
| H5 | 1.252 | 0.095 | 0.226 | 0.024 | 0.092 | 2.447 | 0.039 |
| H6 | 1.289 | 0.104 | 0.226 | 0.024 | 0.087 | 2.593 | 0.040 |
| H7 | 1.257 | 0.097 | 0.232 | 0.018 | 0.094 | 2.467 | 0.039 |
| H8 | 1.296 | 0.106 | 0.232 | 0.018 | 0.088 | 2.622 | 0.040 |

The method for predicting the mean overtopping discharge is determined in accordance with the guidelines in EurOtop 2018 Chapter 7 Vertical and Steep Wall. In the designed experimental setup, there is a foreshore slope with a slope of 1/30 before reaching the vertical wall. On the other hand, all tested waves break at the structure, and this creates "impulsive overtopping" conditions. This condition checked with the $\frac{h^2}{H_{m0} * L_{m-1,0}} < 0.23$. Finally, the $\frac{R_c}{H_{m0}} < 1.35$ status is checked and the equation that will determine the design and evaluation approach is decided. The data is within the range of $0.1 < \frac{R_c}{H_{m0}} < 0.35$ which means all datas are low freeboard condition. The EurOtop (2018) formula that satisfies all these boundary conditions is provided below:

$$\frac{q}{\sqrt{g * {H_{m0}}^3}} = 0.011 * \left(\frac{H_{m0}}{h * s_{m-1,0}}\right)^{0.5} exp\left(-2.2\frac{R_c}{H_{m0}}\right), \quad 0.1 < \frac{R_c}{H_{m0}} < 1.35 \tag{4. 1}$$

According to EurOtop (2018) for a design or assessment approach, it is recommended to increase the average discharge by about one standard deviation which is,

$$\frac{q}{\sqrt{g * {H_{m0}}^{3}}} = 0.0155 * \left(\frac{H_{m0}}{h * s_{m-1,0}}\right)^{0.5} exp\left(-2.2\frac{R_c}{H_{m0}}\right), \qquad 0.1 < \frac{R_c}{H_{m0}} < 1.35 \tag{4. 2}$$

Figure 4.16 presents a comparison of the experimental results from the Reference Case with the formula developed in the EurOtop (2018), which is based on the extensive overtopping measurements compiled in the CLASH database. Additionally, the figure includes experimental studies conducted by Kisacik et al. (2019) and Bahadiroğlu et al. (2024). According to Kisacik et al. (2019) , main sources of differences can be attributed to model effects, variations in the number of waves in one run, and the wave generation spectrum type. On the other hand, there is foreshore slope difference between the datasets. Kisacik et al. (2019) has 1/20 foreshore slope and relative freeboard is between $0.2 < \frac{R_c}{H_{m0}} < 2.0$. The vertical wall experiments by Bahadiroğlu et.al. (2024) were conducted at the LABIMA, University of Florence, Italy. In that study, the relative freeboard range was set between $0.35 < \frac{R_c}{H_{m0}} < 0.75$, with a transition slope of 1/30. All comparative experimental studies were performed with random waves using the JONSWAP spectrum. Notably, the experimental results conducted at IZTECH and LABIMA exhibit a consistent behavior along the same trendline as predicted by the EurOtop (2018) formula. While most of the data points lie slightly below the trendline, a smaller portion is positioned slightly above it, but remains close, reflecting the overall reliability of the experimental observations. This consistency across results suggests that the experimental setup and methodology are both reproducible and capable of yielding reliable outcomes, even when conducted in different experimental facilities. Such findings underscore the robustness of the experimental approach and reinforce the applicability of the results for broader coastal engineering practices.

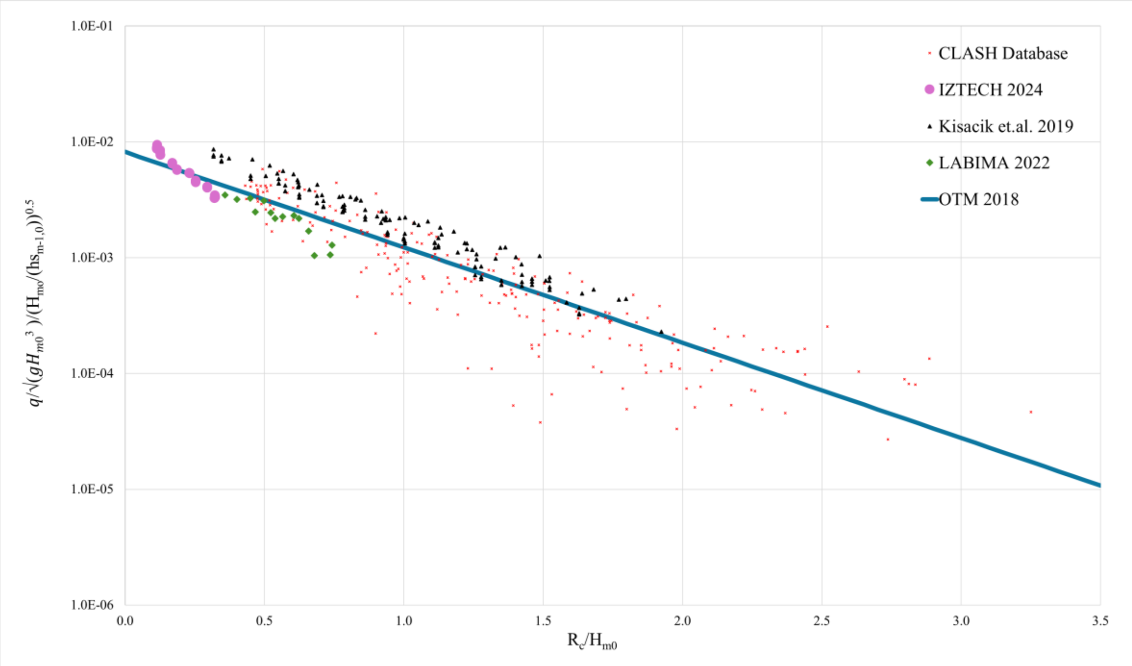


Figure 4.16. EurOtop database comparison of mean overtopping discharge for vertical seawalls: Kisacik et al. (2019), LABIMA (2022), and IZTECH (2024).

## 4.3. Impact of Submerged Breakwater on Vertical Seawall Overtopping Discharge

The Model Y test matrix, which examines the effect of a submerged breakwater on overtopping discharge for a vertical seawall, is provided in Table 3.7. Model Y includes tests on 15 different submerged breakwater geometries. To assess the reduction effect of the submerged breakwater on overtopping discharge, experiments conducted for the simple vertical wall case are compared with Model Y data. Consequently, the simple vertical wall case, serving as a reference for Model Y, is referred to as the "reference case."

For both scenarios, tests were conducted under four different hydrodynamic conditions, comprising two water depths and two target wave height and periods. The results, presented in Figure 4.17 and Figure 4.18, demonstrate that all Model Y configurations successfully reduced overtopping discharge relative to the reference case. Figure 4.17 shows the reduction achieved across all hydrodynamic conditions at a constant relative freeboard, $R_c/H_{m0}$. Meanwhile, Figure 4.18 illustrates the reduction associated with various geometric configurations when compared to the reference case.

A key finding is that the largest submerged breakwater geometry, G15, with a breakwater height of h5' and a crest width of B4 (see Table 3.1), achieved the greatest reduction in overtopping discharge. Additionally, as shown in Figure 4.18, it was observed that as the cross-sectional area of the submerged breakwater decreases, the reduction effect tends to decrease as well. However, the extent of this reduction requires comprehensive analysis for a deeper understanding.

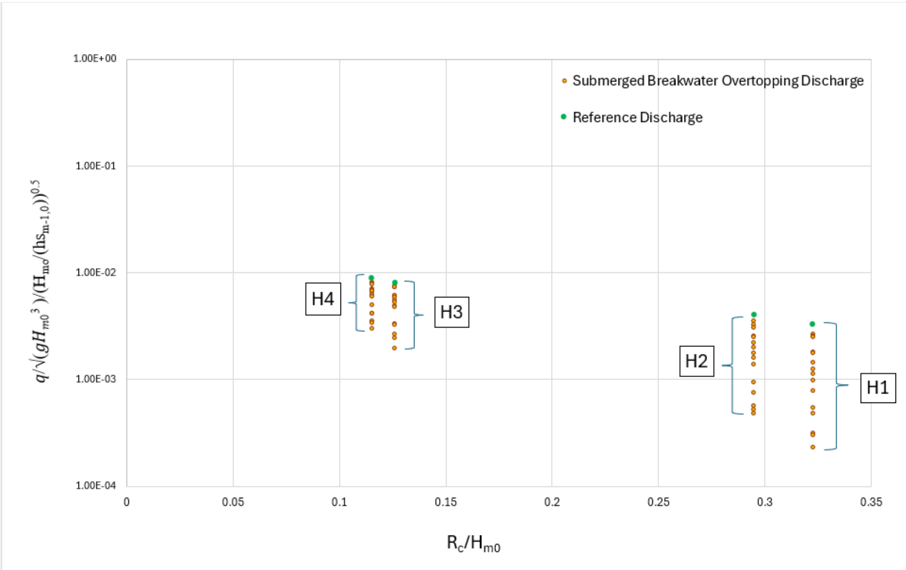


Figure 4.17. Relative overtopping rate comparison of Reference Case and Model Y

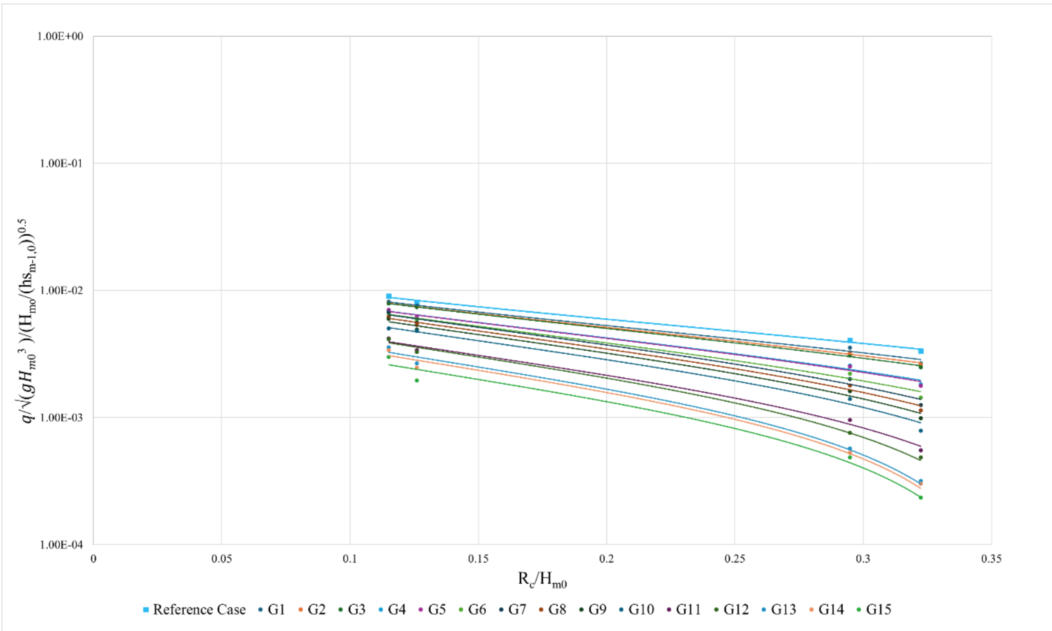


Figure 4.18. Relative overtopping rate comparison of Reference Case and Model Y with different geometric configurations

## 4.4. Overtopping at Model Y

In Model Y, where the submerged breakwater is placed in front of a vertical seawall, the reduction effect is clearly illustrated in Figure 4.17 and Figure 4.18 for each geometric configuration and hydrodynamic condition. To quantify this reduction, a submerged breakwater reduction factor is incorporated into Eq. 4. 2 from EurOtop (2018), which is formulated for vertical seawalls. Since 60 different experiments were conducted within the framework of Model Y, 60 different values of $\gamma_{sub}$ are calculated accordingly. This calculation involves taking the ratio of each experiment's overtopping discharge to the overtopping discharge in its corresponding reference test.

$$\frac{q_{ref}}{\sqrt{g * H_{m0}{}^{3}}} = 0.0155 * \left(\frac{H_{m0}}{h * s_{m-1,0}}\right)^{0.5} exp\left(-2.2\frac{R_c}{H_{m0}}\right), \quad \left(0.1 < \frac{R_c}{H_{m0}} < 0.35\right) \tag{4.3}$$

Where ($q_{ref}$) is reference case overtopping discharges.

$$\frac{q_{sub}}{\sqrt{g * H_{m0}{}^{3}}} = 0.0155 * \left(\frac{H_{m0}}{h * s_{m-1,0}}\right)^{0.5} exp\left(-2.2\frac{R_c}{H_{m0}}\frac{1}{\gamma_{sub}}\right), \quad \left(0.1 < \frac{R_c}{H_{m0}} < 0.35\right) \tag{4.4}$$

Where ($q_{sub}$) is laboratory experiments overtopping discharge for Model Y

Then when the relative ratio $\frac{q_{ref}}{q_{sub}}$ is considered, the method for calculating $\gamma_{sub}$ proceeds as follows.

$$\frac{\dfrac{q_{ref}}{\sqrt{g * H_{m0}{}^{3}}} = 0.0155 * \left(\dfrac{H_{m0}}{h * s_{m-1,0}}\right)^{0.5} exp\left(-2.2\dfrac{R_c}{H_{m0}}\right)}{\dfrac{q_{sub}}{\sqrt{g * H_{m0}{}^{3}}} = 0.0155 * \left(\dfrac{H_{m0}}{h * s_{m-1,0}}\right)^{0.5} exp\left(-2.2\dfrac{R_c}{H_{m0}}\dfrac{1}{\gamma_{sub}}\right)} \tag{4.5}$$

$$\frac{q_{ref}}{q_{sub}} = \frac{exp\left(-2.2\frac{R_c}{H_{m0}}\right)}{exp\left(-2.2\frac{R_c}{H_{m0}}\frac{1}{\gamma_{sub}}\right)} \tag{4.6}$$

$$\frac{q_{ref}}{q_{sub}} = \frac{e^{\left(-2.2\frac{R_c}{H_{m0}}\right)}}{e^{\left(-2.2\frac{R_c}{H_{m0}}\frac{1}{\gamma_{sub}}\right)}} \tag{4.7}$$

$$\frac{q_{ref}}{q_{sub}} = e^{-2.2\frac{R_c}{H_{m0}}-\left(-2.2\frac{R_c}{H_{m0}}\frac{1}{\gamma_{sub}}\right)} \tag{4.8}$$

$$ln\left(\frac{q_{ref}}{q_{sub}}\right) = ln\left(e^{-2.2\frac{R_c}{H_{m0}}-\left(-2.2\frac{R_c}{H_{m0}}\frac{1}{\gamma_{sub}}\right)}\right) \tag{4.9}$$

$$ln\left(\frac{q_{ref}}{q_{sub}}\right) = -2.2\frac{R_c}{H_{m0}} + \left(2.2\frac{R_c}{H_{m0}}\frac{1}{\gamma_{sub}}\right) \tag{4.10}$$

$$ln\left(\frac{q_{ref}}{q_{sub}}\right) = -2.2\frac{R_c}{H_{m0}}\left(1-\frac{1}{\gamma_{sub}}\right) \tag{4.11}$$

$$\frac{ln\left(\frac{q_{ref}}{q_{sub}}\right)}{-2.2\frac{R_c}{H_{m0}}} = \left(1-\frac{1}{\gamma_{sub}}\right) \tag{4.12}$$

$$\left(\frac{1}{\gamma_{sub}}\right) = 1 - \frac{ln\left(\frac{q_{ref}}{q_{sub}}\right)}{-2.2\frac{R_c}{H_{m0}}} \tag{4.13}$$

$$\left(\frac{1}{\gamma_{sub}}\right) = 1 - \left(ln\left(\frac{q_{ref}}{q_{sub}}\right) * -2.2\frac{H_{m0}}{R_c}\right) \tag{4.14}$$

$$(\gamma_{sub}) = \frac{1}{1-\left(ln\left(\frac{q_{ref}}{q_{sub}}\right) * -2.2\frac{H_{m0}}{R_c}\right)} \tag{4.15}$$

With the Eq. 4.15, 60 different $\gamma_{sub}$ values are calculated and reduction factor variation is in the range of $0.16 \leq \gamma_{sub} \leq 0.82$. Reduction factor $\gamma_{sub}$ indicates that the effectiveness of the submerged breakwater in mitigating wave overtopping varies significantly under different conditions.

According to Figure 4.19 low $\gamma_{sub}$ values indicate that the submerged breakwater has a high reduction of wave overtopping Conversely, a higher $\gamma_{sub}$ value (closer to 0.82) implies that the breakwater is less effective, allowing more wave energy and wave overtopping discharge.

The choice and calibration of this reduction factor can depend on multiple parameters, including breakwater geometry (height, crest width, slope), wave characteristics (height, period), and water depth. In practical terms, understanding and accurately defining this reduction factor is crucial because it allows optimizing designs to prevent coastal flooding, and related risks. As shown in Figure 4.19 The reduction factor decreases in a linear manner as the submerged breakwater cross-sectional area increases. The cross-sectional area of the submerged breakwater is,

$$Area(A) = \frac{(2B + 4h') \times h'}{2} \tag{4.16}$$

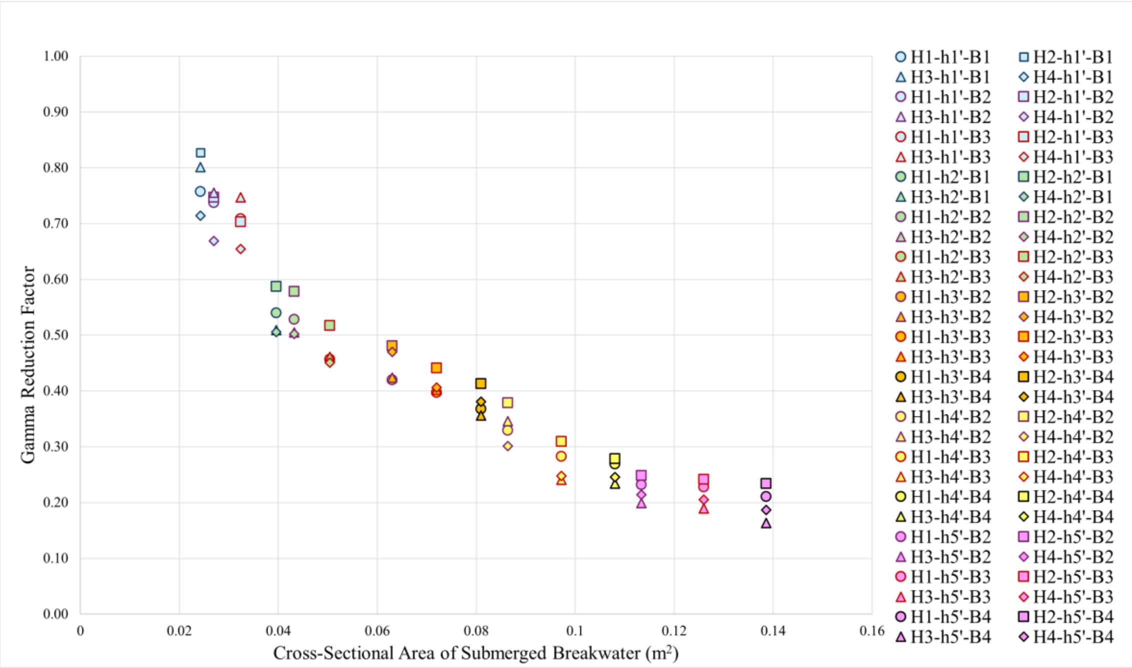


Figure 4.19. Relation between gamma reduction factor ($\gamma_{sub}$) and submerged breakwater cross-sectional area

The significance of the submerged breakwater's cross-sectional area in mitigating overtopping is clearly illustrated through the reduction percentage defined in Eq. 4.17 and presented in Figure 4.20 , which highlight the decrease in overtopping discharge relative to the reference case.

$$\text{Reduction Percentage} = \frac{q_{reference} - q_{sub}}{q_{reference}} \times 100 \tag{4.17}$$

In Figure 4.19 and Figure 4.20, it is observed that when the reduction percentage is less than 10% - 15%, the reduction factor approaches almost 1. This indicates that the submerged breakwater is relatively ineffective in reducing overtopping discharge particularly under H3 and H4 hydrodynamic conditions. The key factor influencing this outcome is the submergence depth, or freeboard (F) of the breakwater. As the freeboard increases, the wave transmission coefficient also increases (see Figure 4.1). Under H3 and H4 conditions, where the water depth at the toe is 23.75 cm, the breakwater is found to be nearly ineffective in scenarios with the largest freeboard which means the smallest h’ values. Consequently, these geometries exhibit minimal reduction in overtopping discharge. Furthermore, as shown in Figure 4.20, the experimental results for reduction percentage form two distinct curves under H1, H2 and H3, H4 hydrodynamic conditions. As expected, for the same breakwater geometries, a decrease in the reduction percentage is observed at higher water levels.

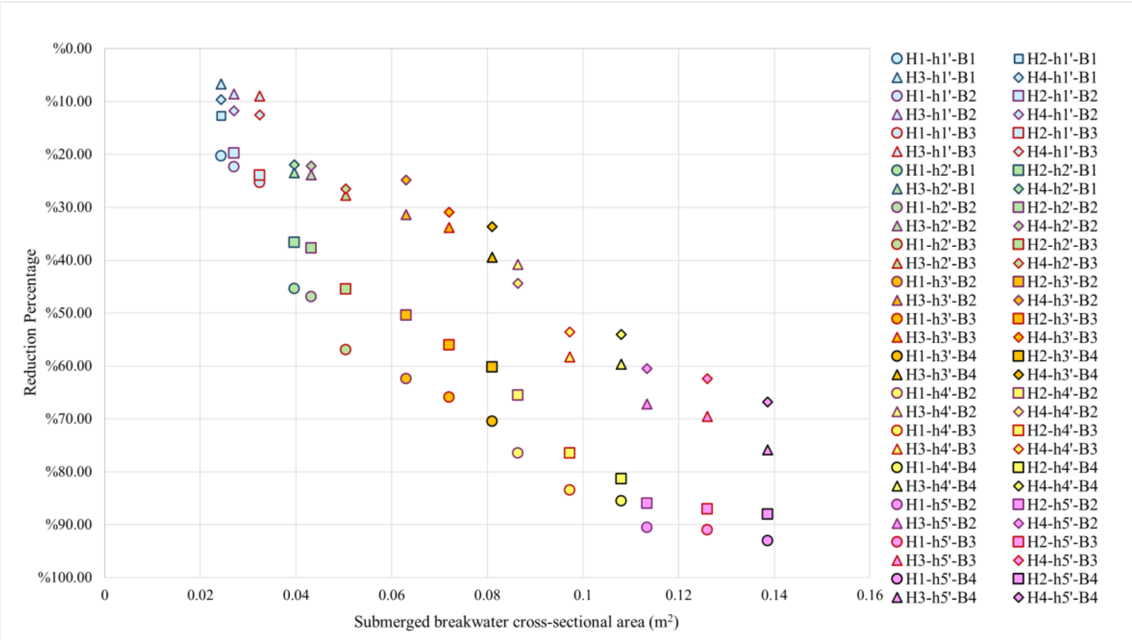


Figure 4.20. Relation between reduction percentage and submerged breakwater cross-sectional area

The main objective of this study is to increase the strength of the existing coastal defense system by adding a submerged breakwater as an additional measure. The cross-sectional area of the submerged breakwater is the most critical design parameter for reducing overtopping discharge, as previously mentioned.

It is appropriate to represent the cross-sectional area in a dimensionless form in order to reduce the impact of scale effect. In this context, efforts have been made to achieve the best correlation using the dimensionless parameters identified through the dimensional analysis presented in Section 3.1.3.

The Table 4.2 below assesses the efficiency of various non-dimensional parameters by utilizing a variety of metrics, such as $R^2$ (Linear, Logarithmic and Exponential), RMSE (Root Mean Squared Error), MAE (Mean Absolute Error), and the difference between RMSE and MAE. The accuracy of the parameters and their ability to fit the data are evaluated by these metrics.

$$RMSE = \sqrt{\frac{1}{n}\sum_{i=1}^{n}(q_{observed} - q_{predicted})^2} \tag{4.18}$$

$$MAE = \frac{1}{n}\sum_{i=1}^{n}|q_{observed} - q_{predicted}| \tag{4.19}$$

where n is the number of observations.

Table 4.2. $R^2$, RMSE and MAE values for non-dimensional parameters

| Non-Dimensional Parameter | Linear $R^2$ | Logarithmic $R^2$ | Exponential $R^2$ | RMSE | MAE | RMSE-MAE |
|---|---|---|---|---|---|---|
| $\frac{L_{m-1,0}}{\sqrt{Area}}$ | 0.94 | 0.94 | - | 7.4823E-04 | 6.6871E-04 | 7.9522E-05 |
| $\frac{h_t \times L_{m-1,0}}{\sqrt{Area} \times H_{m0i}}$ | 0.935 | 0.933 | - | 7.3828E-04 | 6.5724E-04 | 8.1049E-05 |
| $\frac{H_{m0i} \times L_{m-1,0}^2 \times h_t}{Area^2}$ | 0.80 | 0.932 | - | 7.6163E-04 | 6.7375E-04 | 8.7880E-05 |
| $\frac{H_{m0i} \times L_{m-1,0}^2}{Area \times h_t}$ | 0.892 | 0.93 | - | 7.5996E-04 | 6.7215E-04 | 8.7803E-05 |
| $\frac{H_{m0i} \times L_{m-1,0}}{Area}$ | 0.896 | 0.928 | - | 7.6332E-04 | 6.7443E-04 | 8.8890E-05 |
| $\frac{H_{m0i} \times L_{m-1,0} \times h_t}{Area^{1.5}}$ | 0.853 | 0.928 | - | 7.6547E-04 | 6.7618E-04 | 8.9293E-05 |
| $\frac{H_{m0i} \times h_t}{Area}$ | 0.890 | 0.92 | - | 7.7321E-04 | 6.8077E-04 | 9.2444E-05 |

(cont. on next page)

Table 4.2. (cont.)

| | | | | | | |
|---|---|---|---|---|---|---|
| $\frac{h_t}{\sqrt{Area}}$ | 0.917 | 0.916 | - | 7.6169E-04 | 6.7276E-04 | 8.8927E-05 |
| $\frac{H_{m0i}}{\sqrt{Area}}$ | 0.906 | 0.910 | - | 7.7060E-04 | 6.8124E-04 | 8.9359E-05 |
| $\frac{H_{m0i} \times L_{m-1,0}}{\sqrt{Area} \times h_t}$ | 0.897 | 0.904 | - | 7.6480E-04 | 6.8000E-04 | 8.4808E-05 |
| $\frac{h_t^2}{Area} \times S_{m-1,0}$ | 0.875 | 0.902 | - | 7.8386E-04 | 6.8558E-04 | 9.8279E-05 |
| $\frac{H_{m0i}^2 \times h_t}{Area \times L_{m-1,0}}$ | 0.868 | 0.901 | - | 7.8754E-04 | 6.8950E-04 | 9.8037E-05 |
| $\frac{H_{m0i} \times h_t}{\sqrt{Area} \times L_{m-1,0}}$ | 0.883 | 0.884 | - | 7.8482E-04 | 6.8588E-04 | 9.8943E-05 |
| $Kt$ | - | - | 0.85 | 7.6097E-04 | 6.6829E-04 | 9.2672E-05 |

Most non-dimensional parameters exhibit high explanatory power, with $R^2$ values that fall within the range of 0.80 to 0.94. Overtopping discharge is affected by the different geometry of the submerged breakwater; therefore, the breakwater's area is incorporated into almost each parameter. Additionally, it can be stated that some parameters are directly affected by wave steepness ($\frac{H_{m0}}{L_{m-1,0}}$), the breaker index ($\frac{H_{m0}}{h_t}$), as well as wave height, water depth, and wavelength. The data is best fit by the parameter $\frac{L_{m-1,0}}{\sqrt{Area}}$ ($R^2$=0.94, logarithmic $R^2$=0.94) and parameter $\frac{h_t \times L_{m-1,0}}{\sqrt{Area} \times H_{m0,i}}$ ($R^2$=0.935, logarithmic $R^2$=0.933), as observed by the highest values. $\frac{h_t \times L_{m-1,0}}{\sqrt{Area} \times H_{m0,i}}$ and $\frac{L_{m-1,0}}{\sqrt{Area}}$ also attain the lowest RMSE and MAE values, with RMSE values of 0.0007383 and 0.0007482, respectively, and MAE values of 0.0006572 and 0.0006687, respectively. These values suggest minimal prediction errors. In contrast, $\frac{{H_{m0i}}^2 \times h_t}{Area \times L_{m-1,0}}$ demonstrates the maximum RMSE (0.000787536) and MAE (0.0006895), which underscores its inferior predictive accuracy in comparison to the other parameters.

The magnitude of significant errors is elucidated by the distinction between RMSE and MAE. The slightest differences are observed for $\frac{L_{m-1,0}}{\sqrt{Area}}$ (0.0000795), suggesting that the errors are consistent and systematic, with minimal influence from outliers.

In general, $\frac{h_t \times L_{m-1,0}}{\sqrt{Area} \times H_{m0,i}}$ and $\frac{L_{m-1,0}}{\sqrt{Area}}$ outperform the others in terms of both explanatory power ($R^2$) and error metrics (RMSE, MAE). These parameters exhibit high accuracy and robustness against large errors, rendering them appropriate for applications that necessitate precision predictions.

The figures below (see Figure 4.21 - Figure 4.38) provide a comprehensive overview of the experiments that were conducted with %95 prediction interval from the t-test for the clear evaluation.

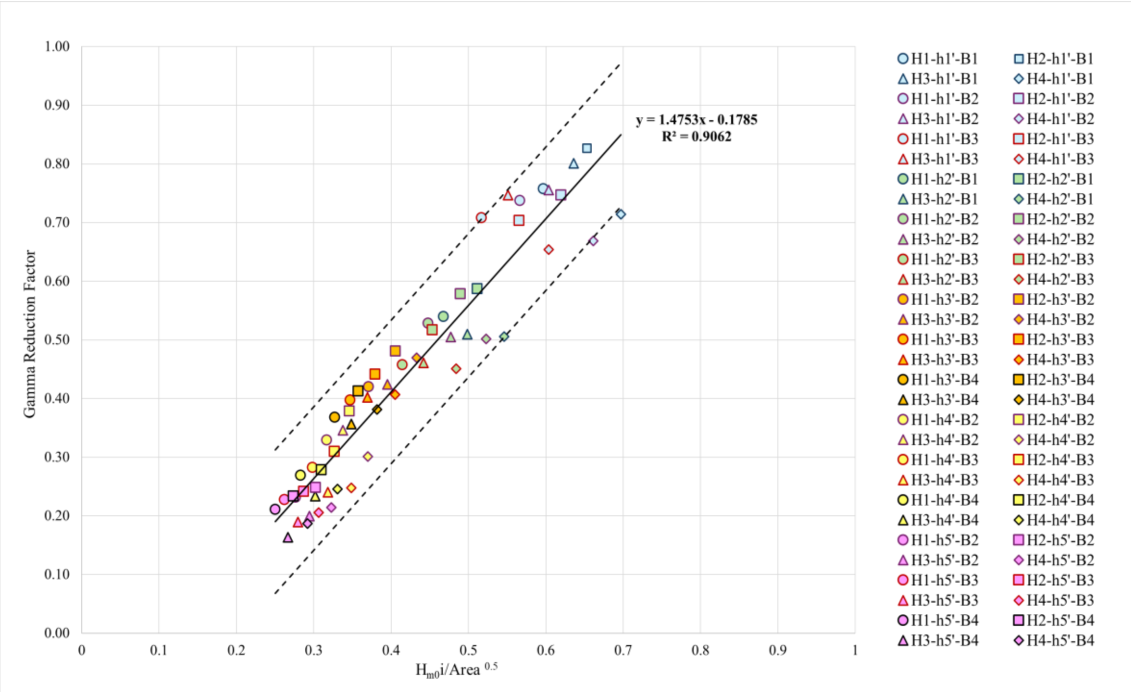


Figure 4.21. Relation between gamma reduction factor ($\gamma_{sub}$) and non-dimensional parameter $\frac{H_{m0i}}{\sqrt{Area}}$ with linear representation and 95% prediction interval

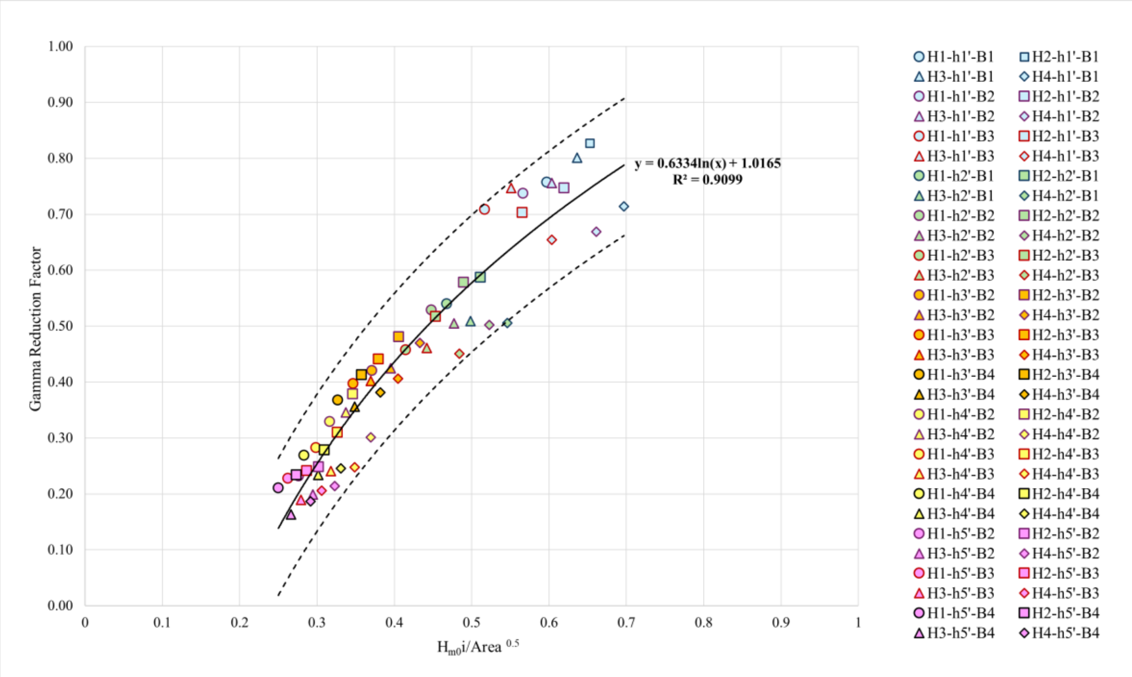


Figure 4.22. Relation between gamma reduction factor ($\gamma_{sub}$) and non-dimensional parameter $\frac{H_{m0i}}{\sqrt{Area}}$ with logarithmic representation and 95% prediction interval

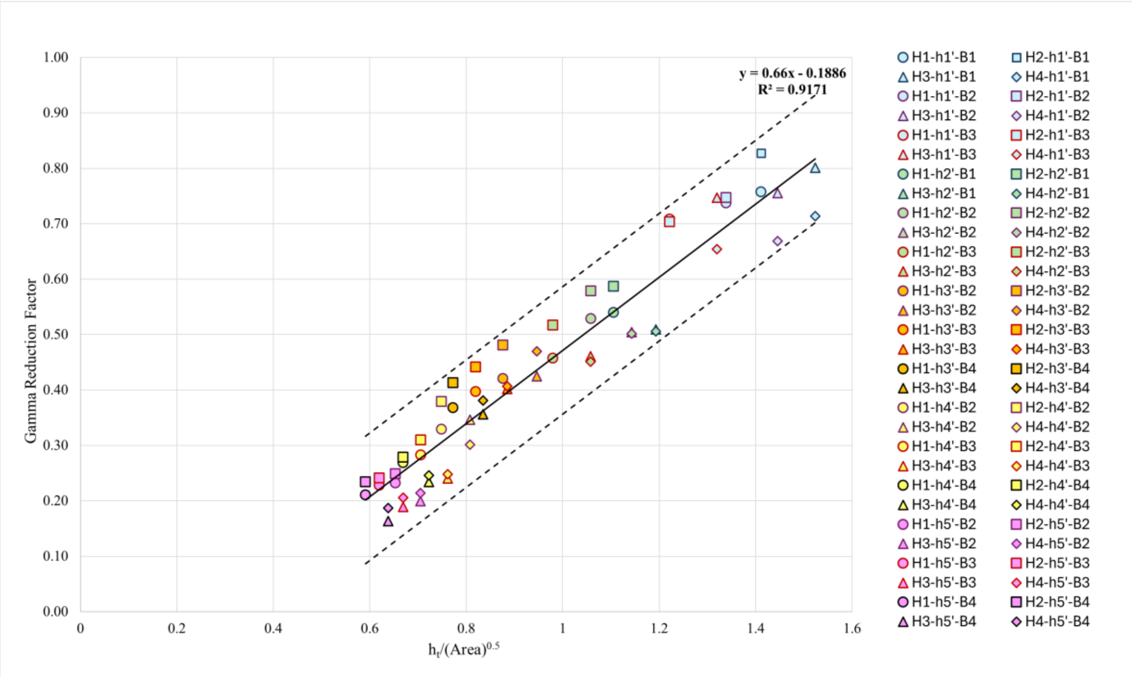


Figure 4.23. Relation between gamma reduction factor ($\gamma_{sub}$) and non-dimensional parameter $\frac{h_t}{\sqrt{Area}}$ with linear representation and 95% prediction interval

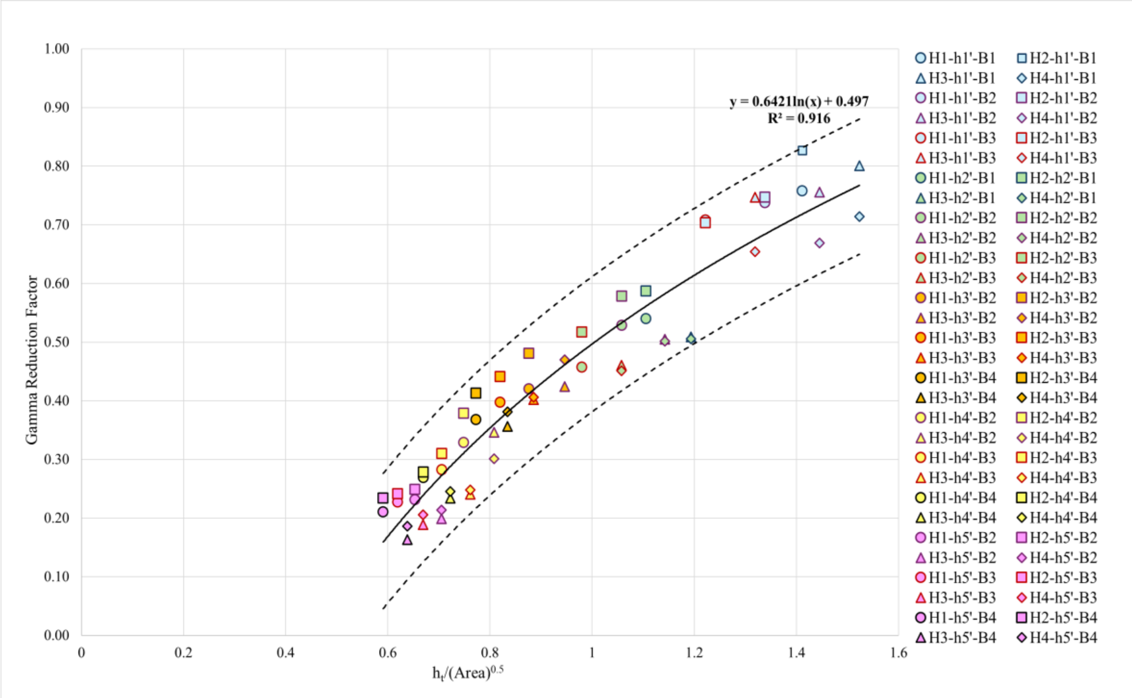


Figure 4.24. Relation between gamma reduction factor ($\gamma_{sub}$) and non-dimensional parameter $\frac{h_t}{\sqrt{Area}}$ with logarithmic representation and 95% prediction interval

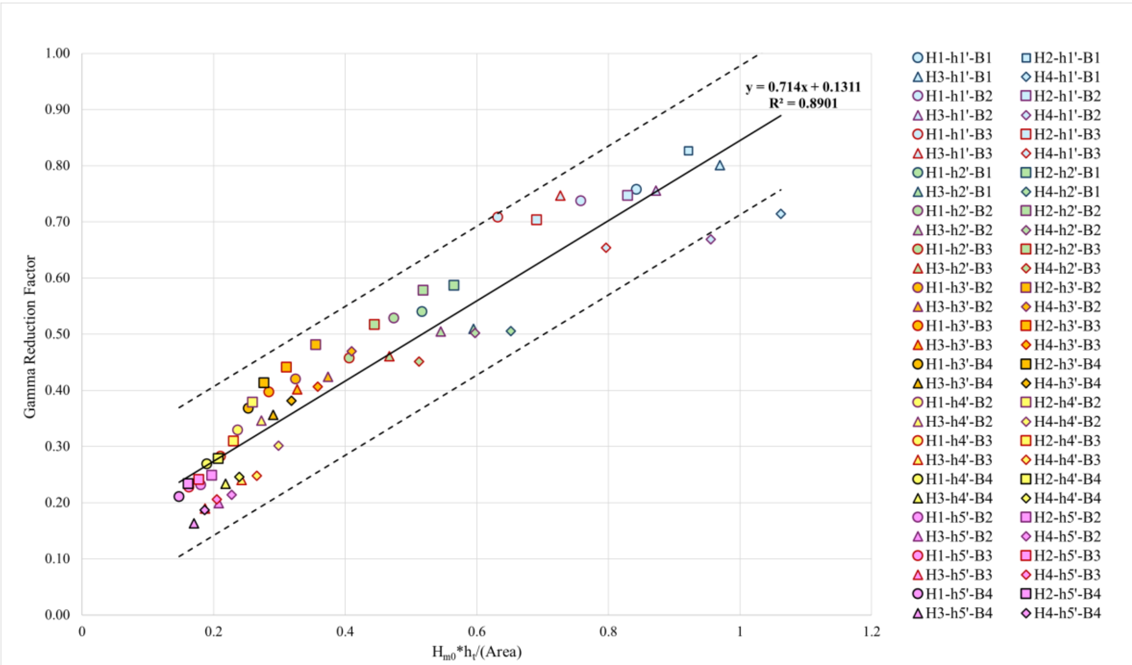


Figure 4.25. Relation between gamma reduction factor ($\gamma_{sub}$) and non-dimensional parameter $\frac{H_{moi} \times h_t}{Area}$ with linear representation and 95% prediction interval

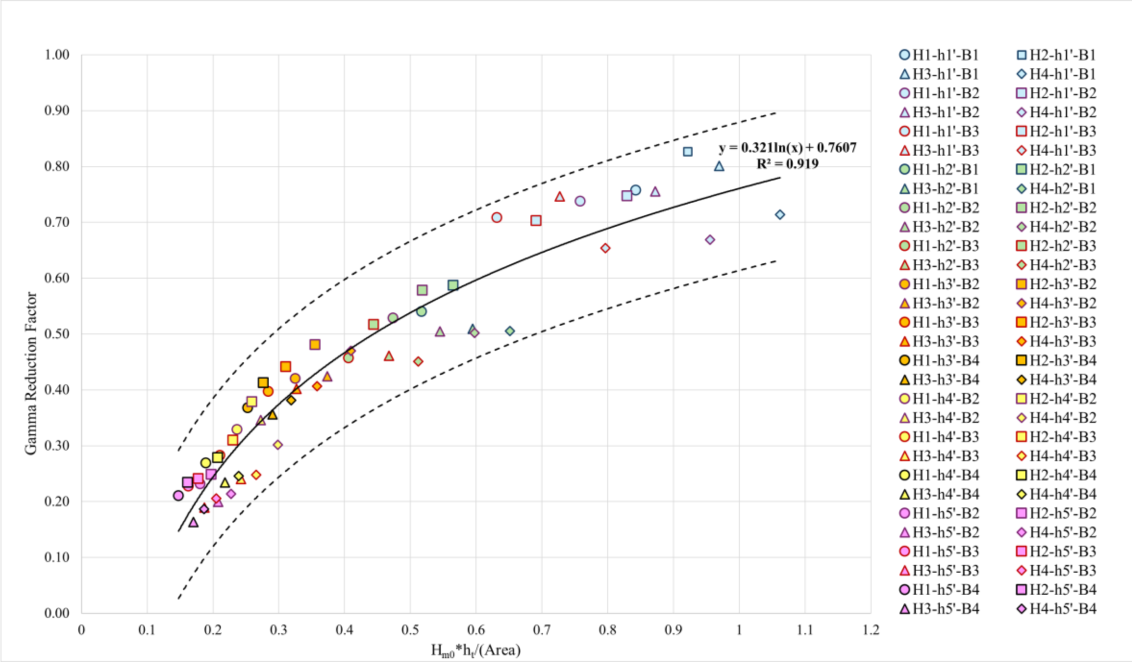


Figure 4.26. Relation between gamma reduction factor ($\gamma_{sub}$) and non-dimensional parameter $\frac{H_{m0i} \times h_t}{Area}$ with logarithmic representation and 95% prediction interval

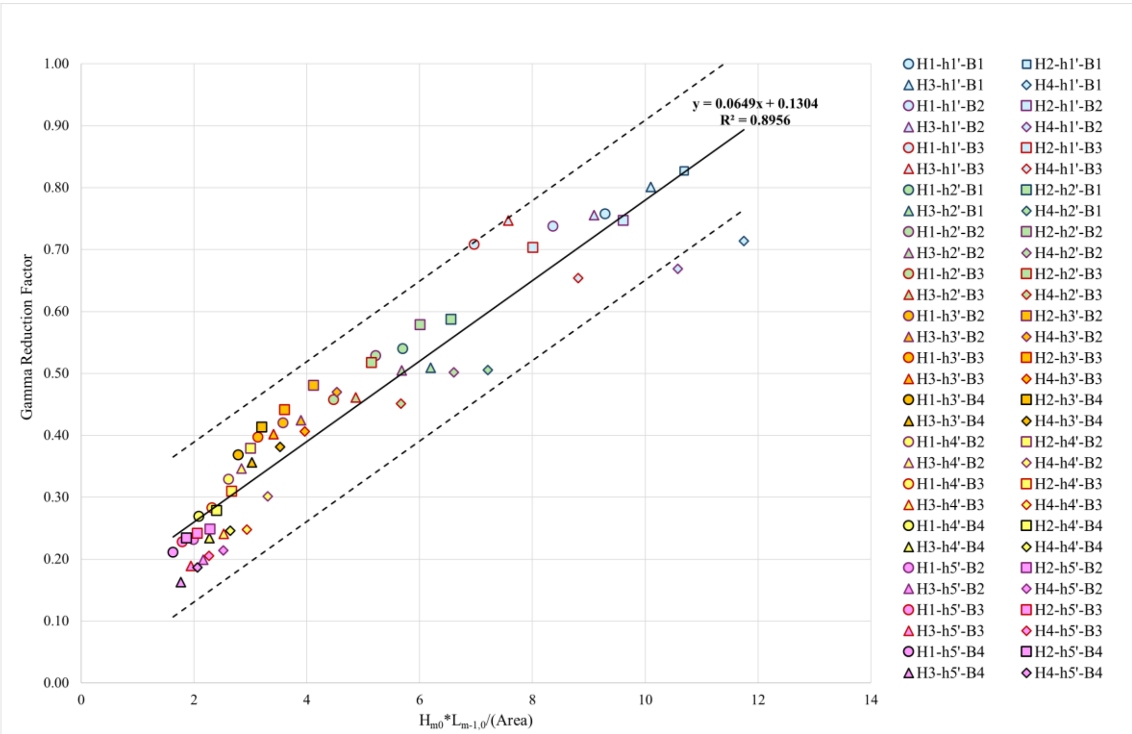


Figure 4.27. Relation between gamma reduction factor ($\gamma_{sub}$) and non-dimensional parameter $\frac{H_{m0i} \times L_{m-1,0}}{Area}$ with linear representation and 95% prediction interval

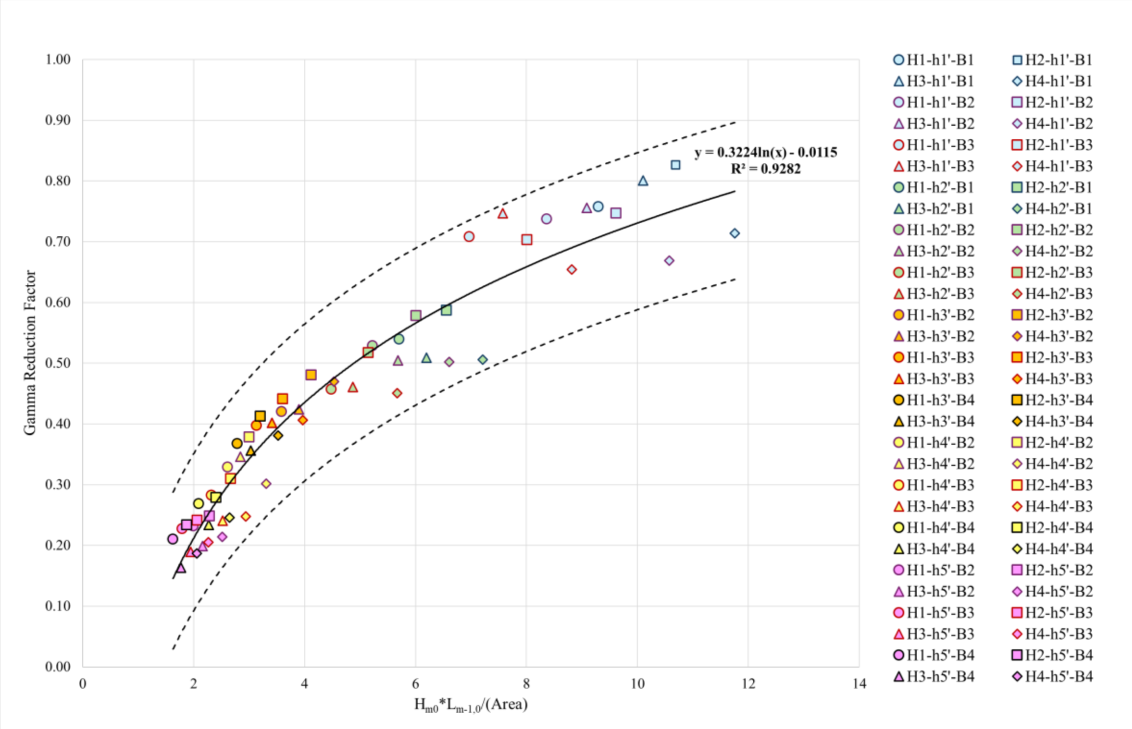


Figure 4.28. Relation between gamma reduction factor ($\gamma_{sub}$) and non-dimensional parameter $\frac{H_{m0i} \times L_{m-1,0}}{Area}$ with logarithmic representation and 95% prediction interval

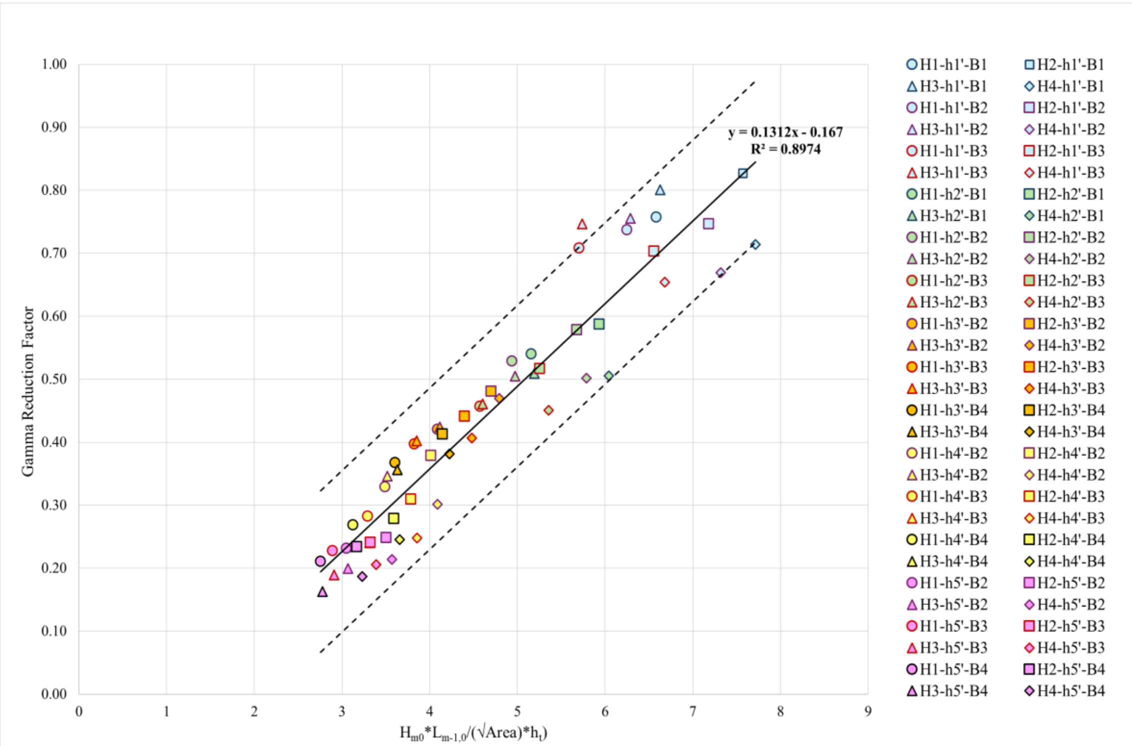


Figure 4.29. Relation between gamma reduction factor ($\gamma_{sub}$) and non-dimensional parameter $\frac{H_{m0i} \times L_{m-1,0}}{\sqrt{Area} \times h_t}$ with linear representation and 95% prediction interval

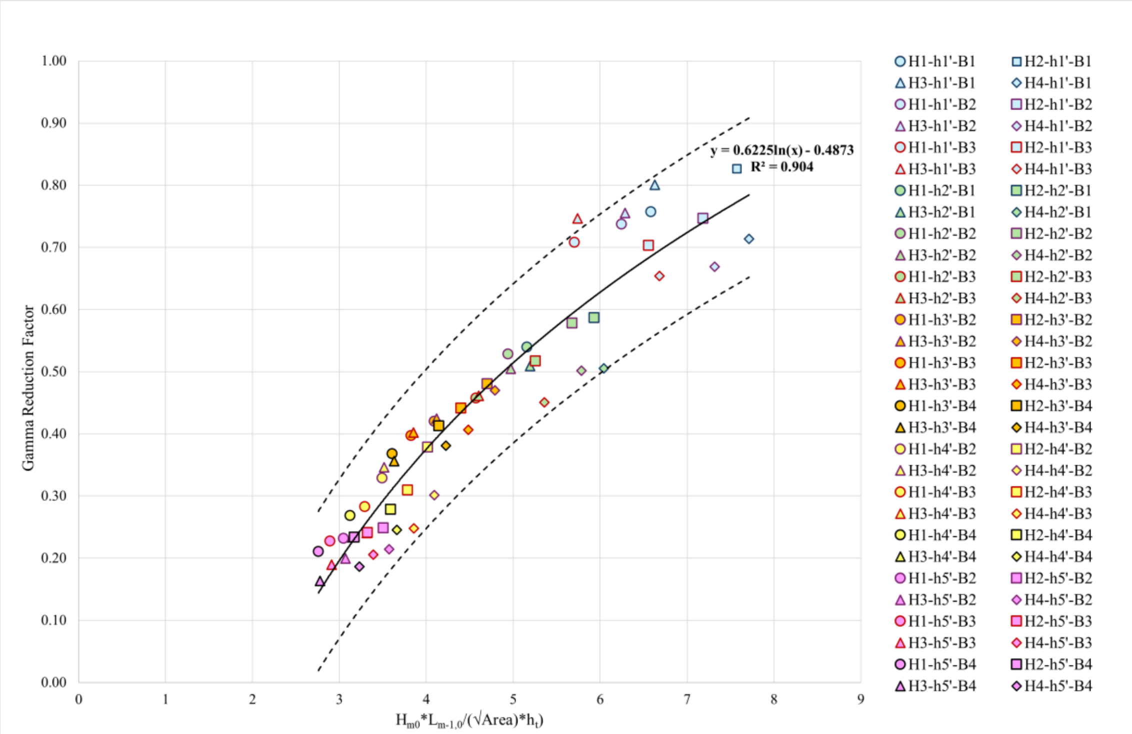


Figure 4.30. Relation between gamma reduction factor ($\gamma_{sub}$) and non-dimensional parameter $\frac{H_{m0i} \times L_{m-1,0}}{\sqrt{Area} \times h_t}$ with linear representation and 95% prediction interval

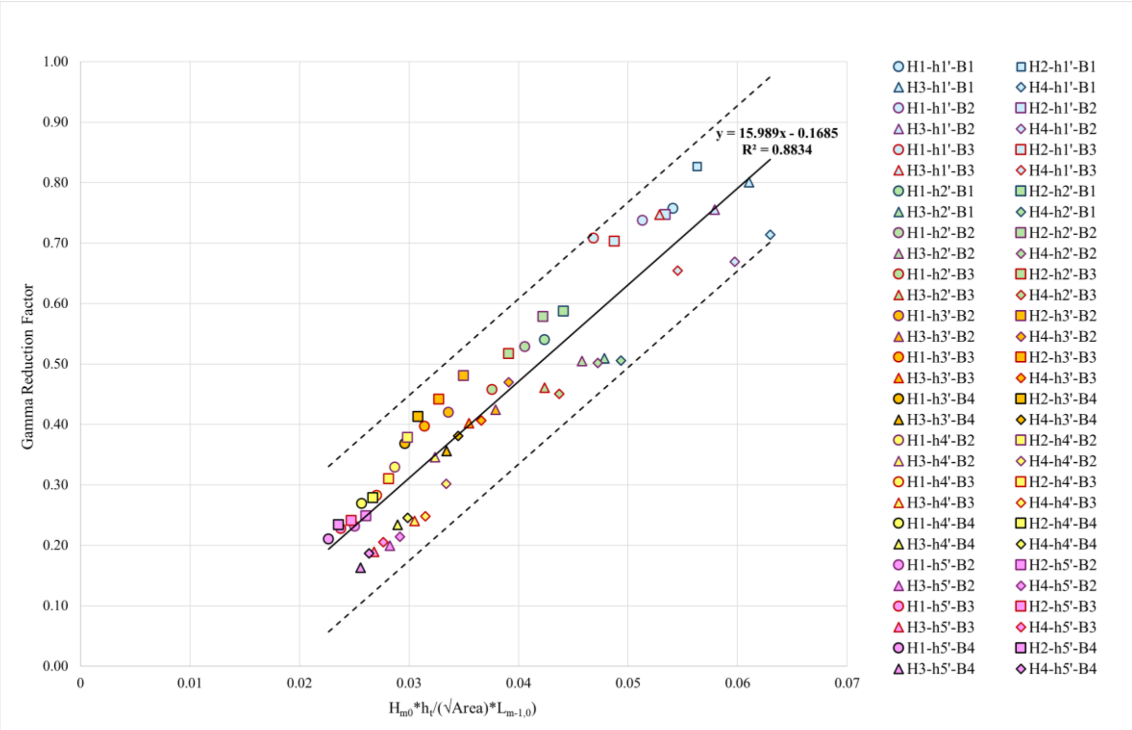


Figure 4.31. Relation between gamma reduction factor ($\gamma_{sub}$) and non-dimensional parameter $\frac{H_{m0i} \times h_t}{\sqrt{Area} \times L_{m-1,0}}$ with linear representation and 95% prediction interval

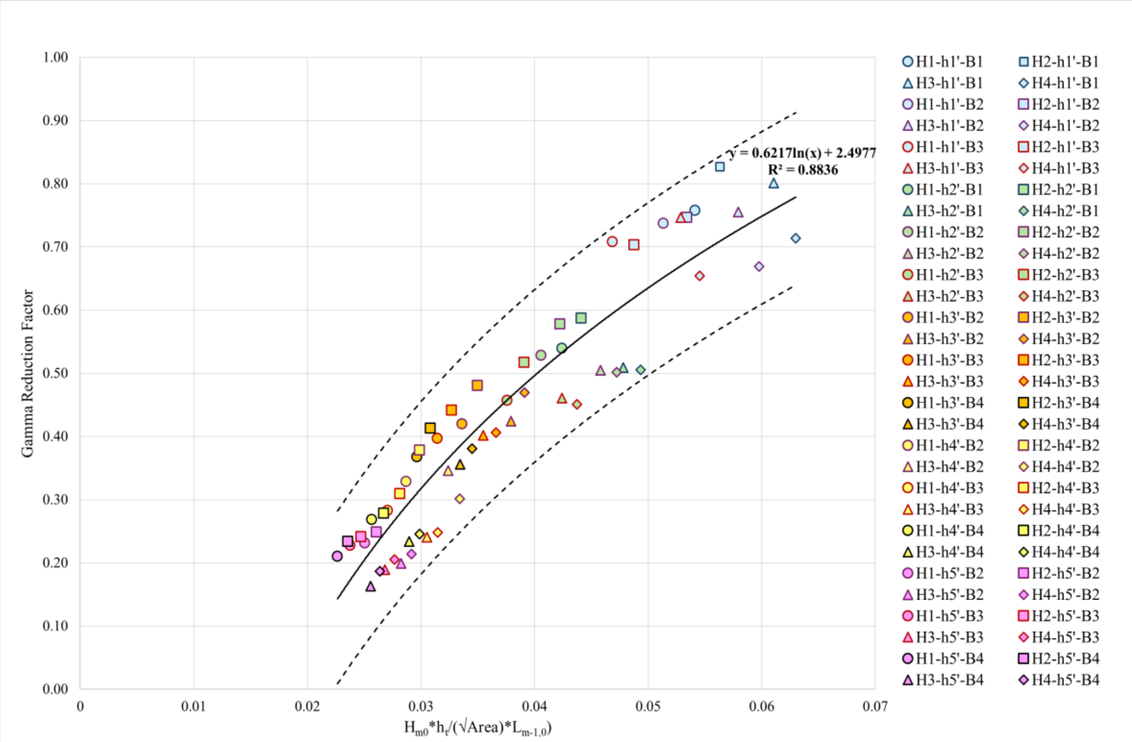


Figure 4.32. Relation between gamma reduction factor ($\gamma_{sub}$) and non-dimensional parameter $\frac{H_{m0i} \times h_t}{\sqrt{Area} \times L_{m-1,0}}$ with logarithmic representation and 95% prediction interval

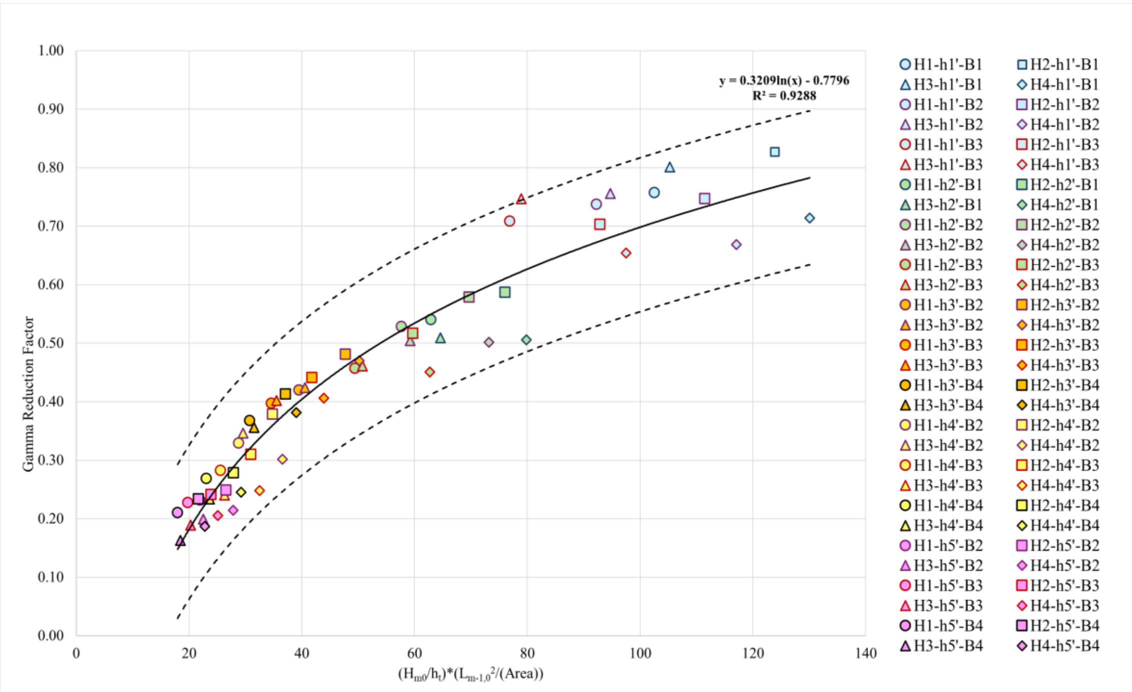


Figure 4.33. Relation between gamma reduction factor ($\gamma_{sub}$) and non-dimensional parameter $\frac{H_{m0i}}{h_t} \times \frac{{L_{m-1,0}}^2}{Area}$ with logarithmic representation and 95% prediction interval

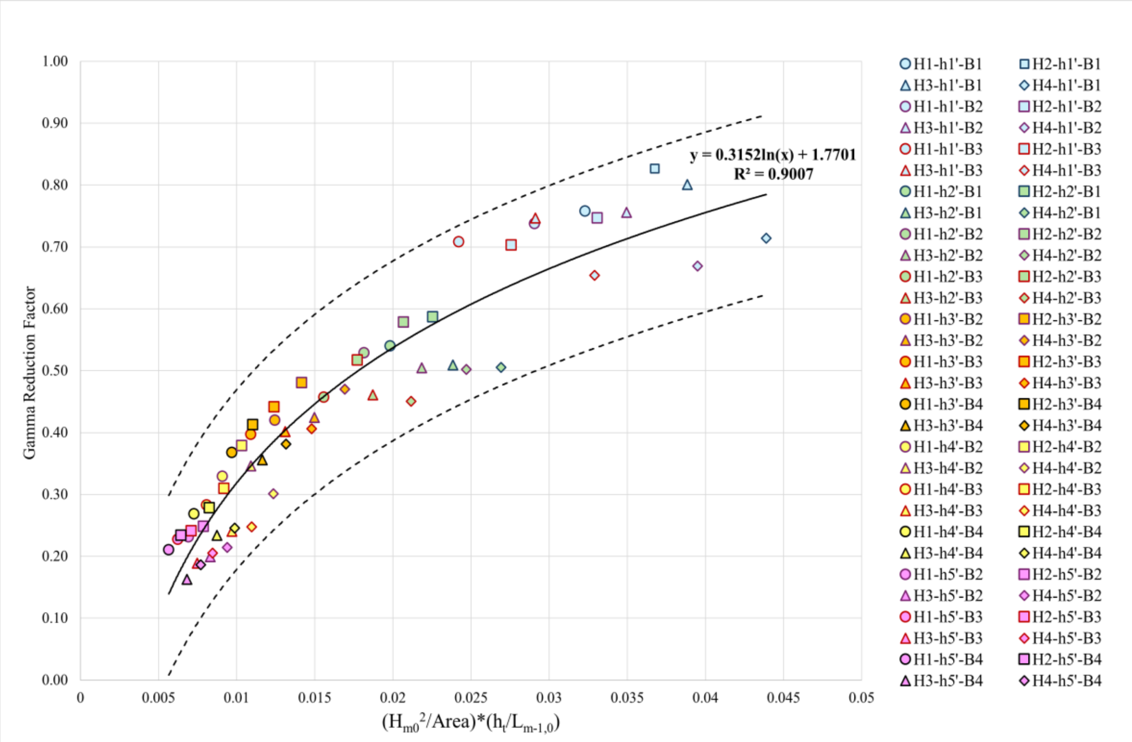


Figure 4.34. Relation between gamma reduction factor ($\gamma_{sub}$) and non-dimensional parameter $\frac{H_{m0i}^{2}}{Area} \times \frac{h_t}{L_{m-1,0}}$ with logarithmic representation and 95% prediction interval

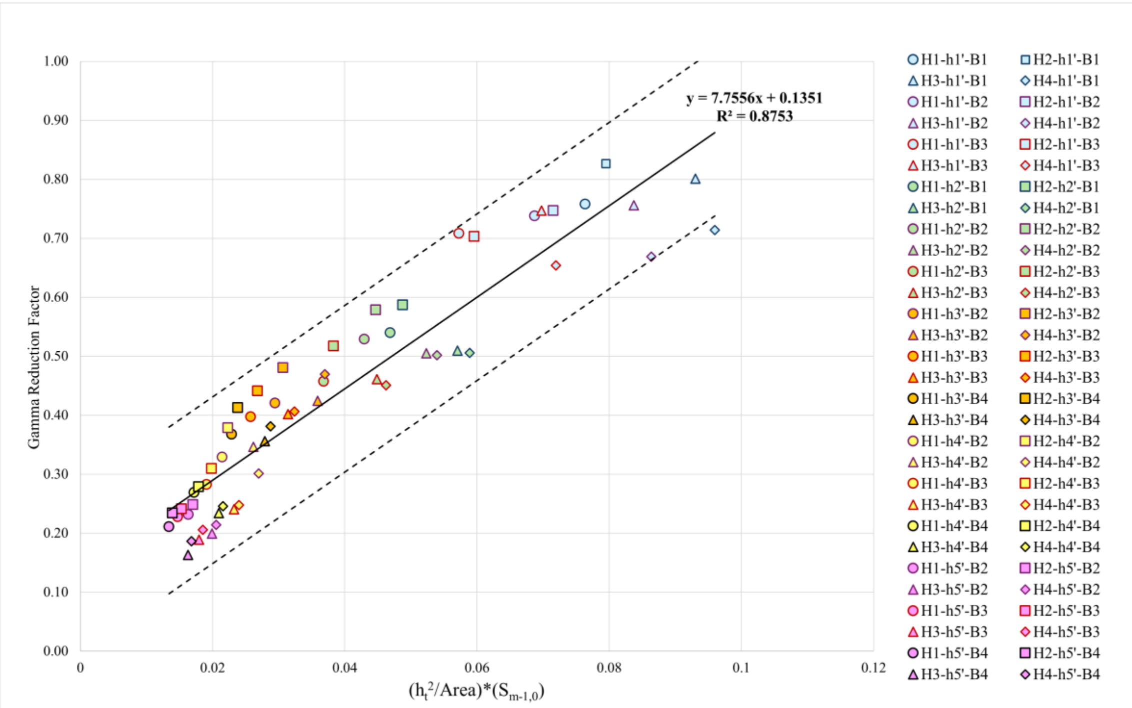


Figure 4.35. Relation between gamma reduction factor ($\gamma_{sub}$) and non-dimensional parameter $\frac{h_t^{2}}{Area} \times S_{m-1,0}$ with linear representation and 95% prediction interval

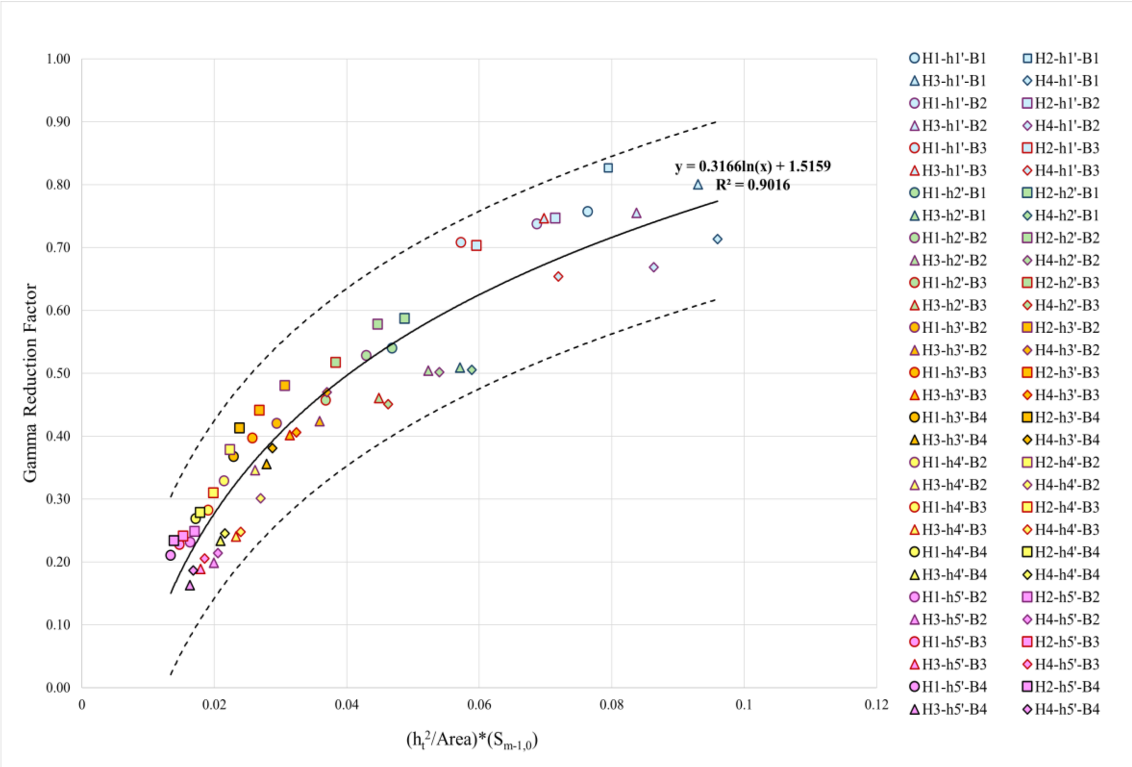


Figure 4.36. Relation between gamma reduction factor ($\gamma_{sub}$) and non-dimensional parameter $\frac{h_t^{\,2}}{Area} \times S_{m-1,0}$ with logarithmic representation and 95% prediction interval

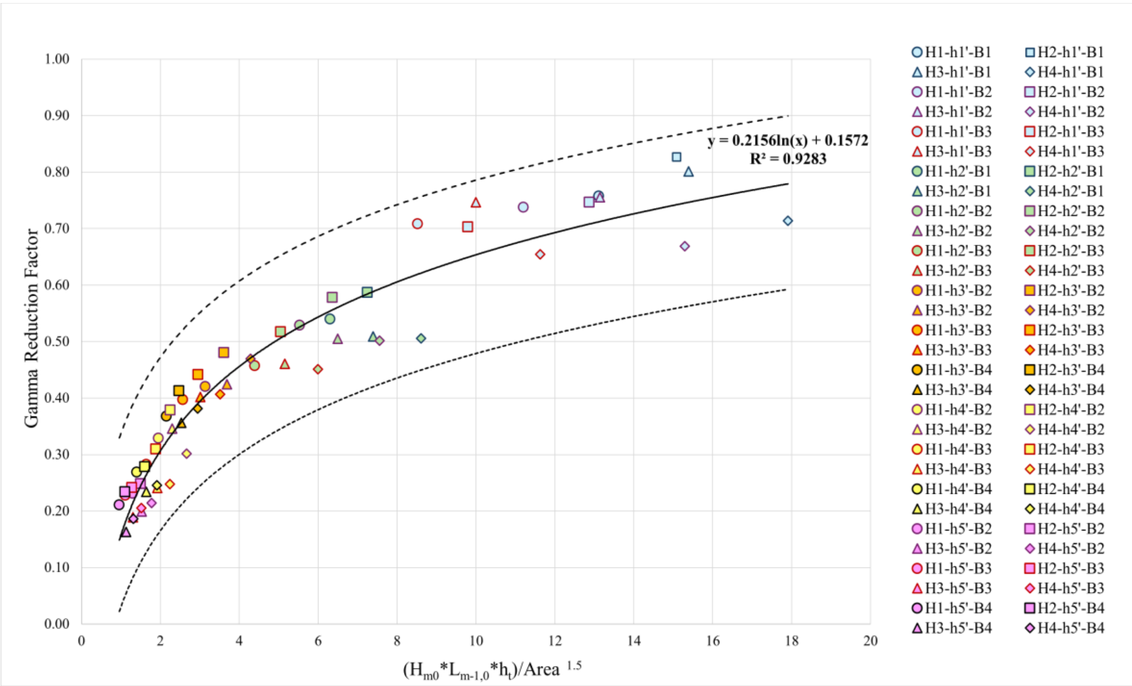


Figure 4.37. Relation between gamma reduction factor ($\gamma_{sub}$) and non-dimensional parameter $\frac{H_{m0i} \times L_{m-1,0} \times h_t}{Area^{1.5}}$ with logarithmic representation and 95% prediction interval

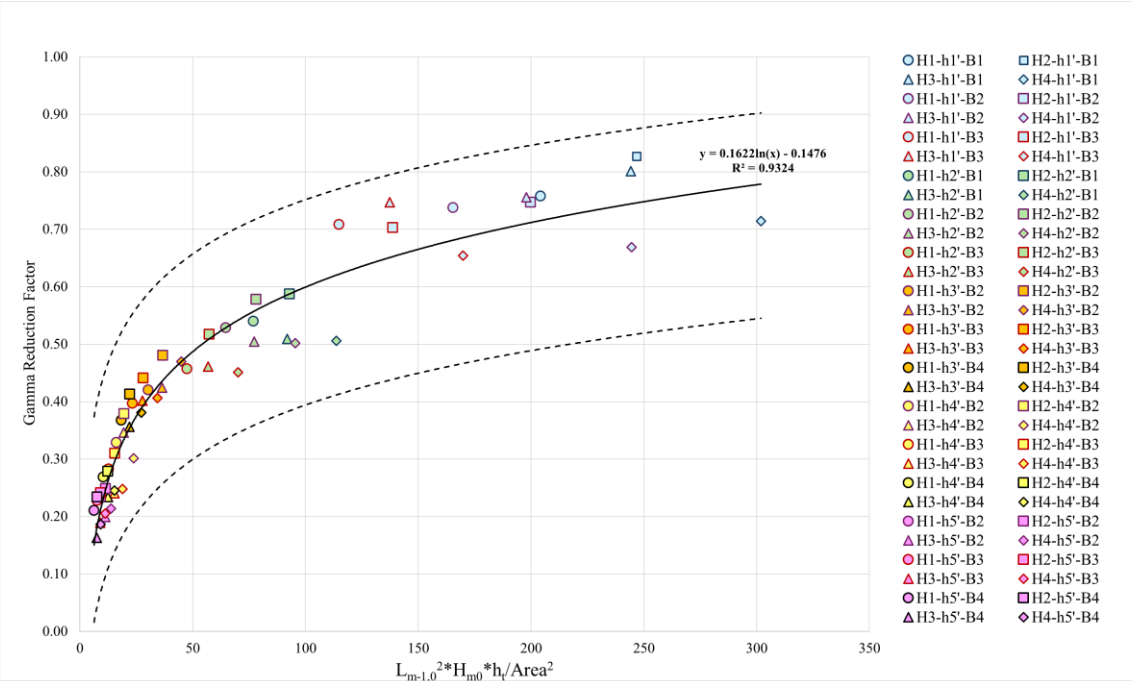


Figure 4.38. Relation between gamma reduction factor ($\gamma_{sub}$) and non-dimensional parameter $\frac{H_{m0i} \times L_{m-1,0}{}^{2} \times h_t}{Area^2}$ with logarithmic representation and 95% prediction interval

### 4.4.1. Best Fit Non-Dimensional Parameters for Gamma Reduction

The proposed formula Eq. 4.20 is plotted in Figure 4.39 which displays the correlation between the reduction factor, $\gamma_{sub}$ and the non-dimensional parameter of submerged breakwater with a linear fit. Eq. 4.20 represents the wavelength normalized by the square root of the breakwater's area.

$$\gamma_{\text{sub}} = 0.0609\left(\frac{L_{m-1,0}}{\sqrt{Area}}\right) - 0.1986 \tag{4.20}$$

The Figure 4.39 shows that an $R^2$ value of 0.94 was achieved, indicating the other strongest fit for this dataset. Moreover, the lower RMSE and MAE values further support the functionality of this parameter. As also observed in the figure, only four points lie above the prediction interval line. The correlation between the predicted from Eq. 4.20 and the observed reduction factors is illustrated in Figure 4.41. The mean overtopping discharges at vertical seawall with submerged breakwater can be estimated by incorporating Eq. 4.20 into Eq. 4.4 , Figure 4.42 illustrates a substantial degree of agreement between the measured and calculated values. A logarithmic representation of the reduction factor is plotted against the same non-dimensional parameter in Figure 4.40. Although data distribution suggests a linear trend, supporting the use of a linear equation for the best fit, this figure is included to provide a visual reference.

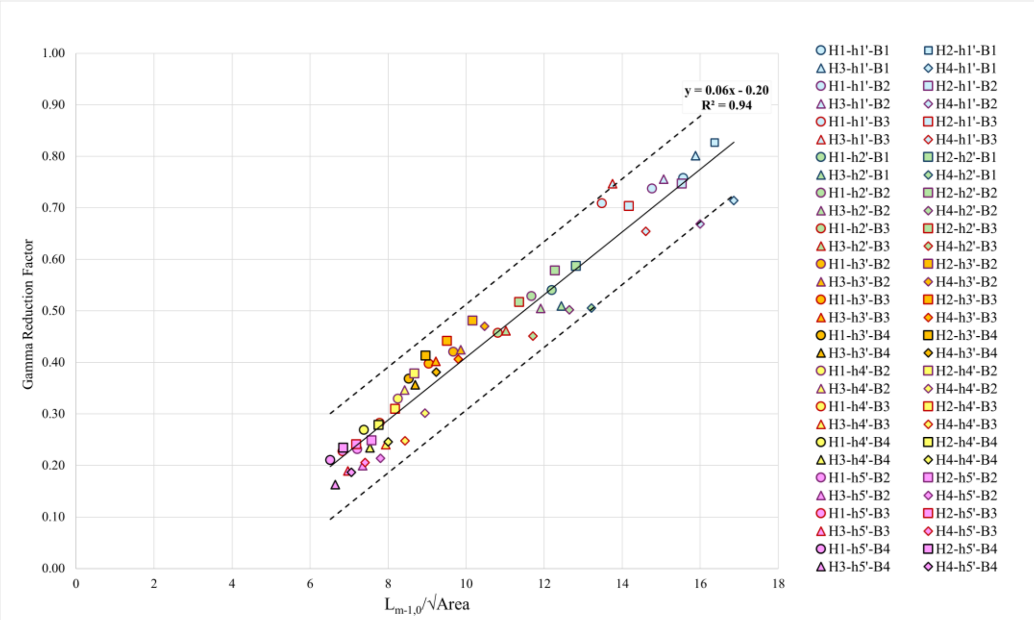


Figure 4.39. Relation between gamma reduction factor ($\gamma_{sub}$) and non-dimensional parameter $\frac{L_{m-1,0}}{\sqrt{Area}}$ with linear representation and 95% prediction interval

The crest width and the height of the submerged breakwater has an influence on the wavelength and the wave form which is directly related to the wavelength.

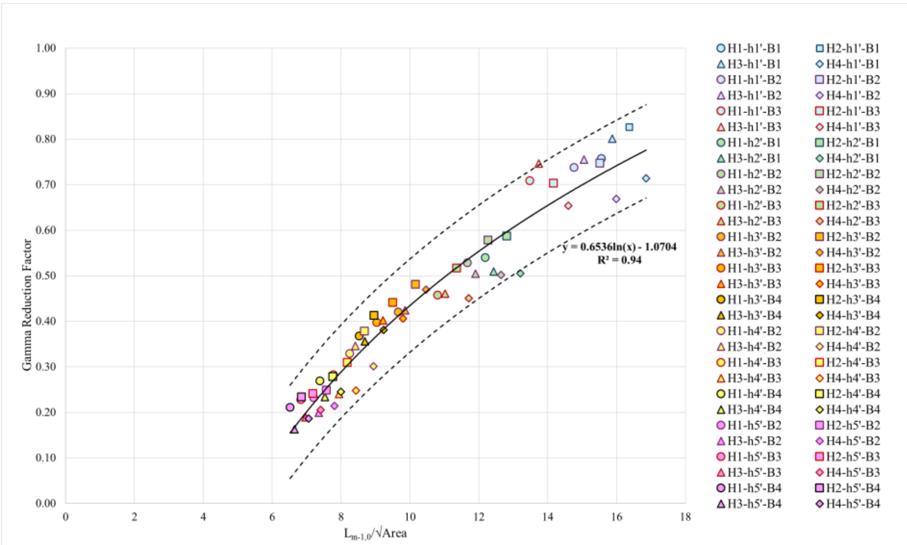


Figure 4.40. Relation between gamma reduction factor ($\gamma_{sub}$) and non-dimensional parameter $\frac{L_{m-1,0}}{\sqrt{Area}}$ with logarithmic representation and 95% prediction interval

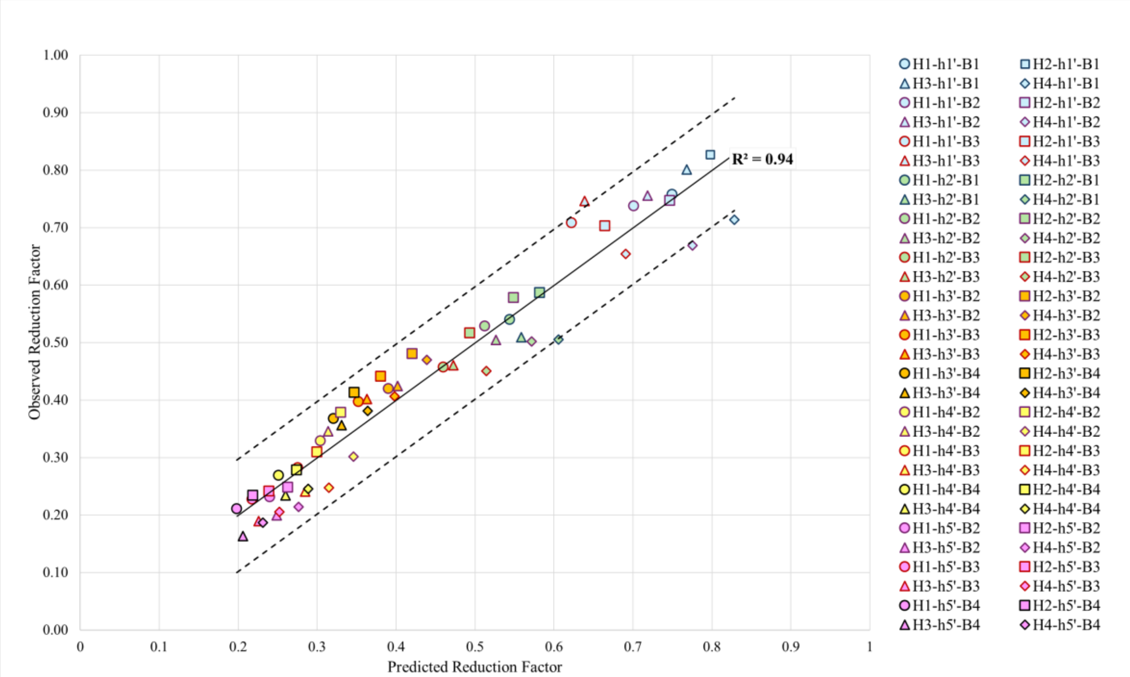


Figure 4.41. Comparison of the observed and predicted reduction factors of submerged breakwater

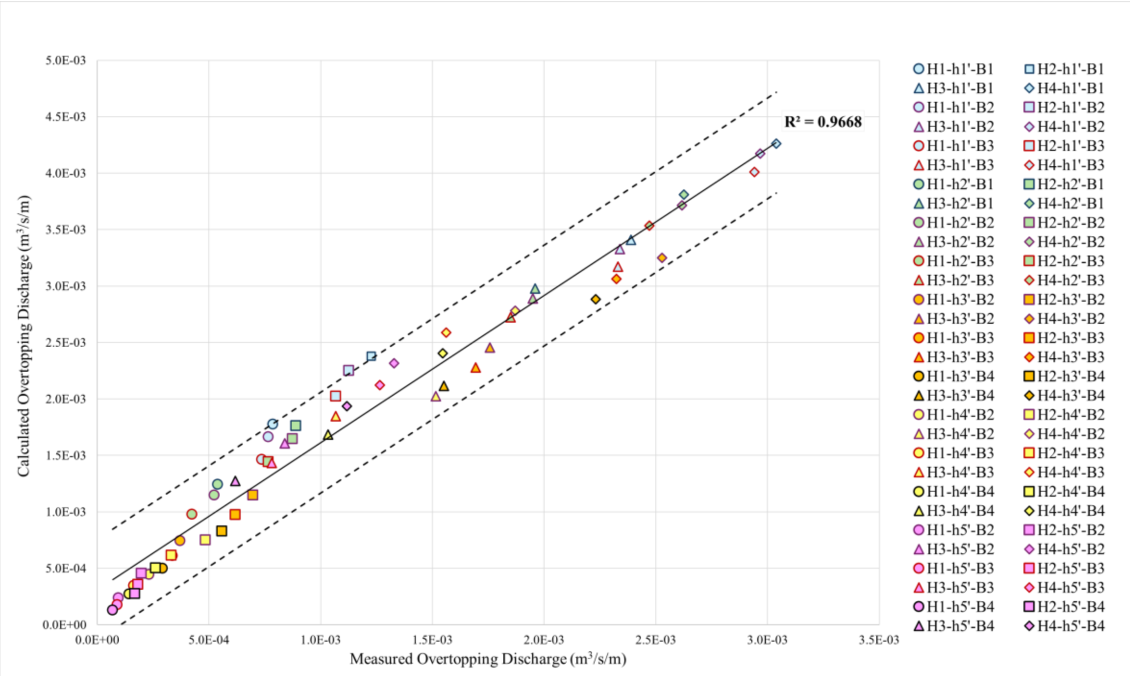


Figure 4.42. Comparison of the calculated and measured mean overtopping discharges

Likewise, another proposed formula Eq. 4.21 is plotted in Figure 4.43, which displays the correlation between the reduction factor, $\gamma_{sub}$ and the non-dimensional parameter of submerged breakwater with a linear fit. The Eq. 4.21 is a function of breaker index and normalized wavelength with square root of the breakwater's area. In other words, it is obtained by multiplying the first proposed parameter by the breaker index. Figure 4.44, on the other hand, provides a logarithmic representation of the reduction factor against the same non-dimensional parameter. While the data distribution appears to follow a linear trend, supporting the recommendation to use a linear equation for the best fit, Figure 4.44 was included for visual reference and comparison.

$$\gamma_{\text{sub}} = 0.0267\left(\frac{L_{m-1,0} \times h_t}{\sqrt{Area} \times H_{m0,i}}\right) - 0.1979 \tag{4.21}$$

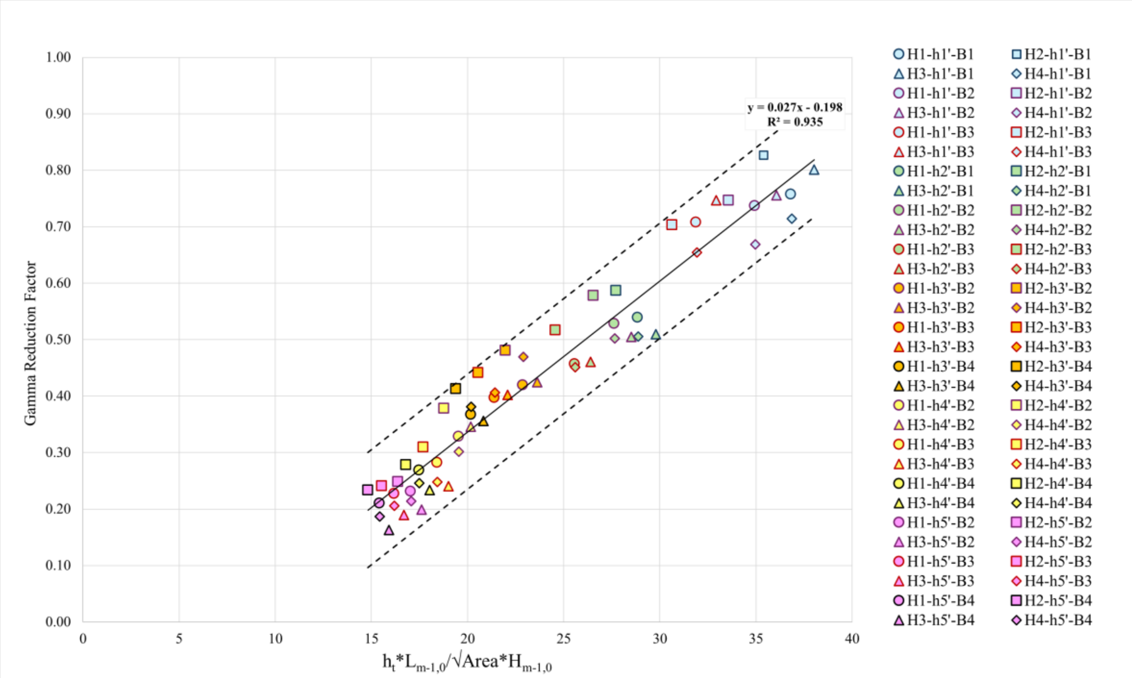


Figure 4.43. Relation between gamma reduction factor ($\gamma_{\text{sub}}$) and non-dimensional parameter $\frac{L_{m-1,0} \times h_t}{\sqrt{Area} \times H_{m0,i}}$ with linear representation and 95% prediction interval

The Figure 4.43 shows that an $R^2$ value of 0.935 was achieved, indicating one of the strongest fit for this dataset. Furthermore, the lowest RMSE and MAE values further support the functionality of this parameter. Additionally, Figure 4.43 shows this parameter has no data points outside the prediction interval line.

The correlation between the predicted from Eq. 4.21 and the observed reduction factors is illustrated in Figure 4.45.

Finally, the mean overtopping discharges at vertical seawalls with submerged breakwater can be estimated by incorporating Eq. 4.21 into Eq. 4.4 , Figure 4.46 illustrates a substantial degree of agreement between the calculated and measured values.

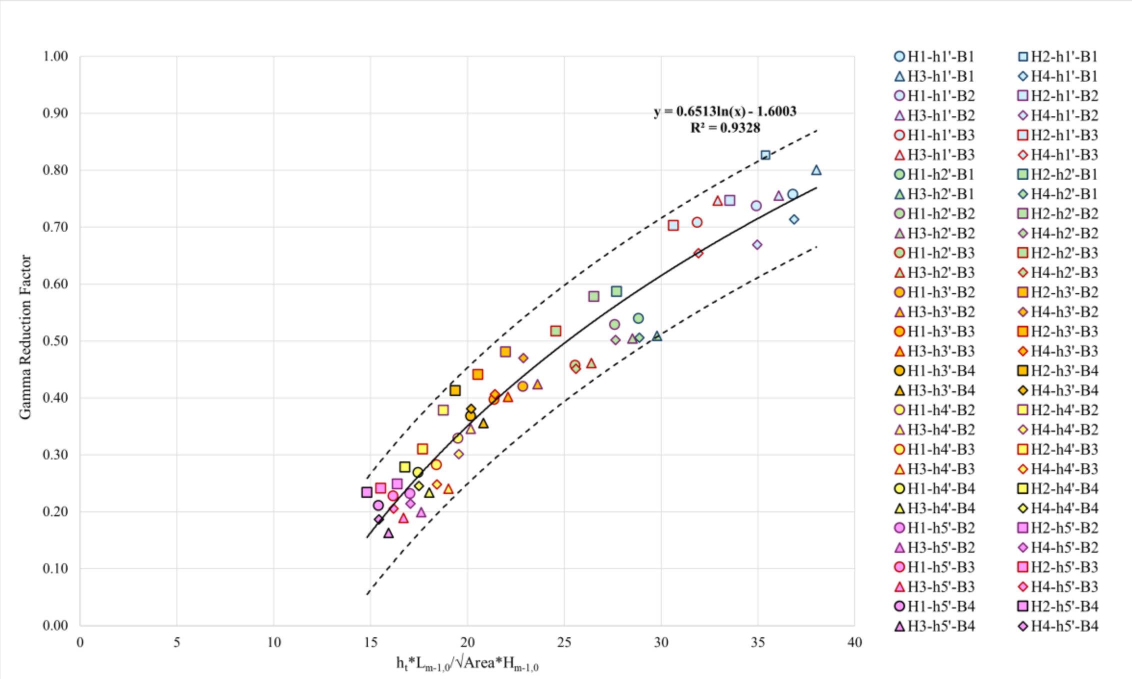


Figure 4.44. Relation between gamma reduction factor ($\gamma_{sub}$) and non-dimensional parameter $\frac{L_{m-1,0}\times h_t}{\sqrt{Area}\times H_{m0,i}}$ with logarithmic representation and 95% prediction interval

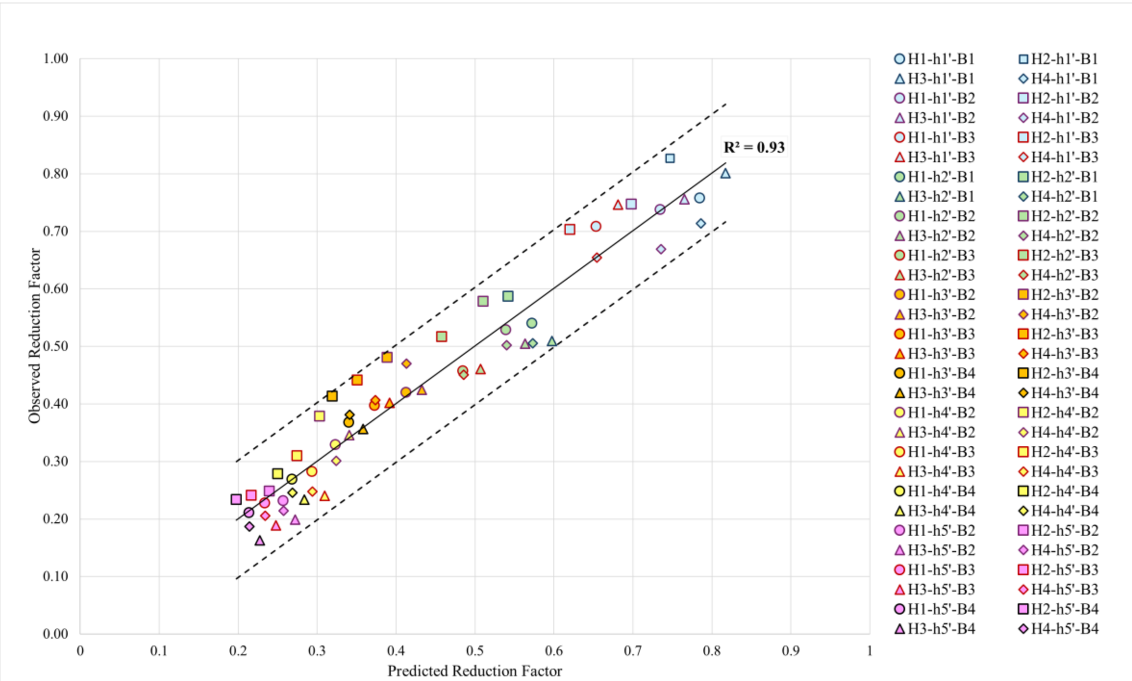


Figure 4.45. Comparison of the observed and predicted reduction factors of submerged breakwater

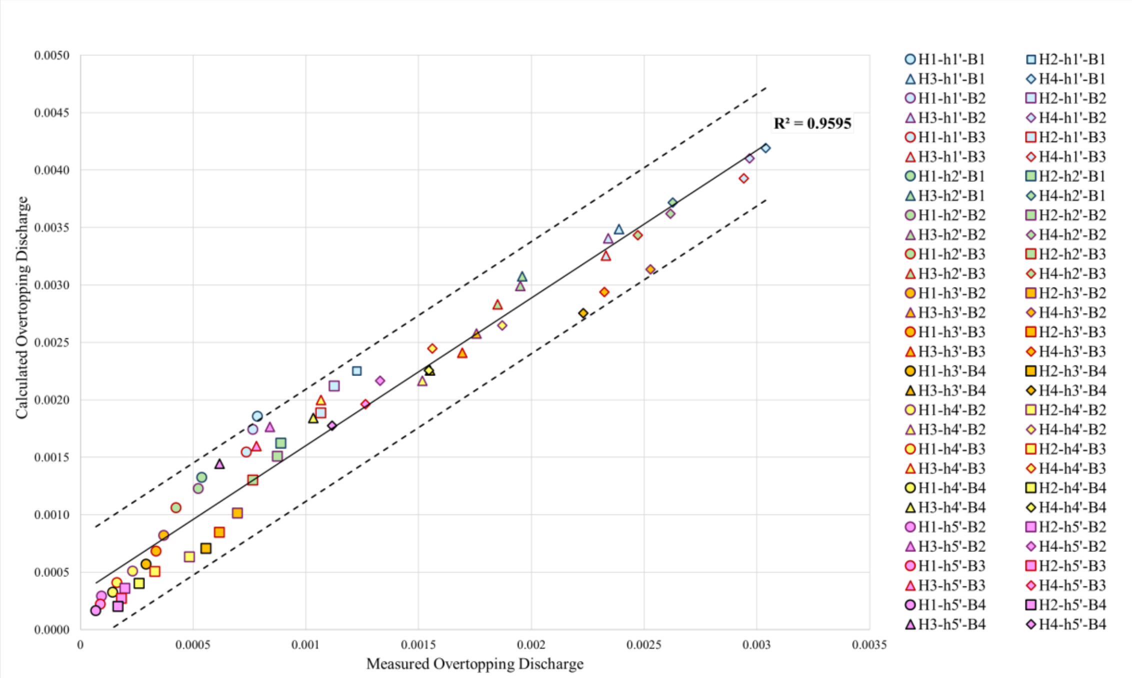


Figure 4.46. Comparison of the calculated and measured mean overtopping discharges

Even though the $R^2$ value of $K_t$ is low when compared to the $R^2$ values of other non-dimensional parameters, it can be suggested that a gamma reduction factor depending on $K_t$ will find a wide applicability since $K_t$ is easy to calculate and well defined in most experimental processes. The physical role of a submerged breakwater is to dissipate wave energy. The parameter that best describes this process is $K_t$. Therefore, the non-dimensional parameter $K_t$ should also be included in the best-fit definitions.

The proposed formula Eq. 4.22 is plotted in Figure 4.47 which shows the correlation between the gamma reduction factor, $\gamma_{sub}$ and the non-dimensional parameter $K_t$ with an exponential fit.

$$\gamma_{\text{sub}} = 0.0478e^{3.0988K_t} \tag{4.22}$$

The correlation between the predicted from Eq. 4.22 and the observed reduction factors is illustrated in Figure 4.48. The mean overtopping discharges at vertical seawall with submerged breakwater can be estimated by incorporating Eq. 4.22 into Eq. 4.4 , Figure 4.49 illustrates a substantial degree of agreement between the measured and calculated overtopping discharge values.

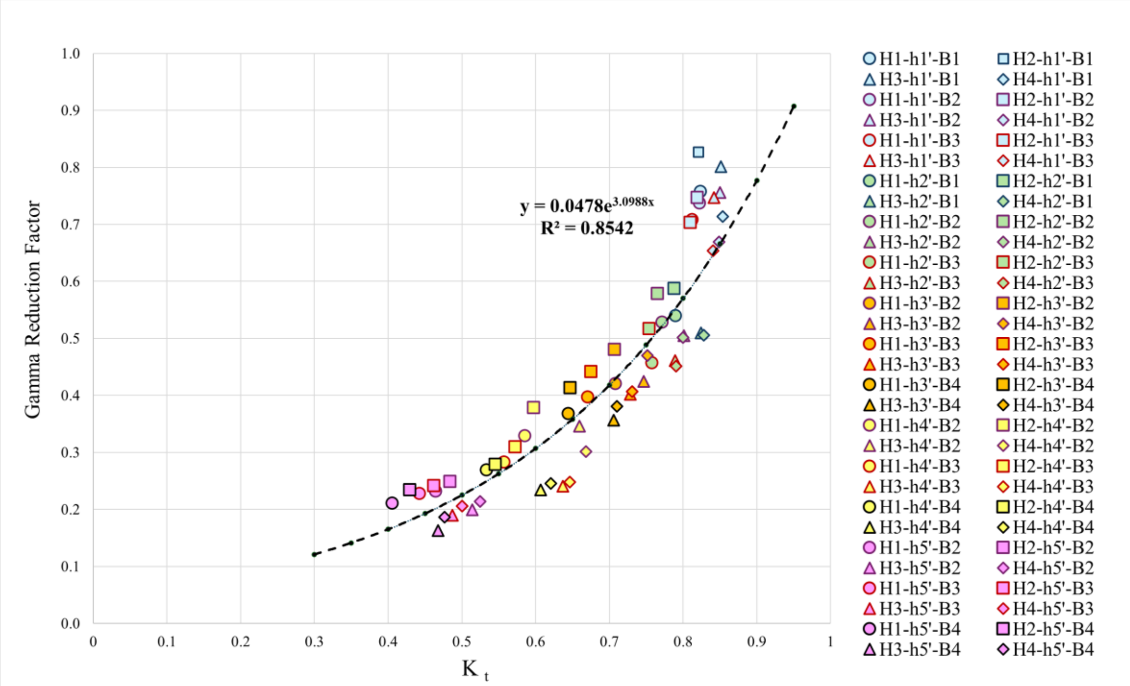


Figure 4.47. Relation between gamma reduction factor ($\gamma_{sub}$) and non-dimensional parameter $K_t$

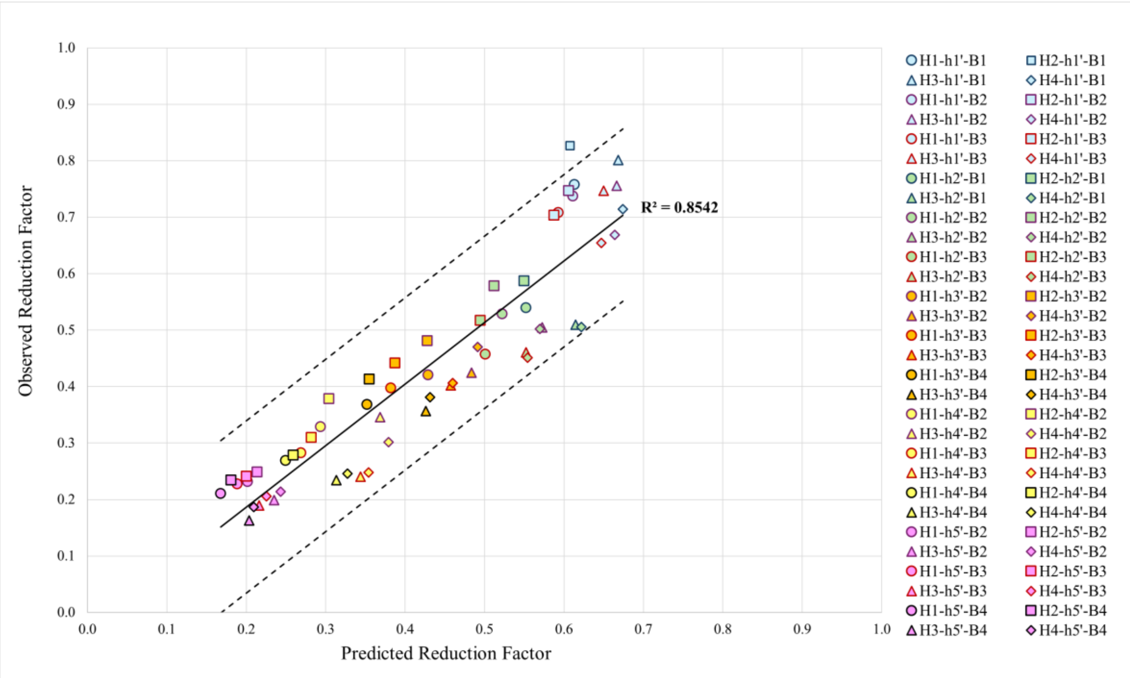


Figure 4.48. Comparison of the observed and predicted reduction factors of submerged breakwater

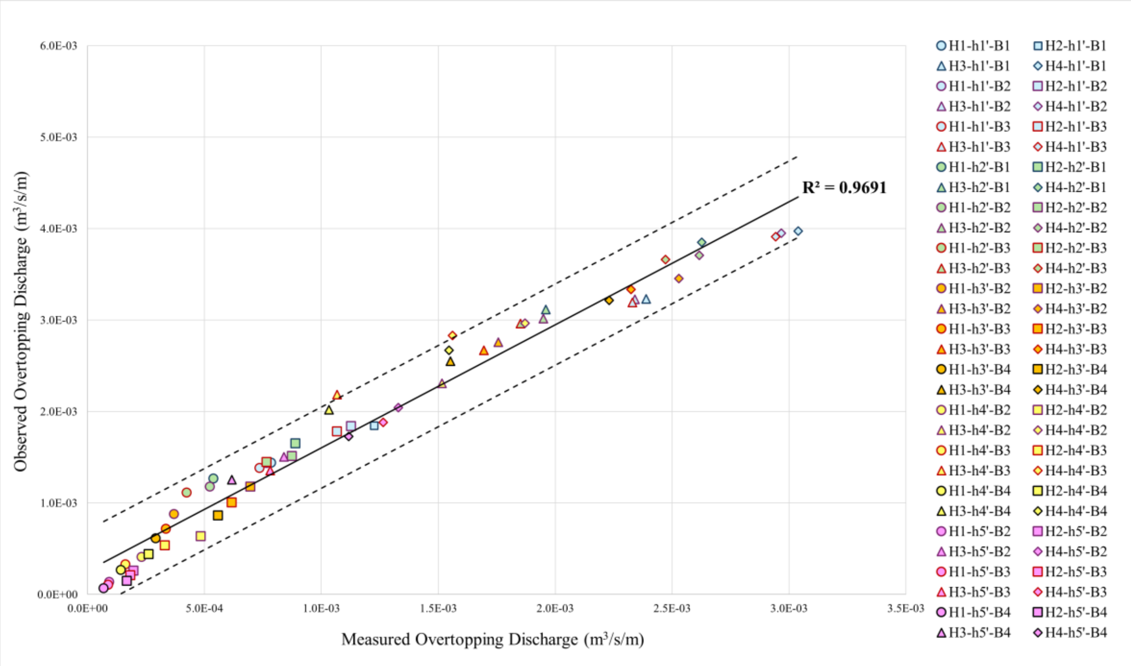


Figure 4.49. Comparison of the measured and calculated mean overtopping discharges

The submerged breakwater decreases the overtopping discharge at the crest of the vertical seawall when it is located in front of it. This reduction is represented by a gamma reduction factor in the traditional formula of EurOtop (2018), Eq. 4. 2.

Gamma reduction coefficient depends on several non-dimensional parameters. First one is wavelength normalizes by the square root of area ($\frac{L_{m-1,0}}{\sqrt{Area}}$), second one is the multiplication of the first one with breaker indices ($\frac{h_t}{H_{m0,i}}$) ; $\frac{L_{m-1,0} \times h_t}{\sqrt{Area} \times H_{m0,i}}$ and the last one is the wave transmission coefficient $K_t$ , which is the ratio of incident wave height to transmitted wave height. The findings indicate that there is no single unique outcome, but rather a combination of various results, as all have similar $R^2$ values, and no single parameter emerges as the definitive best-fit, even though ($\frac{L_{m-1,0}}{\sqrt{Area}}$) may have a slightly higher $R^2$ value compared to the others. The used data range of relative crest width ($\frac{B}{L_{m-1,0}}$), relative freeboard ($\frac{F}{Hm0_i}$), steepness ($S_{m-1,0}$), and breaker index ($\frac{Hm0_i}{ht}$) are written in Eq. 4.23 below.

$$0.03 < \frac{B}{L_{m-1,0}} < 0.1$$

$$0.8 < \frac{h'}{Hm0_i} < 2.3$$

$$-1.5 < \frac{F}{Hm0_i} < -0.09 \tag{4.23}$$

$$3 < \frac{B}{L} < 10$$

$$0.4 < \frac{Hm0_i}{ht} < 0.5$$

$$0.038 < \frac{H_{m0i}}{L_{m-1,0}} \; or \; S_{m-1,0} < 0.042$$

This data includes uncertainties related to laboratory effects, scale effects, 3D effects, and the use of pure freshwater instead of saline water. Therefore, it should be validated by using prototype data.

From the Figure 4.43, Figure 4.39 , Figure 4.47 and Equations 4.21, 4.20, 4.22 it can be observed that the overtopping discharge, which is influenced by the submerged breakwater, is significantly affected by wavelength, incident wave height, water depth and $K_t$ parameter. Therefore, these parameters exhibit strong correlations with the gamma reduction factor.

# CHAPTER 5

# CONCLUSIONS AND RECOMMENDATIONS

Coastal zones, including Izmir Bay, are at a substantial risk of experiencing natural disasters that are further worsened by climate change and sea level rise, such as increased storm intensity and wave heights. The necessity for innovative and adaptive solutions has been prompted by the limitations of conventional coastal protection structures, such as rubble mound breakwaters and vertical seawalls, in addressing these challenges.

The objective of this research was to assess the effectiveness of submerged breakwaters in reducing wave overtopping at vertical seawalls with the help of physical model tests. The influence of the submerged breakwater is reflected by a gamma reduction factor. This factor is included in the traditional EurOtop formulation.

The experimental investigations conducted at the Izmir Institute of Technology (IZTECH) have provided valuable insights into the performance of submerged breakwaters under varying hydrodynamic conditions. Random waves were used in the experimental study and 128 different 2D small scale experiments were conducted.

The experimental data demonstrated that, in certain cases, submerged breakwaters reduced wave overtopping at vertical seawalls by as much as 90%. However, this significant reduction was observed under specific geometric and hydrodynamic conditions. The geometric parameters of submerged breakwater (i.e. height and crest width) are directly correlated with its reduction factor. To evaluate the impact of the submerged breakwater on wave overtopping reduction, experiments were performed with and without the submerged breakwater.

It is important to note that submerged breakwaters are fixed structures, and as sea level rise is a gradual process, their effectiveness is expected to decrease over time. This theoretical projection highlights the need to consider future sea level scenarios during the design and implementation phases to ensure long-term resilience.

After validating overtopping discharge measurements for a vertical seawall without a submerged breakwater using the EurOtop (2018) guidelines, a reduction factor related to the submerged breakwater was defined, considering factors such as wave climate, water depth, and environmental conditions to help reduce overtopping discharge and protect urban infrastructure against storm surge events.

The gamma reduction factor of the submerged breakwater was found to be inversely proportional to its area. To model this dependency, two different equations have been proposed. Also, considering the importance of the wave transmission coefficient ($K_t$) in this analysis, an additional equation including $K_t$ is also developed. The final equations are,

$$\gamma_{\text{sub}} = 0.0609\left(\frac{L_{m-1,0}}{\sqrt{Area}}\right) - 0.1986\ , \qquad 6 < \frac{L_{m-1,0}}{\sqrt{Area}} < 17$$

$$\gamma_{\text{sub}} = 0.0267\left(\frac{L_{m-1,0} \times h_t}{\sqrt{Area} \times H_{m0,i}}\right) - 0.1979\,, \qquad 15 < \frac{L_{m-1,0} \times h_t}{\sqrt{Area} \times H_{m0,i}} < 37$$

$$\gamma_{\text{sub}} = 0.0478e^{3.0988K_t}\ , \qquad 0.40 < K_t < 0.86$$

The variation of reduction factor is in the range of $0.16 \leq \gamma_{\text{sub}} \leq 0.82$ and the new forms of nondimensionalized exponential form equations are expressed as,

$$\frac{q}{\sqrt{g * {H_{m0}}^3}} = 0.0155 * \left(\frac{H_{m0}}{h * s_{m-1,0}}\right)^{0.5} exp\left(-2.2\frac{R_c}{H_{m0}}\frac{1}{\gamma_{sub}}\right), \qquad 0.1 < \frac{R_c}{H_{m0}} < 0.35$$

These formulas indicate that parameters such as wavelength, wave height and water depth play an important role in determining the gamma reduction factor. The results highlight the strong correlations between these variables and the reduction factor and their critical impact on the overall performance of submerged breakwaters.

In addition, experiments with the submerged breakwater existing alone in the flume were conducted to investigate the wave transmission through a submerged breakwater. The data set analyzed in this study showed strong correlations with the formulas proposed in the literature. Among those examined, the formula proposed by Van Gent et al. (2023), Eq. 2.21 provide the strongest correlation.

Low wave transmission coefficients are directly related to low wave overtopping discharge, highlighting the complementary role of submerged breakwaters in enhancing coastal protection systems. The results of this study demonstrate that submerged breakwaters can be an effective supplementary measure to address flooding risks and enhance the resilience of vertical seawalls.

To improve the accuracy and reliability of this study, it is essential to acknowledge the disadvantages associated with submerged breakwaters. Constructing these structures on the seaward side is more challenging and costly compared to landward crest modifications. Additionally, submerged breakwaters pose navigation hazards due to their low visibility during high tides or rough sea conditions, potentially endangering boats and other watercraft. Their ecological impacts are also notable, as they can alter marine habitats and disrupt the behavior of aquatic species, with some facing habitat loss or disturbances in sedimentation patterns.

Given these challenges, it is advised to incorporate supplementary datasets that cover a wider range of incident wave heights to improve the accuracy and reliability of this study. A more comprehensive explanation of the behavior of submerged breakwaters under varying hydrodynamic conditions would be facilitated by the incorporation of a wider range of wave height scenarios. This will enhance the understanding of the relationships among wave height, wave overtopping, and wave transmission, ensuring the findings are relevant across a wider range of hydrodynamic conditions. Also, such data will improve understanding of submerged breakwater performance under extreme wave conditions, leading to improved modeling design recommendations.

Lastly, the differences induced by scale effects can be further mitigated by undertaking in-situ measurement or using larger-scale model results. Moreover, physical investigations can be complemented by advanced numerical modeling techniques, which enable the validation of results at a variety of scales. The reliability and applicability of the findings to real-world scenarios will be enhanced by these methods.

# REFERENCES


Ahrens, John P. 1987. “Characteristics Of Reef Breakwaters.”

Allsop, N. W. H., Besley, P., and Madurini, L. 1995. “Overtopping performance of vertical walls and composite breakwaters, seawalls and low reflection alternatives.” Final Rep. of Monolithic Coastal Structures Project, Univ. of Hannover, Hannover, Germany.

Ak, Salih. 2021. “Investigation of Coastal Flood Problem in Izmir Bay.” M. Sc. – Master’s Degree Program, İzmir Institute of Technology.

Aktaş, Kadir. 2020. “Wave Generation and Analysis in the Laboratory Wave Channel to Conduct Experiments on the Numerically Modeled Spar Type Floating Wind Turbine.” M. Sc. – Master’s Degree Program, İzmir Institute of Technology.

Bahadıroğlu, Nisa, Doğan Kısacık, and Lorenzo Cappietti. "Using Stilling Wave Basin for Adaptation Measures to Sea Level Rise in Coastal Areas." Abstract presented at ICCE 2024, 2024. Abstract ID: 697.

Briganti, Riccardo, Jentsje Der Van Meer, Mariano Buccino, and Mario Calabrese. 2003. “Wave Transmission behind Low-Crested Structures.” In Coastal Structures 2003 - Proceedings of the Conference, 580–92. https://doi.org/10.1061/40733(147)48.

Calabrese, Mario, Diego Vicinanza, and Mariano Buccino. 2003. “Large-Scale Experiments On The Behaviour Of Low Crested And Submerged Breakwaters In Presence Of Broken Waves.” In, 1900–1912. *World Scientific Pub Co Pte Lt.* https://doi.org/10.1142/9789812791306_0160.

Cappietti, Lorenzo. 2011. “Converting Emergent Breakwaters into Submerged Breakwaters.” *Journal of Coastal Research SI 64:479–83.* https://www.researchgate.net/publication/266889192.

Charles Friebel, Harry, and Lee E Harris. 2003. “Re-Evaluation of Wave Transmission Coefficient Formulae from Submerged Breakwater Physical Models.”

CIRIA, CUR, CETMEF. 2007. The Rock Manual. The use of rock in hydraulic engineering (2nd edition). C683, CIRIA, London.

d'Angremond K., J.W. van der Meer and R.J. de Jong. 1996. Wave transmission at low crested structures. Proc. 25th Int. Conf. on Coastal Engineering, ASCE, 3305-3318.

Daemen, I. F. R. 1991. Wave Transmission at Low-Crested Structures. Thesis, Delft Hydraulics/Delft University of Technology, February.

EurOtop, 2007. In: Pullen, T., Allsop, N.W.H., Bruce, T., Kortenhaus, A., Schüttrumpf, H., van der Meer, J.W. (Eds.), EurOtop — Wave Overtopping of Sea Defences and Related Structures: Assessment Manual. nvironment Agency (UK), Expertise Netwerk Waterkeren (NL), Kuratorium fr Forschung im Ksteningenieurwesen (DE). www.overtopping-manual.com.

EurOtop, 2016. In: Van der Meer, J.W., Allsop, N.W.H., Bruce, T., De Rouck, J., Kortenhaus, A., Pullen, T., Schüttrumpf, H., Troch, P., Zanuttigh, B. (Eds.), Manual on Wave Overtopping of Sea Defences and Related Structures. An Overtopping Manual Largely Based on European Research, but for Worldwide Application. www. overtopping-manual.com.

EurOtop, 2018. In: Manual on Wave Overtopping of Sea Defenses and Related Structures, an Overtopping Manual Largely Based on European Research, but for Worldwide Application, second ed. 2018. http://www.overtopping-manual.com/

Franco, L, M De Gerloni, and J W Van Der Meer. 1994. "Chapter 75 Wave Overtopping On Vertical And Composite Breakwaters."

Gent, Marcel R.A. van, Guido Wolters, and Alex Capel. 2022. "Wave Overtopping Discharges at Rubble Mound Breakwaters Including Effects of a Crest Wall and a Berm." *Coastal Engineering 176* (September). https://doi.org/10.1016/j.coastaleng.2022.104151.

Gent, Marcel R.A. van, Lisanne Buis, Jeroen P. van den Bos, and Davide Wüthrich. 2023. "Wave Transmission at Submerged Coastal Structures and Artificial Reefs." *Coastal Engineering 184* (September). https://doi.org/10.1016/j.coastaleng.2023.104344.

Gent, Marcel R.A. Van. 2024. "Submerged Low-Crested Structures in Front of Coastal Structures*." Journal of Coastal and Hydraulic Structures 4* (March). https://doi.org/10.59490/jchs.2024.0033.

Goda, Yoshimi, and Yasumasa Suzuki. 1976. "Chapter 48 Estimation of Incident and Reflected Waves in Random Wave Experiments."

Goda, Yoshimi, 2000. In: Random Seas and Design of Maritime Structures, second ed. *World Scientific Publishing*, Singapore.

İzmir Metropolitan Municipality. 2022. “Sponge City Izmir.” https://sungerkent.izmir.bel.tr.

Kısacık, Dogan and Gökhan Kaboğlu 2017. İzmir İç Körfezde Yaşanan Fırtına Taşkınlarının Araştırılması ve Tainaron Önlenmesi İçin Bir Öneri: Durgun Dalga Havuzu Modeli Projesi (BAP-2016.KB.FEN.014) 1. Development Report. DEÜ-BAP: İzmir.

Kisacik, Dogan, Gulizar Ozyurt Tarakcioglu, and Cuneyt Baykal. 2019. “Stilling Wave Basins for Overtopping Reduction at an Urban Vertical Seawall – The Kordon Seawall at Izmir.” *Ocean Engineering 185* (August):82–99. https://doi.org/10.1016/j.oceaneng.2019.05.033.

Kisacik, Dogan, Gulizar Ozyurt Tarakcioglu, and Lorenzo Cappietti. 2022. “Adaptation Measures for Seawalls to Withstand Sea-Level Rise.” *Ocean Engineering 250* (April). https://doi.org/10.1016/j.oceaneng.2022.110958.

Kurdistani, Sahameddin Mahmoudi, Giuseppe Roberto Tomasicchio, Felice D′Alessandro, and Antonio Francone. 2022. “Formula for Wave Transmission at Submerged Homogeneous Porous Breakwaters.” *Ocean Engineering 266* (December). https://doi.org/10.1016/j.oceaneng.2022.113053.

Mansard, E.P.D., and E.R. Funke. 1980. “The Measurement of Incident And Reflected Spectra Using A Least Squares Method.” *Coastal Engineering Proceedings, no. 17* (January), 8. https://doi.org/10.9753/icce.v17.8.

McGranahan, Gordon, Deborah Balk, and Bridget Anderson. 2007. “The Rising Tide: Assessing the Risks of Climate Change and Human Settlements in Low Elevation Coastal Zones.” *Environment and Urbanization 19* (1): 17–37. https://doi.org/10.1177/0956247807076960.

Meer, Jentsje W Van Der, (1990a) Data on Wave Transmission due to overtopping. Delft Hydraulics report no. H986, prepared for CUR C67.

Meer, Jentsje W Van Der, and F R Daemen. 1994. “Stability and Wave Transmission at Low-Crested Rubble-Mound Structures.”

Meer, Jentsje W. van der, Riccardo Briganti, Barbara Zanuttigh, and Baoxing Wang. 2005. “Wave Transmission and Reflection at Low-Crested Structures: Design Formulae, Oblique Wave Attack and Spectral Change.” *Coastal Engineering 52* (10–11): 915–29. https://doi.org/10.1016/j.coastaleng.2005.09.005.

Meer, Jentsje van der, and Tom Bruce. 2014. “New Physical Insights and Design Formulas on Wave Overtopping at Sloping and Vertical Structures.” *Journal of Waterway, Port, Coastal, and Ocean Engineering 140* (6). https://doi.org/10.1061/(asce)ww.1943-5460.0000221.

Owen, M. W. 1980. Design of seawalls allowing for wave overtopping. Hydraulics Research Station, Wallingford. https://eprints.hrwallingford.com/35/1/EX924.pdf

Rambabu, Nimma, S M Asce, V K Srineash, and Aff M Asce. 2024. “Numerical Investigation on the Hydrodynamics of Vertical Seawalls Defended by a Submerged Breakwater.” https://doi.org/10.1061/JWPED5.WWENG-2144.

Romano, A., G. Bellotti, R. Briganti, and L. Franco. 2015. “Uncertainties in the Physical Modelling of the Wave Overtopping over a Rubble Mound Breakwater: The Role of the Seeding Number and of the Test Duration.” *Coastal Engineering 103* (September):15–21. https://doi.org/10.1016/j.coastaleng.2015.05.005.

Seabrook, Stuart R, and Kevin R Hall. 2000. “Wave Transmission at Submerged Rubblemound Breakwaters.”

Small, Christopher, and Robert J Nicholls. 2003. “A Global Analysis of Human Settlement in Coastal Zones.” Source: *Journal of Coastal Research*. Vol. 19. https://about.jstor.org/terms.

SWAN team (2017). SWAN Scientific and Technical Documentation. SWAN Cycle III version 41.20 Delft University of Technology, Netherlands.

TAW, 2002. In: van der Meer, J.W. (Ed.), Technical Report on Wave Run-Up and Wave Overtopping at Dikes. Technical Advisory Committee on Flood Defence. The Netherlands. www.tawinfo.nl.